The Physiological and Behavioral Roles of Cholinergic and GABAergic Signaling to *Drosophila* Circadian Clock Neurons

by

Jenna L. Persons

A dissertation submitted in partial fulfillment
of the requirements for the degree of
Doctor of Philosophy
(Molecular, Cellular, and Developmental Biology)
in the University of Michigan
2019

Doctoral Committee:

Professor Richard I. Hume, Co-chair
Professor Orie T. Shafer, Co-chair
Associate Professor Sara J. Aton
Associate Professor Laura A. Buttitta
Professor Scott D. Pletcher

Jenna L. Persons

clemjenl@umich.edu

ORCHID iD: 0000-0002-8807-9678

Dedication

To my Mamaw and grandma Jane, who saw in me a willful girl who might someday make her parents proud.

Acknowledgments

The work published herein is the combined effort of a community, to which I owe a great deal of gratitude and admiration. Thank you all. First, I acknowledge my mentor Dr. Orie Shafer whose enthusiasm for science is unmatched. I've enjoyed working with him for the past two years at Michigan, and though our time together was measurably shorter than that of most graduate careers, I've learned more in this span than all years prior. I appreciate greatly his persistent faith in my abilities as a scientist and for focusing my efforts on performing the best experiment, that win or lose will tell us something new. I wish to thank Dr. Monica Dus, for inspiring me to do research that challenges the prescriptive, merges disparate scientific fields and where there is need, creating tools to investigate previously unanswerable questions. Without Monica's fearless scientific mind, I wouldn't have found my footing at Michigan. An enormous thank you to Drs. Michael Bradley, Stacy Jones, and Casey McNeil at my undergraduate institution, Newman University. I am grateful for their mentorship, positive energy and seeing in me the potential to pursue this work.

Thank you to my committee members and mentors at Michigan, Drs. Laura Buttitta, Sara Aton, Rich Hume, and Scott Pletcher, for their thoughts on my work and importantly, their support of my scientific career. They were voices of clarity and reassurance when I needed it the most. I extend a special thank you to Dr. Scott Pletcher for telling me sincerely that 'people might tell you that you can't do this, but [he] knew I could.' I will not soon forget their faith in me. I must express my gratitude to my lab mates,

colleagues and collaborators throughout the years. Their contributions to this work and my development as a scientist prove that great work is the result of many hands and minds. These include Dr. Rob Jackson, Dr. Maria paz de la Fernandez, Dr. Zepeng Yao, Charles Davey, Dr. Swathi Yadlapalli, Andy Kernbach, Hannah Pettibone, Deepika Pandian, Alyssa Kalsbeek, Lorraine Horwitz, Matt Gaidica, Sara Lennox, Krystal Harrison, and Dr. Olga Grushko. To all my students at Michigan for challenging me to work harder and think differently. I deeply enjoyed teaching, and though it's a common trope for educators, they taught me more than I think I ever taught them.

My upmost thanks for Shyama Nandakumar, Christina May, and Hadley Freeman and Wyatt Bigley. Their friendships and brilliance are invaluable sources of support, joy and laughter. I truly never expected to be so lucky and I wish to thank them for being there when it mattered and showing me how powerful true friends can be. Finally, I must acknowledge my family for their enduring love and support. I literally- in the fullest sense of the word- would not be here without them. My love goes to Veronica and Alex Varela, their two incredible girls Gwen and Sophie, and Jonte Jones. Thank you to my brothers in blood and spirit, Dan, Corbin Adams, Andy Heinrich, Kevin Kinkaid, Andrew Corbin, Adam Rhodes, Kamren Reilly, Caleb McCormick, and Pat Stuchlik. To my grandparents, to whom this work is dedicated. They've encouraged me in word and deed to keep my head up, and do the 'next, right thing.' Lastly, my Mam and Dad. Thank you for sharing this life with me. We've made it so far, together. I could not wish for better parents, mentors and models of love.

Table of Contents

List of Tables

List of Figures

Abstract

Circadian clocks allow organisms to track and anticipate rhythms in time-giving environmental cues (Zeitgebers) caused by Earth's 24-hour rotation. In many organisms, master neuronal clocks are essential to synchronize physiology and sleep-wake behavior with daily light and temperature rhythms. Neuronal timekeepers each possess an endogenous molecular clock causal to circadian sleep-wake behavior. The molecular clock's rhythms approximate the solar day with near 24-hour transcriptional-translational feedback loops. Their slight deviation from the day's 24-hour cycle requires that clock neurons be reset daily, and stably "entrain" to Zeitgebers to maintain synchrony with the environment. Understanding entrainment is central to understanding circadian clocks; though the precise neurophysiological and molecular mechanisms through which organisms entrain to their environment to coordinate sleep-wake rhythms remains mysterious.

Foundational work in circadian model organisms suggests that communication through neuropeptides and transmitters underlies circadian behavior and timing of sleep-wake rhythms. While the criticality of neural communication to circadian behavior is certain, the functions of only a handful of transmitter types within the network's repertoire have been explored. Remarkably, clock neuron networks exhibit conservation in form and function across network size and separate evolutionary lineages. The clock network of *Drosophila melanogaster* is spatially and functionally organized similar to mammalian model networks, but with fewer than 1/100th the neurons. Despite their economical scale,

Drosophila clock neurons retain many of the neurochemicals that function in mammalian clock networks, and neural connections between clock neuron populations, input and output centers that produce quantifiable circadian rhythms and sleep-wake behavior.

My work leverages the *Drosophila* model's unique advantages to define the roles of fast-neurotransmitters in circadian neuron physiology and sleep-wake behavior. Using live-neuronal imaging, I characterized the physiological roles of ionotropic GABAergic and acetylcholinergic communication to a critical clock neuron population. I validated the use of a genetically-encoded voltage sensor to directly study membrane excitability without electrophysiology in the *Drosophila* clock network. I used classic circadian mutants to determine the physiological roles of the molecular clock and light-mediated inputs in setting daily rhythms in transmitter receptivity. Finally, with behavioral studies I determined the functions of GABA and acetylcholine in coordinating circadian rhythmicity and sleep-wake behavior. My biological findings support that fast-neurotransmitters may represent distinct "day" and "night" physiological and behavioral states. Fast-neurotransmitter signaling in mammalian networks is correlated, and perhaps causal to circadian entrainment. In an effort to develop standardized, quantitative measures to study entrainment behavior in *Drosophila*, I co-developed a free MATLAB-based program, PHASE, to define Activity, Sleep, and Entrainment behavior in data acquired from the universally used DAM-system (TriKinetics, Waltham MA). I demonstrated that PHASE measures entrainment and classic elements of sleep-wake behavior in wild-type flies and circadian mutants in behavior paradigms with equinox light, long- and short-days, and 23- and 25-hour periods. PHASE, when coupled with *Drosophila*'s extensive

genetic tools, may provide key insight into the molecular and neuronal basis of circadian entrainment.

Chapter 1. Introduction

Circadian clocks

Circadian clocks equip organisms with an internal sense of time to synchronize daily behavior with rhythms in the environment (Moore, 1982). Biological timekeeping is present in nearly every tissue of every terrestrial organism; from cyanobacteria, plants and invertebrates, to humans (Vansteensel et al., 2008). Remarkably, clock molecular architecture and functionality is conserved across these independent evolutionary lineages (Rosbash, 2009). The circadian clock's rhythms are driven by a cellular transcription-translation feedback loop that oscillates with near 24-hour periodicity, even in the absence of time-giving "Zeitgebers" or environmental cues (Zheng and Sehgal, 2008). The resulting rhythms in transcriptional and translational programming coordinate cellular physiology that gives rise to sleep, wake, feeding and reproductive behaviors (Ko and Takahashi, 2006).

The endogenous molecular clock in most organisms runs longer or shorter than 24-hours. Their imperfect approximation of the solar day requires clocks to be reset, and entrained by Zeitgebers. Entrainment properties- the type of input and dynamic range over which Zeitgebers set circadian rhythms' pace- vary widely across model systems and clock-possessing tissues (Challet et al., 2003; Rohling et al., 2011; Schlichting et al., 2016; Sehadova et al., 2009; Yadlapalli et al., 2018). A consensus remains despite this intra- and inter- specific heterogeneity: clock entrainment to light, temperature and food-cues is critical to synchronize cellular and behavioral rhythms with the environment

(Herzog, 2007; Nitabach and Taghert, 2008). A network consisting of many diversely entrained clocks may allow organisms to adapt to their habitats as they change temporally with the solar day and season, though the physiological and mechanistic basis for this coordination between molecular clocks and the environment remains elusive.

Mammalian circadian structure and physiology

In most animals, master clock neurons in the brain orchestrate the body's circadian systems to coordinate endogenous clock rhythms with entraining information from the environment (Buhr et al., 2010; Mohawk et al., 2012). Mammalian rodent model organisms are central to our understanding of the neurophysiological mechanisms through which clock neurons produce rhythms in daily behavior. The rodent central clock network consists of 20,000 neurons in the suprachiasmatic nuclei (SCN) of the hypothalamus that receive direct retinal light inputs and communicate with each other and target centers in the brain and periphery (Golombek and Rosenstein, 2010) (Figure 1A). SCN neurons are subdivided into anatomically and functionally distinct core and shell populations that produce synchronized 24-hour rhythms in neuronal activity (as inferred by voltage and firing patterns) through a network of direct synaptic connections and paracrine signals (Enoki et al., 2017; Welsh et al., 2010) (Figure 1B). At the single-cell level, SCN neurons' are diverse in neuronal firing rate and range in molecular clock periodicity from 22 to 30 hours (Herzog et al., 2004). Daily resetting cues from the environment play an important role in maintaining rhythms in neural activity and behavior. However, the natural variation of SCN neurons' clocks renders them diverse in entrainment properties, and under exotic environmental conditions can even uncouple the timing of activity rhythms in the SCN (Evans et al., 2015). To ensure that circadian

behavior is robust to acute perturbation, but adaptive to rhythmic, daily and seasonal changes in light and temperature, the SCN employs neurophysiological mechanisms that communicate between neurons of the clock network (Welsh et al., 2010).

Neurons generally, and those of the SCN, communicate by releasing neurochemicals that change the excitability of members within their network (Reghunandanan and Reghunandanan, 2006). Chemical release can lead to varying effects spatially as signals can be received locally at direct synaptic connections, or far away from their origin through peptides and hormones. Response duration and magnitude also vary; linked to the volume of release, and the recipient neurons' repertoire of receptors and downstream programming. Despite the multi-modal implications of neural signaling, neurotransmission in the SCN strengthens and synchronizes molecular clock and neuronal activity rhythms across the network (Aton et al., 2006). Interestingly, SCN "tone" or excitability to neurochemical signals and entrainment cues varies across the day (Diekman and Forger, 2009; Freeman et al., 2013; Kingsbury et al., 2016; Wagner et al., 2001; Wang et al., 2012). The finding that the SCN is more excitable at day during wake and more inhibited at night during sleep, suggests that timed release of and receptivity to excitatory and inhibitory signals, and the resultant physiological state of the network may be causal to daily behavioral rhythms (Colwell, 2011; DeWoskin et al., 2015; Rohling et al., 2011; Wang et al., 2012). The precise origins and relevance of these physiological rhythms remain unknown. However, the emerging view is that many parallel pathways generate the SCN's rhythms to sync sleep-wake cycles with rhythms in the environment (Welsh et al., 2010). A recent study suggests that a combination of cell intrinsic methods and neurotransmission to the SCN's underlies its physiological rhythms

(Enoki et al., 2017; Herzog, 2007). Sleep-wake centers and neurons of the retinohypothalamic tract make functional physiological connections with the SCN (Golombek and Rosenstein, 2010; Welsh et al., 2010). These input and output pathways provide critical feedback to the SCN about the environment and vigilance state via neuropeptides and transmitters including acetylcholine and glutamate (Bina et al., 1993; S.M. et al., 2013; Yang et al., 2010).

Within the SCN, the actions of the peptide vasoactive intestinal polypeptide (VIP) and inhibitory neurotransmitter GABA appear to be the most consequential for circadian rhythms. While the SCN is globally GABAergic, neuropeptides are spatially distributed between ventral core and dorsal shell populations. Many neurons in the shell produce the peptide arginine vasopressin (AVP), while many neurons of the core produce VIP (Yan et al., 2007). Core VIP signaling strengthens and synchronizes the SCN's molecular clock and neuronal activity rhythms (Aton et al., 2005). Consequently, VIP is required for rhythmic, consolidated bouts of daily behavior both when entrained to light and under constant conditions without environmental time cues (Figure 2). The strength and precision of network rhythms imposed by VIP signaling are modulated by global GABA receptivity (Aton et al., 2006; DeWoskin et al., 2015; Evans et al., 2013; Liu and Reppert, 2000). GABA signals are conducted primarily through the fast- ionotropic receptor GABA-AR that mediates 90% of all excitatory and inhibitory communication in SCN networks (Freeman et al., 2013) (Figure 3). In contrast to VIP's clear role in SCN neural activity rhythms and behavior coherence with environmental cues, GABA both facilitates and opposes this synchrony in a manner dependent on the physiological state of the network and entrainment paradigm (Albers et al., 2017; Evans et al., 2013). GABA's ability to

modulate the “meaning” of VIP signaling across the solar day and season suggests that combinations of neurochemicals, and the SCN’s resultant excitatory-inhibitory tone, may physiologically represent and time distinct behavioral states (Kingsbury et al., 2016). Determining the contributions of communication between SCN neurons, up- and downstream sleep-wake centers, and cell intrinsic mechanisms to the SCN’s physiological states, entrainment and circadian behavior remains a critical area of investigation. However, it is made challenging by the size (number of neurons) and genetic scale of mammalian model networks.

Drosophila melanogaster as a circadian model organism

Drosophila melanogaster is an ideal model to examine the roles of transmitter systems to circadian network function. In invertebrate and mammalian brains alike, endogenous timekeeping mechanisms and physiological coupling within the clock neuron network and to environmental Zeitgebers synchronize daily rhythms in behavior. The fly model has three primary advantages particular to this line of inquiry. 1) Due to their genomic scale, flies have a single gene copy of each molecular clock component and are scaled down in neurochemical signaling machinery relative to mammalian model systems. Clock neurons therefore have considerably less redundancy in neurotransmitter and peptide receptor subunits which makes defining the contributions of specific systems easier. 2) The structure of fly and mammal systems is conserved. The network has the same dorsal, ventral (lateral, in *Drosophila*) structure and function of mammalian networks but with 1/100th the neurons. These neurons receive communication by classic fast-neurotransmitters GABA, glutamate and acetylcholine. *Drosophila* also have a functionally homologous VIP-like peptide, pigment-dispersing factor (PDF) which

coordinates rhythms in neural activity, molecular clocks and facilitate daily entrainment. 3) Finally, powerful tools are available in the fly to genetically isolate and manipulate specific neuron types within the clock network (Allada and Chung, 2010a; Nitabach and Taghert, 2008; Pfeiffenberger et al., 2010a).

The *Drosophila* clock networks' 150 neurons are subdivided into anatomically distinct classes, many of which now have defined roles in diurnal behavior. Under equinox light:dark cycles, PDF+ ventral lateral neurons (LNvs) and dorsal neurons (DN1s) drive peaks in morning wakefulness, dorsal lateral neurons (LNds) and the 5th s-LNv promote evening wakefulness (Helfrich-Förster et al., 2007). *Drosophila* clock neuron activity rhythms as inferred by Ca2+ transients are coincident with and causal to their behavioral roles and are consequentially, asynchronous to one another (Liang et al., 2016). This mimics the asynchronous phases of Ca2+ rhythms in the SCN, but it remains unknown whether the fly circadian clock neuron network (CCNN) exhibits global synchrony in neural firing and voltage rhythms like that of the SCN in equinox light (Enoki et al., 2017). The precise roles of these two neural activity patterns remains a mystery in either organism. It is thought that voltage synchrony may coordinate uniform entrainment to sensory cues, while Ca2+ asynchrony coordinates circuit specific functions (Enoki et al., 2017). Regardless, in both organisms neurochemical communication helps coordinate the network's neural activity rhythms and maintain coherent behavior-environment rhythms (Houben et al., 2014; Nitabach, 2006). The fly network's repertoire of peptides and neurotransmitters reaches well beyond PDF and though the arborizations between, and to a lesser degree to, clock populations are well-mapped, the complexity and consequences of signaling at these sites remain elusive. The extensive, stereotyped

arborizations between CCNN populations indicative of direct synaptic connections suggest that local, fast-neurotransmission through GABA, acetylcholine and glutamate may complement the network's peptidergic signaling (Schubert et al., 2018). Together, *Drosophila*'s rich history in molecular circadian biology, the model's similarity to mammalian systems and aforementioned technical advantages, makes it uniquely suited to examine the roles of fast-neurotransmission in circadian network physiology, molecular timekeeping and circadian behavior.

Drosophila timekeeping

Mechanistic models of circadian timekeeping based on work in *Drosophila* are central to our understanding of the molecular, genetic basis of the circadian clock and it's contributions to timekeeping in the brain (Hardin, 2011). The genetic basis for the core feedback loop protein PER was first discovered by Ron Konopka and Seymour Benzer who characterized mutants that shortened and lengthened circadian periodicity, or caused behavioral arrhythmicity in constant conditions (Konopka and Benzer, 1971) (Figure 4). Later work demonstrated that PER protein oscillates with near 24-hour periodicity in cells throughout the fly body. In constant conditions without entrainment cues however, cell autonomous oscillations were most robust in photoreceptor cells of the eye and a handful of central brain neurons (Ewer et al., 1992). Over 40 years of foundational work later, *Drosophila* circadian research has 1) casually linked the timekeeping abilities of flies and other organisms to molecular clocks in the central brain, 2) dissected the clock's molecular architecture, and 3) identified key regulators and targets of the clock's endogenous oscillations (Ewer et al., 1992; Hardin and Yu, 2006; Zeng et al., 1994). The following sections summarize key findings and provides current

models of *Drosophila*'s molecular clock, and the central clock neuron network's anatomy and physiology.

Cellular clocks have independent evolutionary lineages in distantly related organisms (Rosbash, 2009). However, almost all known molecular clocks center around an endogenous transcriptional-translational feedback loop that oscillates with approximately 24-hr periodicity (Rosbash, 2009). In *Drosophila*, *period (per)* and *timeless (tim)* genes in the nucleus are activated by the binding of the positive transcriptional regulators CYCLE and CLOCK (Allada et al., 1998; Darlington et al., 1998; Hao et al., 1997). (In mammals the homologous proteins are BMAL1 and CLOCK, respectively.) Transcriptional activation produces *per* and *tim* mRNA, which exits the nucleus and is translated by ribosomes into PER and TIM proteins that dimerize to increase stability. The accumulation of *per* and *tim* mRNA, protein and dimers reach a peak during the middle of the night (Curtin et al., 1995; Shafer et al., 2002; Vosshall et al., 1994). At this peak, PER-TIM complexes enter the nucleus and interact with CYCLE/CLOCK to block transcriptional activation at the sites of their own genes and at the many other transcriptional targets of CYCLE/CLOCK (Bae et al., 2000; Lee et al., 1998). PER-TIM dimers are degraded early in the morning by the proteasome and light-dependent mechanisms that destabilize TIM under light:dark cycles (Myers et al., 1996). When too few PER-TIM dimers are available to repress CYCLE/CLOCK transcriptional activation, another 24-hour cycle begins. The molecular feedback loop and downstream cellular transcriptional programming is timed with, and casual to the cellular activities underlying normal cycles of sleeping and waking (Yang and Sehgal, 2001).

The central circadian neuron network (CCNN)

The molecular clock's core components PER, TIM, CLOCK and CYCLE, the core mechanism underlying oscillations and the requirement of this molecular clock in specific neural networks are conserved between invertebrates and mammals. These remarkable similarities and the relative simplicity of the flies central nervous system, established *Drosophila* as a powerful circadian model system (Vansteensel et al., 2008). While there are over 20,000 central neurons in the SCN, the *Drosophila* brain houses less than 1% the clock neurons of mammalian models (Herzog, 2007). The *Drosophila* CCNN comprises 75 pairs of neurons that are anatomically distinct and definable by their expression of a wide-diversity of neuropeptides and proteins (Figure 5). These consist namely of the PDF-positive ventral lateral neurons with four pairs each of small (s-LNvs) and large (l-LNvs) subsets, and the PDF-negative classes; six pairs of dorsal lateral neurons (LNds), three pairs of lateral posterior neurons (LPNs), and approximately 60 pairs of dorsal neurons (DNs) spread across DN1s anterior and posterior, DN2s and DN3s (Helfrich-Förster et al., 2007; Kaneko and Hall, 2000). Approximately half of all clock neurons express the receptor for PDF, PDFR and the protein CRY, the latter of which renders them directly receptive to photic information (Im and Taghert, 2010; Im et al., 2011; Yoshii et al., 2008, 2016) (Figure 5A). The anatomical connections between populations in the *Drosophila* CCNN are well characterized though their roles remain largely unexplored. Nearly all clock neuron classes send projections to the dorsal protocerebrum. The l-LNvs have additional projections to the surface of the medulla and to the contralateral hemisphere. Neurons in the dorsal classes (LNds, DN1ps, and DN3s) also project toward the LNvs within the accessory medulla where the latter receive direct inputs from photoreceptor cells in the retina and the HB-eyelet (Schubert et al., 2018).

Drosophila are diurnal and bimodal, with daily bouts in activity that anticipate the transitions between daytime and nighttime. The autonomous nature of each neuron's molecular clock allows rhythmic behavior to persist in constant conditions a mere half-hour shorter than the solar day without resetting light or temperature cues. Genetic manipulations that leveraged the GAL4 system and the network's mosaic expression of proteins has defined the contributions of specific neuron populations to behavioral rhythms. The GAL4 system is a powerful tool to control gene expression in isolated cell populations (Brand and Perrimon, 1993). It consists of two parts: the yeast *gal4* gene and the upstream activation sequence (UAS) to which GAL4 protein binds and activates transcription of genes downstream of the UAS. Fly model systems have a complete library of stable lines with transgenic GAL4 and UAS elements for nearly every genomic element that by themselves have little to no effect on health or behavior of individuals. The progeny of a GAL4- fly and UAS- fly mating, however, allows manipulation of gene product levels downstream of the UAS in sparsely GAL4-defined cell populations. Without CRY+ cells (using a CRY-GAL4 that defines half of the LNds and DNs, and all PDF+ neurons) or their ability to keep time, rhythmic behavior is completely absent in constant conditions. Flies without PDF+ neurons that retain functional dorsal classes still have evening activity peaks, while those with only PDF+ neurons have morning peaks (Stoleru et al., 2004). Years of molecular and genetic characterization has produced the "morning-evening" (M-E) model of the CCNN (Figure 6A). The PDF+ ventral lateral neurons (LNvs) drive peaks in morning behavior, and are required for endogenous timekeeping under constant conditions, i.e., constant darkness and temperature (Renn et al., 1999; Stoleru et al., 2005, 2007). The PDF- dorsal lateral neurons and the 5th s-LNV promote evening

behavior and appear to set timekeeping most dominantly under long days and constant light (Picot et al., 2007). Central to this M-E model is the PDF+ neurons' role as "leader" neurons that receive environmental information and set the pace of rhythms in "follower" dorsal classes (Helfrich-Förster, 2001). This simplified model is elegant, but cannot explain many experimental observations. In entrainment paradigms outside of standard, equinox light for example, "follower" classes alone are able to coordinate rhythmic behavior (Busza et al., 2007; Bywalez et al., 2012; Green et al., 2015; Yoshii et al., 2012). Additionally, speeding up and slowing down the pace of PDF+ neurons does not uniformly direct the rhythms of so-called "follower" dorsal lateral neurons (LNds) (Yao and Shafer, 2014; Yao et al., 2016). This was due to the fact that the follower neurons display various modes of coupling strength to the PDF+ neurons (Yao et al., 2016). Taken together, recent behavioral and neurogenetic observations increasingly support the conclusion that circadian entrainment, behavior and endogenous timekeeping is distributed across the network (Figure 6B). It also suggests that neural communication to and between clock neurons particular to the entrainment environment defines the dominate pacemaker and resultant behavior rhythms.

Physiology of the CCNN

Light and temperature information that informs diurnal behavior is received by the network through a combination of intrinsic mechanisms (CRY expression) and sensory inputs (Cusumano et al., 2009; Yoshii et al., 2016). Light sensitive cells in the retina and HB-eyelet of the compound eye synapse directly on the ventral lateral clock neurons (LNvs), releasing the neurotransmitters acetylcholine and histamine to convey time of day and day-length (Schlichting et al., 2016). Light information is subsequently relayed

between LNv classes and to dorsal clock classes through the release of PDF and perhaps, other neurochemicals (Seluzicki et al., 2014; Zhang et al., 2010). In addition, a subset of the dorsal neurons (DN1ps) receive temperature information primarily from peripheral sensory organs (Yadlapalli et al., 2018). The variable coupling of CCNN populations to light and temperature cues and parallel nature of environmental input pathways likely supports *Drosophila*'s ability to entrain to a wide range of constantly changing and noisy environmental light and temperature rhythms. Though save studies implicating the centrality of PDF, the precise molecular and neurophysiological basis of this ability remains a mystery (Yoshii et al., 2009).

The extensive overlapping arborizations of the various clock neuron classes suggest that direct, synaptic communication between classes may mediate coupling within the network. Electrically silencing the PDF+ neurons through the overexpression of hyperpolarizing K+ channels severely reduces behavioral rhythmicity in constant conditions (Nitabach, 2006; Nitabach et al., 2002) (Figure 7). Blocking neurotransmitter release from the dorsal lateral neurons (LNds) decreases the anticipation of lights-on and lights-off transitions and dampens rhythmicity in either entrained or constant conditions (Guo et al., 2014). These experiments and others confirm that neural activity, and communication of clock neurons is essential for entrainment and endogenous timekeeping behavior (Nitabach et al., 2005). The essentiality of PDF to *Drosophila* circadian rhythms is undeniable. In constant and entrained light conditions, PDF receptivity coordinates peaks in neuronal activity in CCNN populations that are synchronous with their behavioral roles but asynchronous to one other (Liang et al., 2016) (Figure 8). However, the LNds are PDF negative; thus, the aforementioned works

suggests a requirement for neurochemical signaling additional to PDF to coordinate the network's circadian functions. They also highlight the underappreciated multi-modal nature of the network and potential for each population to signal with and receive a diversity of neurochemical signals.

In addition to PDF in the LNvs, clock neuron subsets releases short neuropeptide F (sNPF), ion transport peptide (ITP), IPNamide (IPNa) and neuropeptide F (NFP), diuretic hormone 31 (DH31) and CCHamide though the functions of these peptides in the network remains largely unexplored (Fujiwara et al., 2018; Hermann-Luibl et al., 2014; Hermann et al., 2010; Kunst et al., 2014; Nässel, 2002). Considerably less is known about the roles of neurotransmitters in timekeeping and physiology of the network, and their consequences for circadian behavior and entrainment. The *Drosophila* network is globally receptive to signaling through metabotropic and ionotropic receptors for GABA, glutamate and acetylcholine (Abruzzi et al., 2017; Aronstein and Ffrench-Constant, 1995; Hamasaka et al., 2007). GABA receptivity promotes consolidated, properly timed sleep at night by inhibiting the excitation of morning wake-promoting clock cells (Agosto et al., 2008; Chung et al., 2009; Hamasaka et al., 2005; Lelito and Shafer, 2012). Glutamate release from a subset of the dorsal neurons inhibits lateral clock neuron's activity and promotes mid-day sleep (Guo et al., 2016). Excluding the dorsal neurons' glutamatergic inputs, the sources of GABAergic, glutamatergic and cholinergic signaling are unmapped. The clock network itself is a possible source of these neurotransmitters. There appears to be only sparse production of these neurochemicals in the CCNN. For example, the 5th s-LNv and a handful of LNds are cholinergic, subsets of the DNs are glutamatergic, and

RNA-sequencing suggests that all clock classes are potentially GABAergic (Abruzzi et al., 2017; Hamasaka et al., 2007; Johard et al., 2009),

Primary questions and findings

My thesis work leverages the conservation of circadian architecture and the genetic malleability of the *Drosophila* nervous system to dissect the physiological and circadian functions of fast neurotransmitters acting on the CCNN. Neurotransmission is fundamental to strengthen coupling between circadian clock neurons in the SCN and produce rhythmic, entrained behavior (Aton et al., 2006; Houben et al., 2014). The *Drosophila* CCNN's global receptivity to GABA, glutamate and acetylcholine suggests the network does not only rely only on peptidergic signaling. Fast-neurotransmission could be fundamental to mediating excitatory and inhibitory signals to clock neurons from sensory inputs that convey environmental cues, and communication between clock neuron populations themselves or downstream behavior centers.

Using a combination of genetic and behavior techniques, pharmacological tools, and live-neuronal imaging, my thesis work characterizes the CCNN's receptivity to fast-synaptic inputs from two major transmitters: GABA and acetylcholine. My studies make use of a newly developed genetically-encoded voltage sensor (GEVI), ASASP2f, to assess changes in membrane voltage to neurotransmitters (Yang et al., 2016). Electrophysiology and genetically encoded sensors for Ca+ and cAMP are commonly used tools in the CCNN to assess neuronal activity (Chen et al., 2013; Tian et al., 2009; Yao et al., 2012). In theory, ASAP2f is uniquely positioned to provide first-line measurements of neural activity, better resolution of inhibitory, hyperpolarizing events, without the invasive measures required in electrophysiology (Yang et al., 2016). Prior to

my studies, voltage sensors like ASAP2f had not been used in the clock network, or to address receptivity to applied neurochemicals. It was also unknown if ASAP2f would be universally useful in the *Drosophila* brain and what potential limitations or challenges researchers might experience using the construct and in the interpretation of imaged responses. My work attempts to fill this knowledge gap by employing ASAP2f in an interneuron population within the clock network, establishing quantitative methods to analyze ASAP2f fluorescence, and interpreting these fluorescence changes in terms of inferred membrane voltage.

I demonstrate that in the dorsal lateral clock neurons (LNds), or evening cells, receptivity to inhibitory GABAergic and excitatory cholinergic inputs physiologically represent night and day, respectively. Acetylcholine's acute depolarizing responses conducted through ionotropic nicotinic receptors are stronger during the day, while the magnitude of hyperpolarizing GABAergic signaling through ionotropic GABA-ARs is greater during the night. These physiological inputs require the molecular clock and light cues to different degrees and have measurable consequences for circadian timekeeping and sleep-wake behavior across the clock network and dorsal lateral clock classes. This work contributes to a growing body of literature that implicates fast-neurotransmission in coupling the *Drosophila* clock network to relevant environmental inputs and to output targets to produce robust behavioral rhythms. It also establishes the *Drosophila* model as a powerful system to investigate the role of particular transmitters in network excitability, entrainment and circadian behavior.

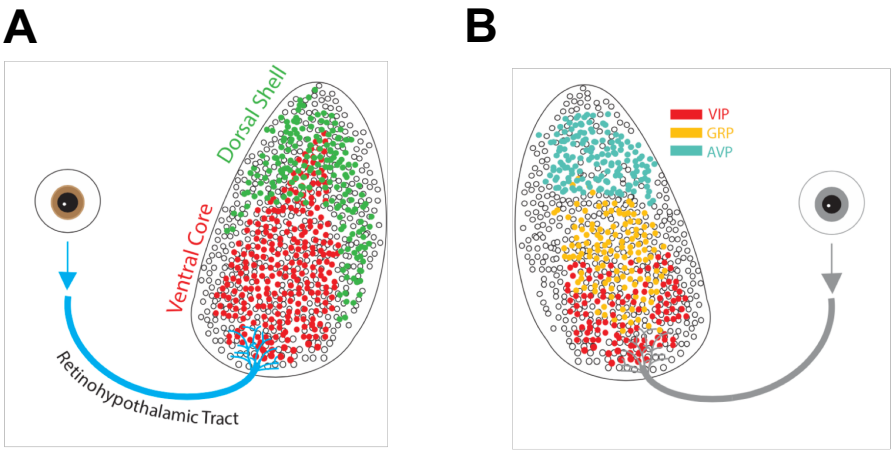

Figure 1.1. The mammalian central circadian system.
A-B. 20,000 neurons in the bilateral suprachiasmatic nuclei (SCN) of the hypothalamus comprise the mammalian circadian neuron network. A. SCN neurons are spatially organized in dorsal shell and ventral core populations. Neurons receive light information from the eye through the retinohypothalamic tract. B. The SCN's expression of critical neurochemicals is spatially distributed. Vasoactive intestinal polypeptide (VIP) is expressed primarily by neurons in the ventral core, while the dorsal shell is populated mostly by vasopressin (AVP) expressing neurons. Figure credit: Andrew Bahle.

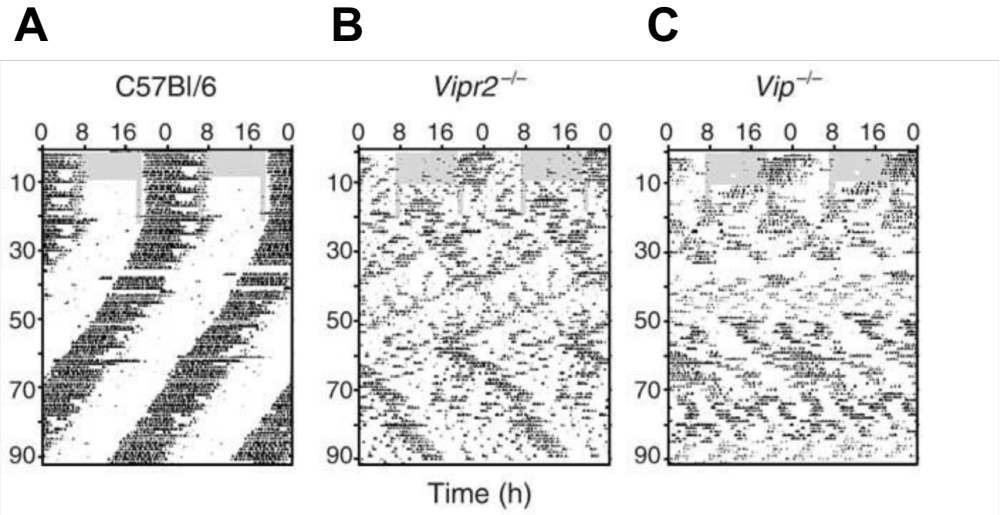

Figure 1.2. VIP neuropeptide, and receptivity is critical to behavioral rhythmicity in constant conditions and entrainment to light.
A-C. Double-plotted actograms of wheel-running activity of representative wildtype (A), VIP-receptor mutant (B), or VIP peptide mutant (C) mice entrained to a 12:12 LD schedule (days 1–10), a skeleton photoperiod (days 11–20), and constant darkness (days 20–90). Gray shading indicates lights on. A. Wildtype mice are nocturnal in both light entrainment paradigms, and rhythmic in constant conditions. B, C. VIP mutations cause arrhythmicity and multi-periodicity in constant conditions and activity in light portions of the day. Figure source data: Aton, et. al. (2005). Nature Neuroscience.

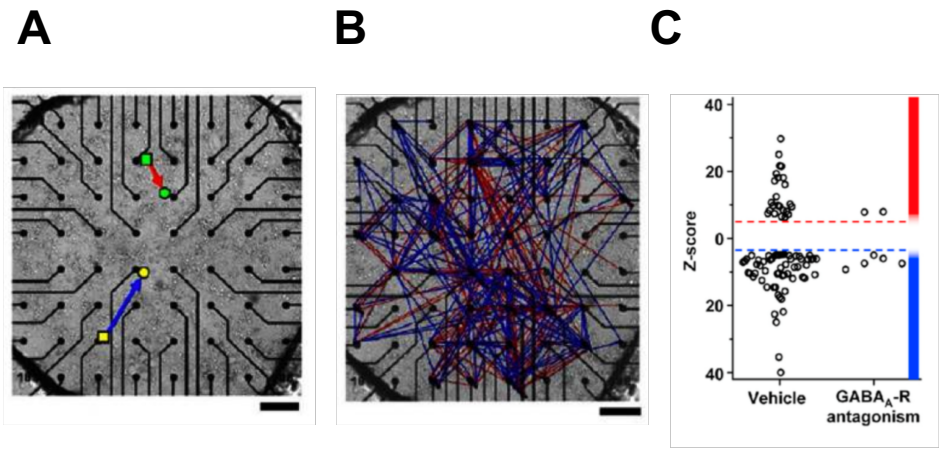

Figure 1.3. GABA mediates the majority of excitatory and inhibitory interactions in mammalian circadian networks.
A-C. SCN neurons' spike trains were recorded on a MEA. Probabilistic interactions between individual neurons during the recording period were converted to a Z-score where negative scores represent inhibitory interactions and positive scores excitatory interactions. A. Spike trains cross-correlated positively, negatively or not at all between each pair of neurons. Changes in firing are illustrated as excitatory (red arrows) or inhibitory (blue arrows) connections on a micrograph of the SCN culture. Colored circles indicate the locations of four representative neurons. B. Interactions from a representative 24-h recording with 103 firing neurons making 542 connections. C. $GABA_A$ receptor antagonists (200 μM bicuculline or 100 μM gabazine) eliminated upwards of 90% of all excitatory and inhibitory connections in SCN cultures relative to vehicle treated cultures. Figure source data: Freeman, et. al. (2013). Neuron.

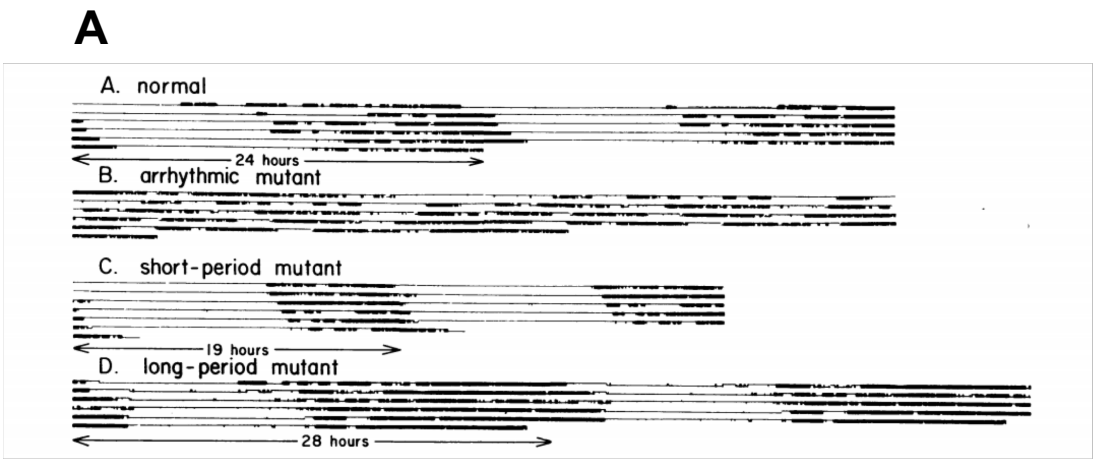

Figure 1.4. Drosophila melanogaster's molecular circadian clock is essential to endogenous timekeeping behavior.
A. Flies are strongly rhythmic in constant darkness, and constant temperature (top, "normal"). Mutations to the molecular clock gene, *period* cause arrthymicity, shortened and lengthened periodicity in constant conditions. Figure source data: Konopka and Benzer. (1971). PNAS.

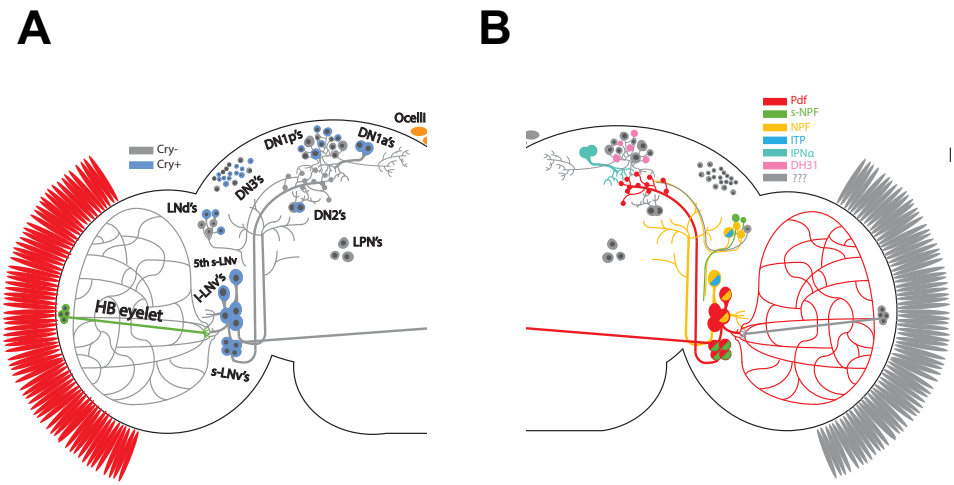

Figure 1.5. The Drosophila central circadian clock neuron network (CCNN).
A-B. 75 pairs of fly circadian neurons in each brain hemisphere are distributed anatomically in to dorsal and ventral classes. Extensive, stereotyped synaptic connections couple clock neurons to each other, and light and temperature sensitive structures in the optic lobes and periphery. A. Light information is received by the ventral lateral neuron (LNvs) from photoreceptive cells in the optic lamina and HB-eyelet. In parallel, expression of the photoreceptive protein CRY (blue) renders approximately half of the network intrinsically sensitive to light. B. Clock neuron classes are diverse in neurochemical machinery. Ventral lateral neurons (s- and l-LNvs) express the critical neuropeptide pigment dispersing factor (PDF). Figure credit: Andrew Bahle.

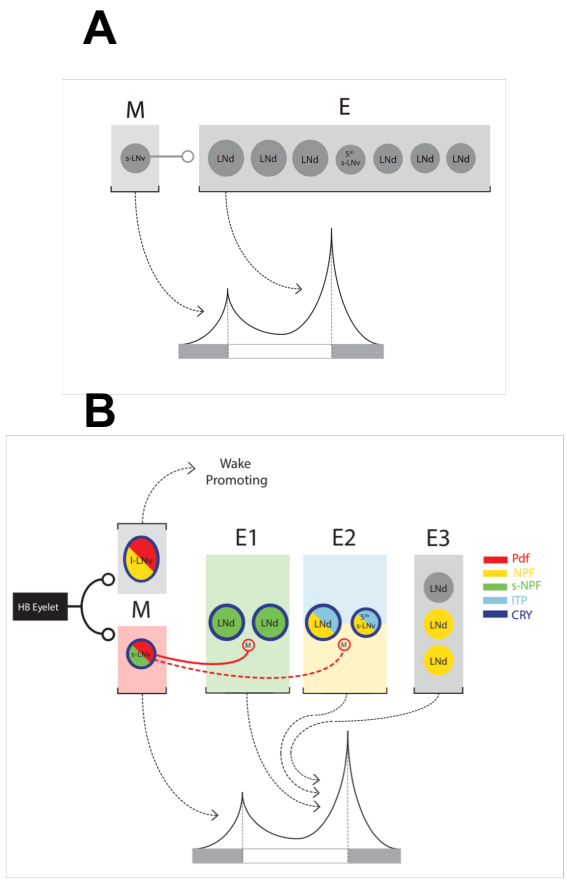

Figure 1.6. Network models of Drosophila's bimodal circadian behavior.
A-B. The distributed network model (B) builds on the simplified M-E model (A). While the latter is more complex, the distributed model better explains experimental observations demonstrating variable coupling of the network's populations to each other and entraining light and temperature information. A. The M-E network model. The ventral lateral neurons (s-LNvs primarily) coordinate morning behavior and dorsal lateral neurons (LNds) coordinate evening behavior. The s-LNvs unidirectionally conduct downstream neuron classes to produce consolidated bouts of behavior around dawn and dusk. B. The updated, distributed model of the CCNN. Light information is received by the PDF+ LNvs (M cells) to promote wakefulness in the morning. They relay this information to heterogeneously coupled LNds (E cells), to coordinate evening activity. The M cells' ability to conduct the actions of E cells is correlated with their expression of peptides and the protein CRY. Figure credit: Andrew Bahle.

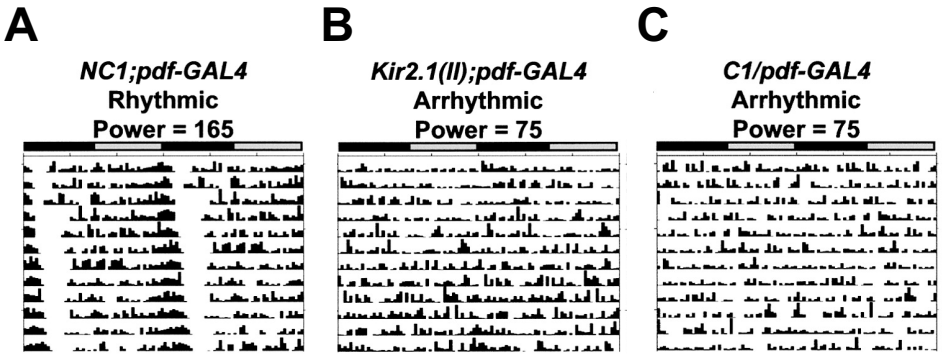

Figure 1.7. The electrical activity of clock neurons is indispensable for strongly rhythmic, circadian behavior in constant conditions.

A-C. Representative actograms of *Pdf-GAL4* flies expressing two functional hyperpolarizing K+ channels *UAS-Kir2.1* (B) or *UAS-dORKΔ-C* and a non-functional channel control, *UAS-dORKΔ-NC* (A) were entrained to light-dark (LD) cycles for least 5 days and then placed in the infrared beam-crossing locomotor assay apparatus in constant darkness (DD) for 12 days. Rhythmic power is a quantification of the strength of the circadian rhythm over 12 days. The power of each arrhythmic fly is defined as 75, which is the $p < .01$ significance threshold for a period of 24 hours (see Experimental Procedures). Flies exhibiting a power greater than 150 are defined as rhythmic. Subjective day (gray) and subjective night (black) are indicated above the actogram. Figure source data: Nitabach, et. al. (2002). Cell.

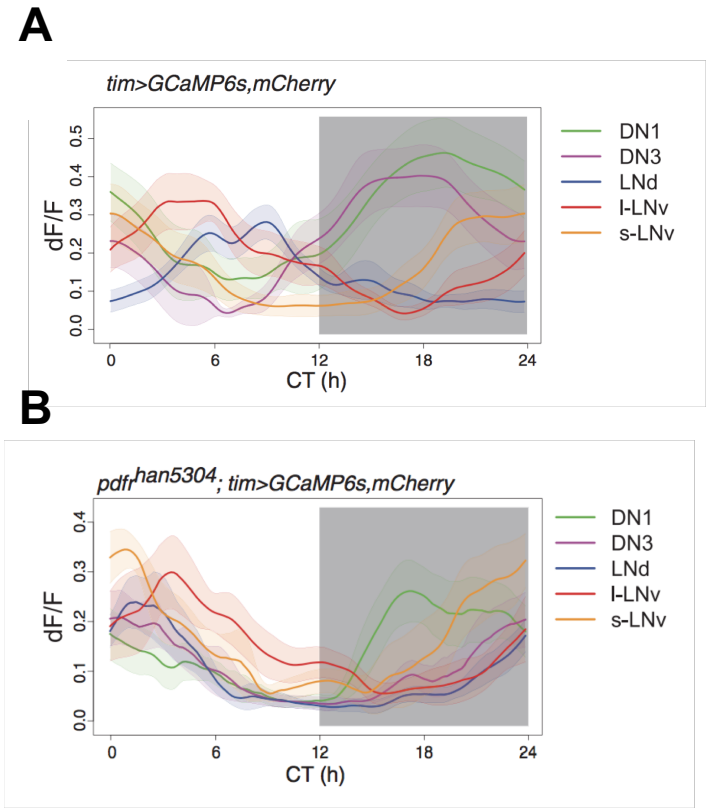

Figure 1.8. Bimodal behavioral rhythms are driven by the CCNN's asynchronous neuronal activity.
A-B. *Tim-GAL4* flies expressing the calcium sensor GCaMP6s were entrained to 6 days of 12:12 LD and released in to constant conditions. Ca2+ levels were subsequently recorded using long-term *in vivo* imaging where the fly's head is immersed in saline and remains attached to the body. Graphs depict average Ca^{2+} transients in each population across circadian time (CT) (n=13 flies). A. CCNN populations' peak neuronal activity (Ca2+ transients) precede, and are causal to rhythms in bimodal daily behavior. M-cells (yellow, red) are active just prior to subjective lights-on, while E-cells (blue) are most active prior to subjective lights-off. B. PDF receptivity in the clock network is essential to producing properly asynchronous neuronal activity and behavior rhythms across the solar day. Figure source data: Liang, et. al. (2016). Science.

References

Abruzzi, K.C., Zadina, A., Luo, W., Wiyanto, E., Rahman, R., Guo, F., Shafer, O., and Rosbash, M. (2017). RNA-seq analysis of *Drosophila* clock and non-clock neurons reveals neuron-specific cycling and novel candidate neuropeptides. PLoS Genet. 13.

Agosto, J., Choi, J.C., Parisky, K.M., Stilwell, G., Rosbash, M., and Griffith, L.C. (2008). Modulation of GABAA receptor desensitization uncouples sleep onset and maintenance in *Drosophila*. Nat. Neurosci. 11, 354–359.

Albers, H.E., Walton, J.C., Gamble, K.L., McNeill, J.K., and Hummer, D.L. (2017). The dynamics of GABA signaling: Revelations from the circadian pacemaker in the suprachiasmatic nucleus. Front. Neuroendocrinol. 44, 35–82.

Allada, R., and Chung, B.Y. (2010). Circadian organization of behavior and physiology in *Drosophila*. Annu. Rev. Physiol.

Allada, R., White, N.E., So, W.V., Hall, J.C., and Rosbash, M. (1998). A mutant *Drosophila* homolog of mammalian clock disrupts circadian rhythms and transcription of period and timeless. Cell.

Aronstein, K., and Ffrench-Constant, R. (1995). Immunocytochemistry of a novel GABA receptor subunit Rdl in *Drosophila melanogaster*. Invertebr. Neurosci. 1, 25–31.

Aton, S.J., Colwell, C.S., Harmar, A.J., Waschek, J., and Herzog, E.D. (2005). Vasoactive intestinal polypeptide mediates circadian rhythmicity and synchrony in mammalian clock neurons. Nat. Neurosci. 8, 476–483.

Aton, S.J., Huettner, J.E., Straume, M., and Herzog, E.D. (2006). GABA and Gi/o differentially control circadian rhythms and synchrony in clock neurons. Proc. Natl. Acad. Sci. U. S. A. 103, 19188–19193.

Bae, K., Lee, C., Hardin, P.E., and Edery, I. (2000). dCLOCK is present in limiting amounts and likely mediates daily interactions between the dCLOCK-CYC transcription factor and the PER-TIM complex. J. Neurosci.

Bina, K.G., Rusak, B., and Semba, K. (1993). Localization of cholinergic neurons in the forebrain and brainstem that project to the suprachiasmatic nucleus of the hypothalamus in rat. J. Comp. Neurol.

Brand, A.H., and Perrimon, N. (1993). Targeted gene expression as a means of altering cell fates and generating dominant phenotypes. Development.

Buhr, E.D., Yoo, S.H., and Takahashi, J.S. (2010). Temperature as a universal resetting cue for mammalian circadian oscillators. Science. 330, 379–385.

Busza, A., Murad, A., and Emery, P. (2007). Interactions between Circadian Neurons Control Temperature Synchronization of *Drosophila* Behavior. J. Neurosci.

Bywalez, W., Menegazzi, P., Rieger, D., Schmid, B., Helfrich-Förster, C., and Yoshii, T. (2012). The dual-oscillator system of *Drosophila melanogaster* under natural-like temperature cycles. Chronobiol. Int.

Challet, E., Caldelas, I., Graff, C., and Pévet, P. (2003). Synchronization of the molecular clockwork by light- and food-related cues in mammals. Biol. Chem.

Chen, T.W., Wardill, T.J., Sun, Y., Pulver, S.R., Renninger, S.L., Baohan, A., Schreiter, E.R., Kerr, R.A., Orger, M.B., Jayaraman, V., et al. (2013). Ultrasensitive fluorescent proteins for imaging neuronal activity. Nature.

Chung, B.Y., Kilman, V.L., Keath, J.R., Pitman, J.L., and Allada, R. (2009). The GABAA Receptor RDL Acts in Peptidergic PDF Neurons to Promote Sleep in *Drosophila*. Curr. Biol. 19, 386–390.

Colwell, C.S. (2011). Linking neural activity and molecular oscillations in the SCN. Nat. Rev. Neurosci.

Curtin, K.D., Huang, Z.J., and Rosbash, M. (1995). Temporally regulated nuclear entry of the *Drosophila* period protein contributes to the circadian clock. Neuron.

Cusumano, P., Klarsfeld, A., Chélot, E., Picot, M., Richier, B., and Rouyer, F. (2009). PDF-modulated visual inputs and cryptochrome define diurnal behavior in *Drosophila*. Nat. Neurosci.

Darlington, T.K., Wager-Smith, K., Ceriani, M.F., Staknis, D., Gekakis, N., Steeves, T.D.L., Weitz, C.J., Takahashi, J.S., and Kay, S.A. (1998). Closing the circadian loop: CLOCK-induced transcription of its own inhibitors per and tim. Science.

DeWoskin, D., Myung, J., Belle, M.D.C., Piggins, H.D., Takumi, T., and Forger, D.B. (2015). Distinct roles for GABA across multiple timescales in mammalian circadian timekeeping. Proc. Natl. Acad. Sci. 112, E3911–E3919.

Diekman, C.O., and Forger, D.B. (2009). Clustering predicted by an electrophysiological model of the suprachiasmatic nucleus. J. Biol. Rhythms 24, 322–333.

Enoki, R., Oda, Y., Mieda, M., Ono, D., Honma, S., and Honma, K. (2017). Synchronous circadian voltage rhythms with asynchronous calcium rhythms in the suprachiasmatic nucleus. Proc. Natl. Acad. Sci. 114, E2476–E2485.

Evans, J.A., Leise, T.L., Castanon-Cervantes, O., and Davidson, A.J. (2013). Dynamic Interactions Mediated by Nonredundant Signaling Mechanisms Couple Circadian Clock Neurons. Neuron 80, 973–983.

Evans, J.A., Suen, T.C., Callif, B.L., Mitchell, A.S., Castanon-Cervantes, O., Baker, K.M., Kloehn, I., Baba, K., Teubner, B.J.W., Ehlen, J.C., et al. (2015). Shell neurons of the master circadian clock coordinate the phase of tissue clocks throughout the brain and body. BMC Biol.

Ewer, J., Frisch, B., Hamblen-Coyle, M.J., Rosbash, M., and Hall, J.C. (1992). Expression of the period clock gene within different cell types in the brain of *Drosophila* adults and mosaic analysis of these cells' influence on circadian behavioral rhythms. J. Neurosci.

Freeman, G.M., Krock, R.M., Aton, S.J., Thaben, P., and Herzog, E.D. (2013). GABA networks destabilize genetic oscillations in the circadian pacemaker. Neuron 78, 799–806.

Fujiwara, Y., Hermann-Luibl, C., Katsura, M., Sekiguchi, M., Ida, T., Helfrich-Förster, C., and Yoshii, T. (2018). The CCHamide1 neuropeptide expressed in the anterior dorsal neuron 1 conveys a circadian signal to the ventral lateral neurons in *Drosophila melanogaster*. Front. Physiol.

Golombek, D.A., and Rosenstein, R.E. (2010). Physiology of Circadian Entrainment. Physiol. Rev.

Green, E.W., O'Callaghan, E.K., Hansen, C.N., Bastianello, S., Bhutani, S., Vanin, S., Armstrong, J.D., Costa, R., and Kyriacou, C.P. (2015). *Drosophila* circadian rhythms in seminatural environments: Summer afternoon component is not an artifact and requires TrpA1 channels. Proc. Natl. Acad. Sci.

Guo, F., Cerullo, I., Chen, X., and Rosbash, M. (2014). PDF neuron firing phase-shifts key circadian activity neurons in *Drosophila*. Elife.
Guo, F., Yu, J., Jung, H.J., Abruzzi, K.C., Luo, W., Griffith, L.C., and Rosbash, M. (2016). Circadian neuron feedback controls the *Drosophila* sleep-activity profile. Nature.
Hamasaka, Y., Wegener, C., and Nässel, D.R. (2005). GABA modulates *Drosophila* circadian clock neurons via GABAB receptors and decreases in calcium. J. Neurobiol. 65, 225–240.
Hamasaka, Y., Rieger, D., Parmentier, M.L., Grau, Y., Helfrich-Förster, C., and Nässel, D.R. (2007). Glutamate and its metabotropic receptor in *Drosophila* clock neuron circuits. J. Comp. Neurol.
Hao, H., Allen, D.L., and Hardin, P.E. (1997). A circadian enhancer mediates PER-dependent mRNA cycling in *Drosophila melanogaster*. Mol. Cell. Biol.
Hardin, P.E. (2011). Molecular genetic analysis of circadian timekeeping in *Drosophila*. Adv. Genet.
Hardin, P.E., and Yu, W. (2006). Circadian Transcription: Passing the HAT to CLOCK. Cell.
Helfrich-Förster, C. (2001). The locomotor activity rhythm of *Drosophila melanogaster* is controlled by a dual oscillator system. J. Insect Physiol.
Helfrich-Förster, C., Yoshii, T., Wülbeck, C., Grieshaber, E., Rieger, D., Bachleitner, W., Cusumano, P., and Rouyer, F. (2007). The lateral and dorsal neurons of *Drosophila melanogaster*: New insights about their morphology and function. In Cold Spring Harbor Symposia on Quantitative Biology.
Hermann-Luibl, C., Yoshii, T., Senthilan, P.R., Dircksen, H., and Helfrich-Forster, C. (2014). The Ion Transport Peptide Is a New Functional Clock Neuropeptide in the Fruit Fly *Drosophila melanogaster*. J. Neurosci.
Hermann, C., Dircksen, H., Helfrich-Forster, C., and Yoshii, T. (2010). The neuropeptides PDF, NPF and ITP operate synergistically in the endogenous clock of *Drosophila melanogaster*. J. Neurogenet.
Herzog, E.D. (2007). Neurons and networks in daily rhythms. Nat. Rev. Neurosci. 8, 790–802.
Herzog, E.D., Aton, S.J., Numano, R., Sakaki, Y., and Tei, H. (2004). Temporal Precision in the Mammalian Circadian System: A Reliable Clock from Less Reliable Neurons. J. Biol. Rhythms.
Houben, T., Coomans, C.P., and Meijer, J.H. (2014). Regulation of circadian and acute activity levels by the murine suprachiasmatic nuclei. PLoS One.
Im, S.H., and Taghert, P.H. (2010). PDF receptor expression reveals direct interactions between circadian oscillators in *Drosophila*. J. Comp. Neurol.
Im, S.H., Li, W., and Taghert, P.H. (2011). PDFR and CRY Signaling Converge in a Subset of Clock Neurons to Modulate the Amplitude and Phase of Circadian Behavior in *Drosophila*. PLoS One 6, e18974.
Johard, H.A.D., Yoishii, T., Dircksen, H., Cusumano, P., Rouyer, F., Helfrich-Förster, C., and Nässel, D.R. (2009). Peptidergic clock neurons in *Drosophila*: Ion transport peptide and short neuropeptide F in subsets of dorsal and ventral lateral neurons. J. Comp. Neurol.

Kaneko, M., and Hall, J.C. (2000). Neuroanatomy of cells expressing clock genes in *Drosophila*: Transgenic manipulation of the period and timeless genes to mark the perikarya of circadian pacemaker neurons and their projections. J. Comp. Neurol.

Kingsbury, N.J., Taylor, S.R., and Henson, M.A. (2016). Inhibitory and excitatory networks balance cell coupling in the suprachiasmatic nucleus: A modeling approach. J. Theor. Biol. 397, 135–144.

Ko, C.H., and Takahashi, J.S. (2006). Molecular components of the mammalian circadian clock. Hum. Mol. Genet.

Konopka, R.J., and Benzer, S. (1971). Clock mutants of *Drosophila melanogaster*. Proc. Natl. Acad. Sci. U. S. A.

Kunst, M., Hughes, M.E., Raccuglia, D., Felix, M., Li, M., Barnett, G., Duah, J., and Nitabach, M.N. (2014). Calcitonin gene-related peptide neurons mediate sleep-specific circadian output in *Drosophila*. Curr. Biol.

Lee, C., Bae, K., and Edery, I. (1998). The *Drosophila* CLOCK protein undergoes daily rhythms in abundance, phosphorylation, and interactions with the PER-TIM complex. Neuron.

Lelito, K.R., and Shafer, O.T. (2012). Reciprocal cholinergic and GABAergic modulation of the small ventrolateral pacemaker neurons of *Drosophila*'s circadian clock neuron network. J. Neurophysiol.

Liang, X., Holy, T.E., Taghert, P.H., Lim, C., Allada, R., Partch, C.L., Green, C.B., Takahashi, J.S., Welsh, D.K., Takahashi, J.S., et al. (2016). Synchronous *Drosophila* circadian pacemakers display nonsynchronous Ca2+ rhythms in vivo. Science.

Liu, C., and Reppert, S.M. (2000). GABA synchronizes clock cells within the suprachiasmatic circadian clock. Neuron 25, 123–128.

Mohawk, J.A., Green, C.B., and Takahashi, J.S. (2012). Central and Peripheral Circadian Clocks in Mammals. Annu. Rev. Neurosci.

Moore, R.Y. (1982). The suprachiasmatic nucleus and the organization of a circadian system. Trends Neurosci.

Myers, M.P., Wager-Smith, K., Rothenfluh-Hilfiker, A., and Young, M.W. (1996). Light induced degradation of TIMELESS and entrainment of the *Drosophila* circadian clock. Science.

Nässel, D.R. (2002). Neuropeptides in the nervous system of *Drosophila* and other insects: Multiple roles as neuromodulators and neurohormones. Prog. Neurobiol. 68, 1–84.

Nitabach, M.N. (2006). Electrical Hyperexcitation of Lateral Ventral Pacemaker Neurons Desynchronizes Downstream Circadian Oscillators in the Fly Circadian Circuit and Induces Multiple Behavioral Periods. J. Neurosci. 26, 479–489.

Nitabach, M.N., and Taghert, P.H. (2008). Organization of the *Drosophila* Circadian Control Circuit. Curr. Biol. 18.

Nitabach, M.N., Blau, J., and Holmes, T.C. (2002). Electrical silencing of *Drosophila* pacemaker neurons stops the free-running circadian clock. Cell.

Nitabach, M.N., Sheeba, V., Vera, D.A., Blau, J., and Holmes, T.C. (2005). Membrane electrical excitability is necessary for the free-running larval *Drosophila* circadian clock. J. Neurobiol.

Pfeiffenberger, C., Lear, B.C., Keegan, K.P., and Allada, R. (2010). Locomotor Activity Level Monitoring Using the *Drosophila* Activity Monitoring (DAM) System. Cold Spring Harb. Protoc. 2010, pdb.prot5518-pdb.prot5518.

Picot, M., Cusumano, P., Klarsfeld, A., Ueda, R., and Rouyer, F. (2007). Light activates output from evening neurons and inhibits output from morning neurons in the *Drosophila* circadian clock. PLoS Biol.

Reghunandanan, V., and Reghunandanan, R. (2006). Neurotransmitters of the suprachiasmatic nuclei. J. Circadian Rhythms.

Renn, S.C.P., Park, J.H., Rosbash, M., Hall, J.C., and Taghert, P.H. (1999). A pdf neuropeptide gene mutation and ablation of PDF neurons each cause severe abnormalities of behavioral circadian rhythms in *Drosophila*. Cell.

Rohling, J.H.T., vanderLeest, H.T., Michel, S., Vansteensel, M.J., and Meijer, J.H. (2011). Phase resetting of the mammalian circadian clock relies on a rapid shift of a small population of pacemaker neurons. PLoS One 6.

Rosbash, M. (2009). The implications of multiple circadian clock origins. PLoS Biol. S.M., A., J.M., A., Q., C., H., M., N., O., C., C., P.E., G., and J.V., S. (2013). Signals from the Brainstem Sleep/Wake Centers Regulate Behavioral Timing via the Circadian Clock. PLoS One.

Schlichting, M., Menegazzi, P., Lelito, K.R., Yao, Z., Buhl, E., Dalla Benetta, E., Bahle, A., Denike, J., Hodge, J.J., Helfrich-Forster, C., et al. (2016). A Neural Network Underlying Circadian Entrainment and Photoperiodic Adjustment of Sleep and Activity in *Drosophila*. J. Neurosci.

Schubert, F.K., Hagedorn, N., Yoshii, T., Helfrich-Förster, C., and Rieger, D. (2018). Neuroanatomical details of the lateral neurons of *Drosophila melanogaster* support their functional role in the circadian system. J. Comp. Neurol.

Sehadova, H., Glaser, F.T., Gentile, C., Simoni, A., Giesecke, A., Albert, J.T., and Stanewsky, R. (2009). Temperature Entrainment of *Drosophila*'s Circadian Clock Involves the Gene nocte and Signaling from Peripheral Sensory Tissues to the Brain. Neuron 64, 251–266.

Seluzicki, A., Flourakis, M., Kula-Eversole, E., Zhang, L., Kilman, V., and Allada, R. (2014). Dual PDF Signaling Pathways Reset Clocks Via TIMELESS and Acutely Excite Target Neurons to Control Circadian Behavior. PLoS Biol. 12.

Shafer, O.T., Rosbash, M., and Truman, J.W. (2002). Sequential nuclear accumulation of the clock proteins period and timeless in the pacemaker neurons of *Drosophila melanogaster*. J. Neurosci.

Stoleru, D., Peng, Y., Agosto, J., and Rosbash, M. (2004). Coupled oscillators control morning and evening locomotor behaviour of *Drosophila*. Nature.

Stoleru, D., Peng, Y., Nawathean, P., and Rosbash, M. (2005). A resetting signal between *Drosophila* pacemakers synchronizes morning and evening activity. Nature.

Stoleru, D., Nawathean, P., Fernández, M. de la P., Menet, J.S., Ceriani, M.F., and Rosbash, M. (2007). The *Drosophila* Circadian Network Is a Seasonal Timer. Cell.

Tian, L., Hires, S.A., Mao, T., Huber, D., Chiappe, M.E., Chalasani, S.H., Petreanu, L., Akerboom, J., McKinney, S.A., Schreiter, E.R., et al. (2009). Imaging neural activity in worms, flies and mice with improved GCaMP calcium indicators. Nat. Methods.

Vansteensel, M.J., Michel, S., and Meijer, J.H. (2008). Organization of cell and tissue circadian pacemakers: A comparison among species. Brain Res. Rev. 58, 18–47.

Vosshall, L.B., Price, J.L., Sehgal, A., Saez, L., and Young, M.W. (1994). Block in nuclear localization of period protein by a second clock mutation, timeless. Science.
Wagner, S., Sagiv, N., and Yarom, Y. (2001). GABA-induced current and circadian regulation of chloride in neurones of the rat suprachiasmatic nucleus. J. Physiol.
Wang, T.A., Yu, Y. V., Govindaiah, G., Ye, X., Artinian, L., Coleman, T.P., Sweedler, J. V., Cox, C.L., and Gillette, M.U. (2012). Circadian rhythm of redox state regulates excitability in suprachiasmatic nucleus neurons. Science.
Welsh, D.K., Takahashi, J.S., and Kay, S.A. (2010). Suprachiasmatic Nucleus: Cell Autonomy and Network Properties. Annu. Rev. Physiol. 72, 551–577.
Yadlapalli, S., Jiang, C., Bahle, A., Reddy, P., Meyhofer, E., and Shafer, O.T. (2018). Circadian clock neurons constantly monitor environmental temperature to set sleep timing. Nature.
Yan, L., Karatsoreos, I., LeSauter, J., Welsh, D.K., Kay, S., Foley, D., and Silver, R. (2007). Exploring spatiotemporal organization of SCN circuits. In Cold Spring Harbor Symposia on Quantitative Biology.
Yang, Z., and Sehgal, A. (2001). Role of molecular oscillations in generating behavioral rhythms in *Drosophila*. Neuron.
Yang, H.H.H., St-Pierre, F., Sun, X., Ding, X., Lin, M.Z.Z., and Clandinin, T.R.R. (2016). Subcellular Imaging of Voltage and Calcium Signals Reveals Neural Processing In Vivo. Cell.
Yang, J.-J., Wang, Y.-T., Cheng, P.-C., Kuo, Y.-J., and Huang, R.-C. (2010). Cholinergic modulation of neuronal excitability in the rat suprachiasmatic nucleus. J. Neurophysiol. 103, 1397–1409.
Yao, Z., and Shafer, O.T. (2014). The *Drosophila* circadian clock is a variably coupled network of multiple peptidergic units. Science.
Yao, Z., Macara, A.M., Lelito, K.R., Minosyan, T.Y., and Shafer, O.T. (2012). Analysis of functional neuronal connectivity in the *Drosophila* brain. J. Neurophysiol.
Yao, Z., Bennett, A.J., Clem, J.L., and Shafer, O.T. (2016). The *Drosophila* Clock Neuron Network Features Diverse Coupling Modes and Requires Network-wide Coherence for Robust Circadian Rhythms. Cell Rep.
Yoshii, T., Todo, T., Wülbeck, C., Stanewsky, R., and Helfrich-Förster, C. (2008). Cryptochrome is present in the compound eyes and a subset of *Drosophila*'s clock neurons. J. Comp. Neurol.
Yoshii, T., Wulbeck, C., Sehadova, H., Veleri, S., Bichler, D., Stanewsky, R., and Helfrich Forster, C. (2009). The Neuropeptide Pigment-Dispersing Factor Adjusts Period and Phase of *Drosophila*'s Clock. J. Neurosci. 29, 2597–2610.
Yoshii, T., Rieger, D., and Förster, C.H. (2012). Two clocks in the brain: An update of the morning and evening oscillator model in *Drosophila*. Prog. Brain Res.
Yoshii, T., Hermann-Luibl, C., and Helfrich-Föorster, C. (2016). Circadian light-input pathways in *Drosophila*. Commun. Integr. Biol.
Zeng, H., Hardin, P.E., and Rosbash, M. (1994). Constitutive overexpression of the *Drosophila* period protein inhibits period mRNA cycling. EMBO J.
Zhang, L., Chung, B.Y., Lear, B.C., Kilman, V.L., Liu, Y., Mahesh, G., Meissner, R.A., Hardin, P.E., and Allada, R. (2010). DN1pCircadian Neurons Coordinate Acute Light and PDF Inputs to Produce Robust Daily Behavior in *Drosophila*. Curr. Biol.

Zheng, X., and Sehgal, A. (2008). Probing the relative importance of molecular oscillations in the circadian clock. Genetics 178, 1147–1155.

Chapter 2. The Physiology of *Drosophila* Clock Neurons Is Tuned by the Fast-Neurotransmitters GABA and Acetylcholine.

Jenna L Persons[1], Rich Hume[1], and Orie T Shafer[1]

[1]Department of Molecular, Cellular and Developmental Biology, University of Michigan, Ann Arbor, MI 48109,

Author Contributions

JLP, conception and design, data acquisition, analysis and interpretation of data, drafting and revising the manuscript; RIH, OTS, conception and design, analysis and interpretation of data, drafting and revising the manuscript.

Abstract

Biological timekeeping is essential for organisms to coordinate behavior with environmental rhythms originating from the earth's 24-hour rotation. Though circadian clocks are present in most terrestrial organisms and tissues across the body, many animals have dedicated brain circuitry indispensable for maintaining rhythmic behavior. Despite the criticality of neurotransmission in coupling clock neuron networks, the contributions of specific transmitter systems remain mysterious due to the complexity of many model systems. We leverage the advantages of the *Drosophila* model system to

describe the roles of major neurotransmitters GABA and acetylcholine to clock neuron network physiology. Using voltage sensor live-imaging studies, we describe the receptivity of the evening activity-promoting cells (LNds) to cholinergic and GABAergic inputs across the circadian day. We find that increases in GABAergic and cholinergic signaling in the LNds physiologically represent night and day, respectively. Finally, we demonstrate that the daily rhythms in GABAergic and cholinergic receptivity rely on the molecular clock and light inputs.

Introduction

Circadian rhythms evolved to both track and anticipate predictable daily and seasonal changes in the environment that are result of the earth's rotation and revolution around the sun. Cellular mechanisms to reliably anticipate and adapt to environmental rhythms are present in all species studied- from bacteria, plants and mammals (Vansteensel et al., 2008). Timekeeping enables organisms to synchronize sleep, wake, feeding and mating behavior with Zeitgebers (time-givers) across appropriate timescales. Biological clocks are themselves oscillators; transcriptional-translational feedback loops whose constituent proteins' abundance and phase recapitulates light and temperature rhythms at a molecular level (Dunlap, 1999; Tataroglu and Emery, 2015; Zheng and Sehgal, 2008). The molecular clocks' rhythms are intrinsic and persist with approximately 0.5-hour deviations from the earth's 24-hour rotation in the absence of external environmental cues (Herzog, 2007; Nitabach and Taghert, 2008). The cellular clock's slightly imperfect periodicity necessitates that they be reset daily and stably "entrained" to extrinsic Zeitgebers. These Zeitgebers connote time-of-day and day length and ensure clocks align with the 24-hour solar day (Buhr et al., 2010; Challet et al., 2003; Sehadova

et al., 2009). Behavior rhythms in many organisms are an emergent property of many individual cellular clocks with diverse physiological characteristics, entrainment properties, and periodicities (Evans et al., 2015; Rohling et al., 2011; Welsh et al., 2010). Nevertheless, the circadian system reliably coordinates behavior across the solar day and seasons suggesting that there are centralized mechanisms to coordinate complex circadian systems.

In animals dedicated circuits in the brain control circadian rhythms. The endogenous timekeeping, synchronized neural activity and network interactions between approximately 20,000 neurons in the mammalian superchiasmatic nuclei (SCN) and their target centers produces regular bouts of sleep and activity (Enoki et al., 2017; Yan et al., 2007). SCN clock neurons range in intrinsic periodicity from 21 to 28 hours, a property that renders them diverse in their entrainment properties (Herzog et al., 2004; Pittendrigh and Daan, 1976). The natural entrainment variation and sheer size of the mammalian clock network provides animals with a diverse clock repertoire to adapt behavior rhythms to changes in the timing, intensity, and modality of Zeitgebers.

Chemical signaling forms the neurophysiological basis for temporal reorganization of mammalian circadian systems with day and season (Golombek and Rosenstein, 2010). Neurotransmission physiologically couples SCN neurons' molecular clocks and coordinates network-wide neural activity rhythms underlying coherent communication between clock neurons in the network, to behavioral output centers, and peripheral sensory organs (Aton et al., 2006; Enoki et al., 2017; Houben et al., 2014). SCN neurons release and receive a variety of peptides and transmitters, though the peptide vasoactive intestinal polypeptide (VIP) and neurotransmitter GABA are the most well studied in

relation to circadian behavior (Reghunandanan and Reghunandanan, 2006). Peptidergic VIP signaling is required for synchronization of network neural activity, molecular rhythms, and rhythmic behavior in light or constant conditions (Aton et al., 2005). Network rhythms imposed by VIP are modulated by GABAergic signaling through the ionotropic receptor GABA-AR, which mediates upwards of 90% of all excitatory and inhibitory communication (Freeman et al., 2013). The consequences of GABA signaling on VIP-mediated neural and behavioral synchrony are not clear: GABA's role in endogenous timekeeping, entrainment and circadian behavior correlates with rhythms in physiological excitability in the SCN (Choi et al., 2008; Evans et al., 2013; Kingsbury et al., 2016). Physiological rhythms in SCN neurons are generated by rhythms in intracellular chloride concentration [Cl^-] which is higher during the day and lower during the nighttime (Wagner et al., 2001). As GABA-ARs are ionotropic chloride channels, they are particularly influenced by the SCN's daily [Cl^-] rhythms. Activation of GABA-ARs causes Cl^- to move down it's concentration gradient, making GABA inherently more excitatory during the day when [Cl^-] on the inside of the neuron is greater and more inhibitory at night when [Cl^-] on the outside of the neuron is greater (DeWoskin et al., 2015; Itri, 2004; Wagner et al., 2001; Wang et al., 2012). Physiological rhythms in neural excitability therefore change the "meaning" of transmitter and peptide communication within the network, including that of GABA and VIP (An et al., 2013; Itri, 2004). They also suggest that the overall tone of the network might signal distinct environment and behavior states though the role of endogenous cell-intrinsic mechanisms, and extrinsic sensory inputs in setting these rhythms remain obscure.

Drosophila melanogaster is an ideal model to define the contributions of neurotransmitter signaling to network physiology and circadian behavior. Like that of mammals, the fly circadian clock neuron network's (CCNN) endogenous timekeeping and network communication coordinates behavior rhythms with light and temperature rhythms across the solar day and season (Dissel et al., 2014; Stoleru et al., 2007). Despite their independent evolutionary origins, remarkably, fly and mammal networks share a number of structural and physiological similarities that make the fly a particular advantageous circadian model (Rosbash, 2009; Tataroglu and Emery, 2014). The *Drosophila* CCNN is spatially organized in to anatomically distinct dorsal and ventral subpopulations. Each systems' clock neurons communicate using the same neurotransmitters and peptides, though in flies there is less redundancy in signaling machinery due to their reduced genomic scale (Hermann-Luibl and Helfrich-Förster, 2015). Flies also have a VIP-like peptide pigment dispersing factor (PDF) that coordinates neural activity and molecular clock rhythms to facilitate entrainment with light and endogenous timekeeping behavior (Liang et al., 2016; Renn et al., 1999; Yoshii et al., 2009). The functional homology of the CCNN conserves these critical elements with 1/100 the neurons of rodent model SCNs, that critically, are easily isolated and manipulated using genetic tools available in the fly model system (Allada and Chung, 2010b; Hendricks and Sehgal, 2004).

The *Drosophila* CCNN's 150 neurons are subdivided into anatomically, and genetically distinct classes. Coordination of diurnal behavior is distributed across the network (Yao et al., 2016; Yoshii et al., 2012). Rather simplistically, the ventral lateral neurons (LNvs) expressing the fly functional homolog of VIP, pigment dispersing factor (PDF) and dorsal neurons (DN1s) drive peaks in morning wakefulness, while the dorsal

lateral neurons (LNds) and the 5th s-LNv promote evening wakefulness (Helfrich-Förster et al., 2007). Much like Ca^{2+} transients in the SCN, fly clock neurons' Ca^{2+} rhythms match their behavioral roles but are asynchronous to one another (Liang et al., 2016). Neurotransmission and peptidergic signaling (VIP and PDF, primarily) is critical for coordinating network molecular rhythms, neural activity and behavior in flies and mammals alike (Nitabach, 2006; Nitabach et al., 2002; Renn et al., 1999; Yoshii et al., 2009). However, the fly network is incredibly rich in neurochemical machinery hinting there may be circadian functions for other transmitter types (Hermann-Luibl et al., 2014; Hermann et al., 2010; Johard et al., 2009). Extensive, stereotyped arborizations synaptically couple clock classes to each other and sensory centers and suggest that fast-neurotransmitters typically communicated at direct, synaptic connections may play a functional role in the network (Helfrich-Förster, 2003; Schubert et al., 2018). This idea is supported by the clock network's global expression of ionotropic receptors to receive signals from classical neurotransmitters like GABA, glutamate and acetylcholine, as well as a growing body of work that positions them as modulators of the clock neuron physiology and sleep-wake behavior (Abruzzi et al., 2017; Guo et al., 2016; Lelito and Shafer, 2012; Muraro and Ceriani, 2015; Parisky et al., 2008).

The CCNN receives daily light information through cell-intrinsic and extrinsic mechanisms (Schlichting et al., 2016; Yoshii et al., 2016). The mosaic expression of the photoreceptive protein CRY renders half of the network directly sensitive to light (Yoshii et al., 2008). In parallel, cholinergic inputs from neurons in the optic lamina and HB-eyelet, and potentially from the choline acetyltransferase (Cha)+ 5th s-LNv and LNds, indirectly send light information to at least the LNvs (Johard et al., 2009; Kolodziejczyk et al., 2008;

Muraro and Ceriani, 2015; Schlichting et al., 2016). Acute, cholinergic signals are conducted primarily through ionotropic nicotinic acetylcholine receptors (nAChRs), though the fly also expresses metabotropic acetylcholine receptors (mAChRs) (Jones et al., 2007). As yet, cholinergic signaling has no defined role in the CCNN's circadian functions, however it is presumed critical for synchronizing the clock network to changes in environmental light intensity and duration. Though the precise sources of GABA input remain unmapped, ionotropic and metabotropic GABA receptors are expressed throughout the CCNN (Abruzzi et al., 2017; Gmeiner et al., 2013; Hamasaka et al., 2005). In addition, RNA-sequencing suggests that the network may express the appropriate synthetic machinery for GABA production (Abruzzi et al., 2017). Of the three potential ionotropic GABA-AR encoding subunits in the fly genome (*Rdl*, *Grd*, *Lcch3*), RDL has documented roles in maintaining and timing nighttime sleep by inhibiting the neural activity of the LNvs (Agosto et al., 2008; Chung et al., 2009; Parisky et al., 2008). As yet, no function has been identified for GABA in the fly's endogenous circadian timekeeping. Interestingly, the strength of acute, nicotinic excitation in the s- and l-LNvs is controlled by GABA suggesting there may be coordination between these two ancient, conserved neurotransmitters (Lelito and Shafer, 2012). The widespread receptivity to GABA and ACh suggests an important role for these transmitters, perhaps together, in maintaining the physiology and behavioral functions of the network either in endogenous timekeeping, entrainment to environmental cues, or both.

Electrophysiology remains the standard to measure the electrophysiological properties of *Drosophila* clock neurons and the effects of neurochemicals on their activity. The l-LNvs, the s-LNvs, and the DN1ps have been characterized electrophysiologically.

Due to their large size and accessible surface location in the fly brain, the electrophysiological properties of the l-LNvs have been analyzed by multiple groups and show both tonic and bursting patterns of action potentials (Cao and Nitabach, 2008; Muraro and Ceriani, 2015; Park and Griffith, 2006; Sheeba et al., 2008). In contrast, only 20% of recorded s-LNvs spontaneously fire, while the DN1ps fire only tonic action potentials (Cao and Nitabach, 2008; Flourakis and Allada, 2015; Seluzicki et al., 2014). Prior to our groups' studies, the LNds remained the only major clock neuron class yet to be characterized electrophysiologically. The LNds are located deep in the fly brain, and are closer in cellular size to the s-LNvs, making them a challenging target for cellular recordings (Schubert et al., 2018). The six LNds are heterogenous in their neurochemistry and coupling to other neurons in the clock network; they are targets of PDF signaling from the LNvs and one-half of the neurons express the photoreceptive protein CRY (Im et al., 2011; Shafer and Yao, 2014; Yao, 2016; Yao and Shafer, 2014). The neural activity of the LNds is causal to the anticipatory peak of activity around dusk and important to light entrainment of endogenous circadian rhythms (Cusumano et al., 2009; Grima et al., 2004; Stoleru et al., 2004; Yao and Shafer, 2014). Z. Yao's electrophysiological recordings from GFP-expressing neurons in the light period of a 12:12 light:dark cycle demonstrated that LNds fire spontaneous tonic and bursting patterns of action potentials (Yao, 2016). Z. Yao also analyzed the effect of classical neurotransmitters GABA and acetylcholine on the LNds. He showed that the LNds are directly excited and inhibited by ionotropic GABA and acetylcholine signaling, respectively. The application of the acetylcholine analog carbamylcholine (CCh), or the nAChR-specific agonist nicotine, caused bursts of action potentials and strong depolarization of the recorded LNds. Z. Yao showed using whole

cell voltage-clamp recordings that the nicotine-induced currents are largely independent of network activity, and are conducted by non-selective cation channels, nAChRs. The LNds' were also receptive to GABA (γ-aminobutyric acid), the major fast inhibitory neurotransmitter in the fly brain (Restifo and White, 1990; Yao, 2016). In contrast to the excitatory effects of acetylcholinergic agonists, Z. Yao found that GABA induced hyperpolarization of the LNds and completely suppressed spontaneous firing. The GABA-induced inward currents persist in the absence of network activity and are conducted by chloride-conducting ion channels, GABA-A receptors (GABA-ARs) (Macdonald and Olsen, 1994; Yao, 2016).

These experiments characterized for the first time the LNds' intrinsic firing modalities and receptivity to classical neurotransmitters. However, we did not examine any time-of-day effects on these metrics nor the roles of light inputs or the circadian clock to the LNds receptivity to transmitters. Herein, we address these questions by dissecting the physiological effects of GABA and acetylcholine in the evening cells, across the circadian day. We used a recently developed genetically encoded voltage sensor (GEVI), ASAP2f, for these studies (Yang et al., 2016). ASAP2f is a membrane-bound GFP construct, fused to a voltage-sensitive domain that bi-directionally responds to changes in membrane potential. ASAP2f decreases in fluorescence upon membrane depolarization, and increases in fluorescence with hyperpolarization. ASAP2f has been successfully utilized to live-image the response of neurons in the *Drosophila* optic lamina to acute light presentation (Yang et al., 2016). ASAP2f is uniquely advantageous for our work in that it offers a first-line measure of relative membrane potential, as opposed to secondary Ca^{2+} or cAMP levels whose relationship to membrane voltage are not

straightforward (Chen et al., 2013; Yao et al., 2012). ASAP2f also differs from commonly used Ca^{2+} sensors in that hyperpolarizing responses result in increased ASAP2f fluorescence, making detection of inhibition more likely. Finally, ASAP2f is compatible with recording neuronal activity of large networks of neurons *in vivo* thereby circumventing the technical limitations of classic electrophysiology, namely its inability to address cellular heterogeneity and the need to remove layers of tissue to access deep brain neurons like the LNds (Yang et al., 2016). Methods to assess neuronal activity directly with electrophysiology, or infer indirectly through genetically encoded sensors for Ca+ and cAMP are widely used in the CCNN (Chen et al., 2013; Yao et al., 2012). Voltage sensors like ASAP2f have not been used in the clock network successfully, nor have they been used to address receptivity to bath-applied neurochemicals. GEVIs offer many advantages to classic electrophysiology, however it is unknown if they will be universally useful in the *Drosophila* brain or the potential limitations to ASAP2f use in new neuronal populations. Among the central efforts of our work, is describing the use of ASAP2f in an interneuron population within the clock network, establishing methods and quantitative measures to analyze ASAP2f fluorescence, and interpreting fluorescence changes in terms of inferred membrane voltage.

Our studies address the receptivity of the LNds to GABAergic and cholinergic inputs across the circadian day. We established curve-fitting methodology using Prism software to reduce ASAP2f fluorescence “noise” while preserving the area of LNds’ responses, and establish metrics to quantitatively compare inferred voltage changes to bath-applied neurotransmitter (GraphPad, Prism version 8.0.2 for Mac, GraphPad Software, San Diego, California USA). We find that the LNds are directly receptivity to the

acute application of nicotine and GABA in a fully intact brain network. Interestingly, we found that GABA hyperpolarization and cholinergic depolarization in the LNds is stronger in the middle of the night and middle of the day, respectively. These observations fit well with the mid-night trough and mid-day peaks in activity of LNds as measured by time course with GCaMP6f Ca^{2+} imaging (Liang et al., 2016). Furthermore, we establish that the molecular clock controls the daily rhythms apparent in GABAergic responses; while cholinergic receptivity is primarily driven by light inputs that themselves are gated by clock-mediated mechanisms. Together our findings suggest that separate neurotransmitters represent distinct “day” and “night” physiological states in the evening-activity promoting neurons. Our experiments suggest a functional conservation across species of neurotransmission and cell-intrinsic mechanisms in the control of circadian neuron activity and behavioral rhythms. In future work, we will describe the roles of ionotropic cholinergic and GABAergic signaling in the circadian timekeeping and sleep behavior of the LNds and more broadly throughout the CCNN. Our use of the ASAP2f sensor outside of the *Drosophila* sensory system, within the clock neuron network required that we create methodology and metrics to quantify and interpret observed voltage changes. Together, these studies set the stage for work in the mechanisms through which GABA and ACh govern timekeeping and sleep and are highly likely to inform our understanding of the physiological basis of circadian timekeeping and entrainment generally.

Results

Nicotinic signaling is stronger during the daytime than nighttime. Acetylcholine (ACh) is the most prevalent fast excitatory neurotransmitter in insect brains. The LNds are

receptive to cholinergic agonists including carbamylcholine (CCh), a structural homolog of acetylcholine that is resistant to the action of cholinesterases and the nAChR-specific agonist, nicotine (McCarthy et al., 2011; Restifo and White, 1990; Yao, 2016). In our groups' prior electrophysiological studies, a 30-second perfusion of 1mM carbamylcholine CCh and nicotine induced a burst of action potentials and a strong depolarization of membrane potential in the LNds (Yao, 2016). We also demonstrated that the acute, nicotine-induced currents are largely independent of network activity and are conducted by nAChRs (Yao, 2016). Given cholinergic signaling's role in fly sleep-wake behavior and it's use to communicate light information from neurons in the optic lamina, we wondered whether there were time-of-day specific effects of cholinergic excitation in the LNds (Kolodziejczyk et al., 2008; Muraro and Ceriani, 2015). We predicted that excitation would be greater during the daytime when most light-mediated information is received. We used GCaMP6f Ca^{2+} transient data to determine the most and least active windows to examine excitatory receptivity using the genetically encoded voltage sensor ASAP2f (Liang et al., 2016). ASAP2f reflects changes in voltage by movement of a charged membrane helix linked to GFP wherein decreased and increased fluorescence represent depolarization and hyperpolarization, respectively (Yang et al., 2016). Therefore, LNds that are excited relative to baseline will exhibit decreases in fluorescence, while those that are inhibited by a stimulus will show increases. We inferred from Yang, et al (2016) that the LNds are most active during ZT4-8 preceding the evening activity peak they coordinate, and least active in the middle of the night from ZT14-18.

We perfused explanted brains dissected from 5-7 day old male flies with 30-seconds of 0.1mM, 0.5mM, and 1mM nicotine during a 200-second time course between

ZT4-8 and ZT14-18 and examined ASAP2f fluorescence of LNds where ASAP2f expression was driven throughout the clock neuron network using the network-wide driver, *CLK856-GAL4* (Gummadova et al., 2009). We imaged the cell bodies of LNds using a confocal microscope with a 488nm laser at 5-10% of total power and acquired frames at 2Hz at the Z-slice with the brightest ASAP2f fluorescence (see Materials and Methods for complete details). Our imaging rate is fast enough to capture global depolarizations and hyperpolarizations at the cell bodies. It is not fast enough to capture the single action potentials previously recorded in our electrophysiological studies, or that of previous ASAP2f publications and is a critical point for the interpretation of the physiological studies herein (Yang et al., 2016; Yao, 2016). The LNds exhibited diverse firing modalities and were sometimes silent in electrophysiological studies (Yao, 2016). This suggests that the LNds baseline membrane potential is not homogenous. Thus, without the ability to infer the baseline membrane voltage or spontaneous firing rate of LNds, depolarizations are not necessarily equal to "excitation" if neurochemical application does not bring the neuron beyond threshold to induce firing and hyperpolarization is not necessarily equal to "inhibition" if it does not prevent or suppress active firing. At our current imaging rate, it is unclear how ASAP2f fluorescence changes correlate with true inhibition or excitation to applied neurotransmitter. However, in our electrophysiology work the LNds depolarized, increased firing with application of cholinergic agonists and hyperpolarized, decreased firing with GABAergic agonists. We reasoned that using the same concentrations of neurotransmitters may produce similar physiological effects and strengthen the interpretive power of our ASAP2f studies.

We developed a post-hoc data processing method to minimize ASAP2f sensor noise due to movement of live brains in the perfusion system that are intensified by imaging single neurons, or sets of neurons at high magnification. We converted raw fluorescence values in 2Hz bins for the duration of the imaging session into percentages computed based on the average of intensity values that preceded vehicle or stimulus presentation. These values are entered in to an X, Y table in the statistical analysis software, Prism, where X-values are each bin's collection "Time" and Y-values are "Percent DeltaF/F" (relative to baseline average) (GraphPad, Prism version 8.0.2 for Mac, GraphPad Software, San Diego, California USA). We chose to represent data using a polynomial fitting method that enables us to compare various fitting methods and acquire confidence intervals (CIs) for fitted traces relative to the original data (GraphPad, Prism version 8.0.2 for Mac, GraphPad Software, San Diego, California USA). Polynomial fitting methods are superior for our purposes because 1) the initial data values have no influence on fitting so pre-fitting data manipulation is not necessary and 2) higher order polynomials have more inflection points that accommodate more twists/turns in data should the responses reflect above and below baseline during the time-course. We chose a centered polynomial because the X-values are consistent across all experiments and do not require fitting, thereby reducing the number of parameters and enabling higher confidence curve prediction. Centering converts each X-value collection bin to XC = X - Xmean. X therefore becomes a constant across all experiments and only the fluorescence values are fitted to the curve. Within experimental replicates, we tested each X-bin's fluorescence values for normality with a D'Agostino-Pearson normality test that assumes that the spread of points for each X-value collection bin is normally distributed between replicates (GraphPad,

Prism version 8.0.2 for Mac, GraphPad Software, San Diego, California USA). All doses and vehicles passed. Finally, we weighed each point equally and automatically removed outliers from trace data using ROUT method with False-discovery rate (FDR) less than 1% (GraphPad, Prism version 8.0.2 for Mac, GraphPad Software, San Diego, California USA).

We found that a centered 6th- order polynomial consistently performed better than lower-order polynomial fitting methods at fitting the original trace data (1A “vehicle”, D “1mM Nicotine”). The 6th- order fitted trace mean fluorescence (black solid line) and fitting method’s 95% confidence bands (black dashed lines) fully encompass the original raw data SEM (blue error lines) (zoomed in, Figure 1B, D). We used this fitting method to analyze all of the imaging studies included herein. Each trace plot has an R^2 value included on the graph title. R^2 vales represent the fitted traces goodness of fit to the original data. We included 95% prediction bands surrounding the fitted mean fluorescence (solid black lines) that enclose the area expected to represent 95% of future data points interpolated from the fitted curve (Figure 1C, F). Prediction bands represent the uncertainty in the true position of the curve (enclosed by the confidence bands), and also account for scatter of data around the curve. We applied the 6th-order polynomial fitting method to each nicotine dose in the data set and compared the mean minimum fluorescence values and signal area of the unfitted and fitted data to ensure that our fitting method eliminated noise but preserved signal total response area (Figure 1G, I). The mean minimum fluorescence values of the fitted data (1G, dark grey or 1H, pink) were consistently and significantly smaller than that of the unfitted data (1G, light grey or 1H, blue). However, the total response area was unchanged between all fitted and unfitted

pairs (Figure 1I, J). This confirms that fitting to a 6th-order polynomial reduced high-frequency noise, but the signal area itself was maintained.

We performed all studies in the presence of 2uM tetrodotoxin (TTX) -from brain explantation to the end of each 200-second imaging session- to examine effects of transmitter directly on LNds. In order to properly interpret our findings for the remainder of these studies, we applied 30-seconds of HL3 vehicle, or HL3 with 2uM TTX during 4-hour time windows across a standard LD cycle (Figure 2A-F). We quantified the total and net response area, and maximum fluorescence in the imaging frames during and after vehicle or TTX presentation (Figure 3). TTX application alone has no significantly different effect from vehicle on the LNds in the mid-day (ZT4-8) and mid-night (ZT14-18) windows assessed with co-application of transmitter for the remainder of experiments in this publication (Figure 3A-C). However, we found that just after light offset, TTX application resulted in significant increases in total response area, net response area and mean maximum fluorescence relative to vehicle and mid-night TTX (ZT14-18) (Figures 3A-C, right). TTX application in the hours after light onset, likewise significantly increased total response area relative to vehicle and mid-day TTX (ZT4-8) and caused trending but non-significant increases in mean maximum fluorescence and net response area (Figure 3A-C, center). This suggests that inputs at nighttime light transitions, and to a lesser extent daytime, exert a net depolarizing action on the LNds. These inputs are blocked by acute application of TTX and result in hyperpolarization (Figure 3A-C, left). Critically, acute TTX application has no significant effect in mid-day (ZT4-8) or mid-night (ZT14-18) and therefore effects observed during these windows for the remaining experiments herein may be attributed primarily to the co-applied transmitter.

The LNds varied in their response to vehicle application alone between the daytime and nighttime experiments (Figure 4A, C). We are imaging too slowly to capture single action potentials, but it suggests that our observations reflect relevant changes in baseline membrane potential or spontaneous LNd firing between daytime and nighttime. Application of 30-seconds of 0.1mM nicotine in the daytime and nighttime produced moderate depolarizations, with the onset of depolarization occurring well into the stimulus presentation window (Figure 4B, D). We quantified and statistically compared the total response area and mean minimum fluorescence of each LNds' trace (Figure 4E, F). The total response area and mean minimum fluorescence of depolarization was not significantly different between daytime and nighttime applications. Relative to their respective vehicle applications, 0.1mM nicotine in either the daytime or nighttime caused significantly greater depolarizations. Interestingly, at this lower dose, responses to nicotine were of greater mean minimum fluorescence during the nighttime than daytime (Figure 4F). 0.5mM nicotine in the daytime and nighttime also caused depolarization in recorded LNds (Figure 5B, D). These depolarizations were significantly greater than their respective vehicle controls in total response area and mean minimum fluorescence change (Figure 5E, F). In contrast to 0.1mM nicotine, 0.5mM nicotine produced significantly greater depolarizations during the daytime than nighttime (Figure 5E, F). Perfusion of 1mM nicotine also caused LNd depolarization (Figure 6B, D). Quantification of total response area and mean minimum fluorescence showed that the recorded LNd depolarizations to 1mM nicotine were significantly greater than vehicle application and also significantly greater during the daytime than nighttime, like that of 0.5mM applications (Figure 6E, F). We quantified and compared LNd responses across the entire dose

response curve (Figure 7). In either the daytime, or nighttime, increasing nicotine dosage from 0.1mM to 1mM increased the total response area (Figure 7A, B) and mean minimum fluorescence (Figure 7C, D). In the nighttime however, the total response area and mean minimum fluorescence of responses is unchanged between 0.1mM and 0.5mM doses suggesting that nighttime applications of nicotine cause less depolarization than those in the daytime (Figure 7B, D).

We noticed that the responses of LNds at lower doses were visibly less coherent, and far more cells were indistinguishable from vehicle, than LNd responses at higher doses. Therefore, we sorted cells into three categories based on their minimum or maximum fluorescence change relative to the vehicle fluorescence mean. To be a depolarized or hyperpolarized responder, a LNd must have a positive or negative fluorescence change that is at least twice the vehicle fluorescence mean. All other cells were called non-responders. We quantified and compared the max and min fluorescence of cells excluding the non-responsive cells for each dose (Figure 8A, D, G). We also visually indicated the response type on trace plots (Figure 8B, E, H) and calculated the percentage of cells in each category (Figure 8C, F, I) for every nicotine dose. After sorting out the non-responders, a comparison of the differences between daytime and nighttime perfusion of 0.1mM nicotine found that there were no longer significant differences between time-of-day (Figure 8A). This is explained by the greater percentage of cells with no response in the daytime (Figure 8B, C, grey). 95% to 100% of the cells in 0.5mM and 1mM nicotine applications responded, and all responses were depolarizations. The significant increase in daytime response mean minimum fluorescence persisted after the expulsion of any non-responders (Figure 8D-I). Together our findings confirm that nicotine

1) directly causes depolarization of the LNds, and 2) that this depolarization is greater during the daytime.

GABA receptivity is greater during the nighttime than daytime. We previously tested the LNds' receptivity to GABA (γ-aminobutyric acid), the major fast inhibitory neurotransmitter in the fly brain (Restifo and White, 1990). In whole-cell current-clamp recordings, perfusion of 1mM GABA induced hyperpolarization of the LNd membrane potential and completely suppressed spontaneous firing (Yao, 2016). The GABA-induced inward currents persisted in low calcium bath solution, nearing the reversal potential for chloride and are almost completely suppressed by the GABA-AR antagonist picrotoxin suggesting that the LNds are directly inhibited by GABA through chloride-conducting ion channels, GABA-A receptors (GABA-ARs) (Yao, 2016). GABA inhibition in SCN neurons of mammals and the CCNN in *Drosophila* promotes proper sleep-wake behavior. In *Drosophila*, ionotropic inhibition through GABA-AR RDL promotes nighttime sleep by inhibiting the morning wake-promoting l- and s-LNvs (Chung et al., 2009; Parisky et al., 2008). The LNd's are also wake-promoting, and their increased mid-day neuronal activity is causal to the fly's evening behavior peak (Guo et al., 2014; Stoleru et al., 2004, 2005).

Our previous studies did not address time-of-day specific effects of GABA signaling to the LNds. We reasoned that inhibitory GABAergic receptivity in the LNds might be greater at nighttime, after their coordination of evening wakefulness (Stoleru et al., 2004, 2005). We used GCaMP6f Ca^{2+} transient data to inform our studies and imaged ASAP2f-expressing LNds during the time of highest (ZT4-8) and lowest (ZT14-18) Ca^{2+} levels reported for these neurons (Liang et al., 2016). All studies were performed in the constant presence of 2uM TTX to assess only those effects of GABA directly on the LNds.

We perfused 30-seconds of 0.25mM, 0.75mM, and 1mM GABA over LNds during the daytime and nighttime windows and examined the ASAP2f responses of LNds in brains dissected from 5-7 day old male flies expressing ASAP2f under control of the clock neuron network-wide driver, *CLK856-GAL4* (Gummadova et al., 2009). We used the same confocal imaging set-up to capture LNds' cell body responses to GABA as described previously for nicotine studies and as detailed in Materials and Methods. We used a 6th-order polynomial to fit the raw data from GABA experiments (9A, D "Raw", and C, F "Fitted"). The fitted mean fluorescence (black solid line) and fitting method's 95% confidence bands (black dashed lines) encompass the original raw data SEM (blue error lines) though with slightly smaller R^2 values than for nicotine experiments (zoomed, Figure 9B, D). We vetted our 6th-order polynomial fitting method on each GABA dose used. The fitting method's effects- high magnitude noise elimination and response area preservation- on raw data were highly similar to those observed in our nicotine experiments. A comparison of mean maximum fluorescence values and total response area of the unfitted and fitted data demonstrated that maximum fluorescence increases were decreased by fitting, while the signal's total response area was unchanged (Figure 9G-J). We applied the 6^{th}-order fitting method to the remainder of our GABA experiments herein.

Perfusing 0.25mM GABA for 30 seconds in the daytime and nighttime produced small hyperpolarizing responses in the LNds (Figure 10B, D). These responses were visibly less coherent in directionality above and below the baseline than we observed with nicotine application, which were coherently depolarizing. Therefore, we calculated the *net response area* (instead of the total response area used in nicotine experiments) to

account for the positive or negative deflection from baseline of each LNds' response to GABA. We quantified and statistically compared the net response area and mean maximum fluorescence of each LNds' response. We found that mean net response area was not significant at this dosage from vehicle controls (Figure 10E). The mean maximum fluorescence of responses was only significantly different than vehicle control during the daytime window (Figure 10F). However, the maximum fluorescence increases displayed by these neurons were not significantly different between daytime and nighttime applications (Figure 10F). We concluded that 0.25mM GABA is not concentrated enough to produce robust hyperpolarizing responses. In contrast, we observed that LNd responses to 0.75mM GABA were visibly more distinguishable from vehicle applications in both day and night windows than in 0.25mM experiments (Figure 11A-D). At this concentration, we found that the LNds were more hyperpolarized relative to vehicle, only in the nighttime (Figure 11E, F). The responses to GABA in the nighttime were significantly greater than those of LNds in daytime (Figure 11E, F). Increasing doses to 1mM GABA caused robust, coherent LNd hyperpolarizations (Figure 12A-D). Quantification of the net response area and mean maximum fluorescence change showed that the imaged LNd responses in day or night were significantly greater than vehicle application (Figure 12E, F). The difference between daytime and nighttime applications was lost at this dose, we speculate due to reaching saturating levels in solution (Figure 12E, F). We quantified and compared LNd responses from the complete dose response curve (Figure 13). Increasing GABA concentration from vehicle or 0.25mM to 1mM increased the total and net response area (Figure 13A, B, E, F) and mean maximum fluorescence change (Figure 13C, D). However, in the daytime the maximum

fluorescence and net response area of traces is unchanged between vehicle and 0.75mM doses suggesting that nighttime applications of GABA cause more hyperpolarization than daytime (Figure 13C, D, E, F). At lower concentrations- 0.25mM and 0.75mM- responses to GABA are less coherently hyperpolarizing in the LNds than at 1mM.

We sorted cells based on their maximum and minimum (positive or negative) fluorescence change relative to the vehicle fluorescence change mean. Depolarized and hyperpolarized responders respectively have a minimum or maximum fluorescence change that is at least twice the vehicle fluorescence mean. All other cells were called non-responders. We quantified and compared the fluorescence of cells excluding the non-responsive cells for each dose (Figure 14). After sorting out the non-responders, daytime and nighttime perfusion of 0.25mM nicotine were no longer significantly different from one another suggesting that our observations were driven by non-responders and depolarizing cells (Figure 14A-C). Sorting cells also identified significantly more depolarizing cells in daytime applications of 0.75mM GABA than nighttime (Figure 14D-F). At both 0.75mM and 1mM doses, far more cells fail to respond to GABA perfusion in the daytime than nighttime (Figure 14F and I, grey). We also confirm that at 1mM, GABA causes hyperpolarization in almost all responding cells (Figure 14F). In summary, we found that the mean maximum fluorescence change, total response area, and percentage of hyperpolarizing responses to GABA increased with increasing dosage. Additionally, while during the nighttime, responses to 0.75mM GABA were primarily hyperpolarizing, we observed significantly more depolarizations to GABA at 0.75mM doses during the daytime than nighttime (Figure 14D). We also found that the mean maximum fluorescence of LNd responses to 0.75mM GABA applications are significantly more

inhibitory during the night (Figure 11B, E). Together, we conclude that GABA causes hyperpolarizing responses in the LNds, and suggest that GABA inhibition to the LNds is greater in the middle of the night than day.

Time of day differences in nicotinic excitation rely on light inputs and the molecular clock. Our ASAP2f imaging demonstrates that the LNds are more hyperpolarized by GABA at night and depolarized by acetylcholine during the day (Yao, 2016). We wondered whether these time-of-day physiological differences were controlled by the molecular clock, light inputs, or a combination of the two. RNA-sequencing from the LNds suggests that the mRNA levels of nAChRs and GABA-AR homolog *Rdl* do not undergo circadian oscillations (Abruzzi et al., 2017). However, this does not exclude the possibility of clock-mediated oscillations at the protein level, or endogenous rhythms in membrane excitability mediated by other channels and receptors. Independent of the molecular clock, light acting directly on the LNds through CRY-mediated photoreception, or indirectly from optic pathways could control membrane potential and transmitter receptivity. To disentangle these possibilities, we examined LNd responses to nicotine and GABA in constant darkness and temperature (DD), and in per^{01} flies with "broken" non-functional molecular clocks. Per^{01} flies are arrhythmic in constant conditions and lack all anticipatory morning and evening activity in LD (Helfrich-Förster, 2001; Konopka and Benzer, 1971). However, they retain acute sensory "startle effects" to the sudden onset and offset of lights in entrained conditions. The molecular clock produces rhythms in behavior and neuronal physiology in the absence of environmental cues. If time-of-day dependent responses persist in constant conditions (DD) we can assume that the molecular clock and not environmental light input controls transmitter receptivity. Thus,

we asked if daily rhythms in receptivity persisted in the absence of clock control by examining LNd physiology under constant conditions in a per^{01} background. Responses that persist in constant conditions and dissipate in a per^{01} background support the conclusion that the molecular clock modulates transmitter receptivity.

We first tested the response of LNds to 30-seconds of 0.5mM nicotine- the most reliable and discriminatory concentration between day and night depolarizations in dose-response experiments (Figure 5 and 8D-F). We entrained ASAP2f-expressing flies to 12:12 LD cycles, and released them into constant darkness and constant temperature for one complete day. Brains were dissected and LNds imaged during 4-hour windows at the middle of the subjective day (CT4-8) and night (CT14-18) in the presence of 2uM TTX. We observed visibly coherent depolarizations to 0.5mM nicotine application relative to vehicle applications (Figure 15A-D). We quantified the total, net response areas, and mean minimum fluorescence change in the imaging frames during and after stimulus application. On the first day of constant conditions, nicotine significantly depolarizes LNds relative to vehicle in the subjective day or night (Figure 16A-C). However, the significant increase in depolarization during the daytime relative to nighttime application we observed in LD does not persist in DD (Figure 16A-C). We sorted LNd responses to control for the effect of non-responding cells- those cells whose maximum or minimum fluorescence change is less than 2X the vehicle controls' mean fluorescence change (Figure 17A, B). We observed no qualitative difference in the distribution of response types, or the mean fluorescence change of responding cells' depolarizations between daytime and nighttime applications (Figure 17C, D). These data suggest that day and night differences in response magnitude for bath application of nicotine do not persist in

constant conditions and are therefore unlikely to be driven by the molecular clock. Instead, it is possible that light or other sensory information prevalent in LD drives these physiological changes.

These findings do not exclude the possibility that the molecular clock contributes to our observations in LD. To test the idea that the molecular clock is contributes to daily changes in cholinergic receptivity in entrained conditions, we expressed ASAP2f in per^{01} mutant flies and examined LNd responses to 0.5mM nicotine in 12:12 LD (Figure 18A-D). Responses to vehicle application in the nighttime were less coherent than we have previously observed in wildtype flies (Figure 18B). Specifically, we observed 4 of 19 recorded LNds hyperpolarizing spontaneously during vehicle applications. LNds coherently depolarized in response to 0.5mM nicotine during daytime and nighttime experiments (Figure 18C, D). Qualitatively, the time to maximum response depolarization occurred later in nighttime nicotine applications than in daytime (Figure 18C, D). Statistically these depolarizations are significantly different than their respective vehicle control, but the total or net response areas, and mean minimum fluorescence of depolarizations between day and night applications of nicotine were not significant in a per^{01} background in LD conditions (Figure 19A-C). We sorted out non-responding cells and confirmed that there were no further differences in mean minimum or maximum fluorescence change or responding cells' modality (Figure 20A-D). We note that non-significant trends towards increased daytime depolarization we previously observed at this concentration in wildtype LNds in LD persist. Thus, our findings in a per^{01} background suggest that the molecular clock plays an important but not singular role in the daytime-nighttime differences in cholinergic receptivity in entrained conditions. Taken together,

our results suggest that light-inputs and the molecular clock together act as important mediators of acute cholinergic receptivity in the LNds.

The molecular clock controls changes in GABA receptivity in daytime and nighttime and the overall polarity of responses. We wondered to what extent the time-of-day changes we observed in LNd receptivity to GABA were due to environmental light, or rhythms generated by the molecular clock. We examined ASAP2f-expressing LNds' response to 1mM GABA, the most consistently hyperpolarizing concentration in LD dose-response experiments (Figure 13), on the first day of constant conditions (DD) during subjective mid-day (CT4-8) and mid-night (CT14-18). All experiments were performed in the presence of 2uM TTX. On the first day of constant conditions, 1mM GABA application for 30-seconds caused visibly more hyperpolarization in LNds than in vehicle treatments (Figure 21A-D). When we quantified the recorded LNd's response mean maximum fluorescence change, total and net response area, these increases were only significantly different from vehicle at nighttime (Figure 22A-C). The maximum response fluorescence was significantly greater during the nighttime than daytime (Figure 22C). We sorted non-responders from responding cells as previously described for each window of GABA application (Figure 23A, B). We observed 24.71% more non-responders during the subjective day compared to subjective night in DD (Figure 23C). Removing non-responding cells from maximum fluorescence calculations eliminates the significant increases in nighttime hyperpolarization we observed in Figure 22C (Figure 23D). Together, these data confirm that without environmental light inputs the LNds retain hyperpolarized responses to 1mM GABA and importantly, that nighttime increases in

GABAergic receptivity persist. This suggests that the molecular clock may control physiological increases and decreases in receptivity to GABA.

To test this idea directly, we expressed ASAP2f in LNds of a *per*^{01} mutant, and applied 1mM GABA on the first day of DD during subjective day and night (Figure 24A-D). If the molecular clock plays a role in time-of-day GABA receptivity, we would expect differences between subjective daytime and nighttime to diminish. To our surprise, we observed incoherent LNd responses to GABA in subjective day, and highly variable, large amplitude responses to GABA during the subjective night (Figure 24C, D). In either GABA treatment window, we observed a combination of hyperpolarization and depolarization that was qualitatively greater during the subjective night. We note that there appear to be spontaneous changes in voltage during vehicle application at nighttime. We previously observed these changes in our *per*^{01} experiments with bath applied nicotine in LD. As flies for these experiments were raised and imaged independently, this suggests that variations in voltage specifically at nighttime may be a consequence of our genetic manipulations to the clock. The total response area of traces we observed in subjective nighttime vehicle application are significantly greater than those of daytime vehicle application (Figure 25A). Relative to daytime vehicle, daytime GABA application causes significant hyperpolarization in *per*^{01} LNds. However, the total and net response area are not significantly different from nighttime applications (Figure 25A, B). Nevertheless, during the subjective night the mean maximum fluorescence change of *per*^{01} LNd responses to GABA remain significantly different from vehicle and daytime GABA application (Figure 25C). To take in to account the directionality of responses, we sorted responders and non-responders whose maximum or minimum fluorescence change in the frames during

or after stimulus were 2X the vehicle controls' fluorescence mean (Figure 26A, B). In stark contrast to the coherently hyperpolarized responses in LD or DD in wildtype flies, *per*^{01} LNds in both the subjective day and night were considerably more depolarized in response to GABA relative to vehicle (Figure 26C). The mean minimum fluorescence change of depolarized cells was increased though non-significantly at nighttime (p= 0.0705, Figure 26D). We previously observed depolarizations in response to GABA at lower GABA concentrations in LD (0.75mM) and in LNds with GABA-AR RNAi (see Chapter 4). Together, we conclude that the molecular clock controls the magnitude of GABAergic receptivity, the increases in transmitter receptivity at nighttime relative to daytime, and overall polarity of responses in LNds.

Discussion

GABA and acetylcholine provide inhibitory and excitatory inputs to the LNds. Acetylcholine is the major excitatory neurotransmitter in the fly brain and is postulated to transmit light information from the fly retina to the lateral, PDF+ clock neurons (Kolodziejczyk et al., 2008; Lelito and Shafer, 2012; Muraro and Ceriani, 2015; Restifo and White, 1990). GABA exerts an important sleep-promoting inhibitory action on the morning wake-promoting neurons of the clock network (Chung et al., 2009; Gmeiner et al., 2013; Hamasaka et al., 2005; Lelito and Shafer, 2012; Parisky et al., 2008). However, GABA's and acetylcholine's physiological actions in other clock cells, effects across the day, and coincident roles in sleep and wake behavior have not been well explored. We previously characterized the responsiveness of LNds to classical fast neurotransmitters acetylcholine and GABA using whole-cell patch-clamp recordings (Yao, 2016). We used the genetically encoded voltage sensor (GEVI), ASAP2f, to assess the physiological roles

of bath-applied neurotransmitters in live, explanted brains (Yang et al., 2016). ASAP2f has been used to live-image the response of sensory neurons to acute light presentation, but never in the *Drosophila* central brain or to bath applied neurotransmitter (Yang et al., 2016). Our studies are the first to use ASAP2f in the *Drosophila* brain outside of primary sensory neurons, and the first GEVI use in the clock neuron network. In live brains under constant HL3 perfusion and confocal imaged at high-magnitude, we noticed that ASAP2f exhibited consistent high frequency "noise." We are imaging too slowly to reliably interpret these high-frequency fluorescence changes as firing patterns. Therefore, we developed a fitting method using Prism software that fits raw LNd response data to a centered-6th order polynomial (GraphPad, Prism version 8.0.2 for Mac, GraphPad Software, San Diego, California USA). The fitting method minimizes high magnitude noise that aberrantly increases the maximum and minimum fluorescence changes, but it preserves the response area and allows us to quantitatively compare true responses between experimental conditions. Our imaging rate is a critical point not only for statistical analysis, but also the interpretation of the changes we observe. Without an independent measurement of LNds' baseline membrane voltage or imaging ASAP2f fluorescence changes fast enough to capture single action potentials, we are unable to call our observations true inhibition (a prevention of firing) or excitation (an increase in firing). However, we can confidently say that there are increases in hyperpolarization (negative charge) or depolarization (positive charge) relative to baseline and vehicle controls.

In an interneuron population, the LNds, bath-applied cholinergic agonists and GABA result in ASAP2f fluorescence decreases (depolarization) and fluorescence increases (hyperpolarization), respectively. These responses are visually and

quantitatively distinguishable from vehicle applications which conversely, remain stable and close to baseline in wildtype LNds throughout the 200-second imaging time course. Using ASAP2f, we confirm that acetylcholine provides depolarizing synaptic inputs to the LNds in a fully intact clock network (Yang et al., 2016). Our results show that nicotinic ionotropic receptors (nAChRs) mediate acute receptivity of the LNds to acetylcholine but do not preclude the expression of metabotropic mAChRs. We also demonstrate using ASAP2f live-imaging that GABA provides hyperpolarizing synaptic inputs onto the LNds. Importantly, the effects we observed from application of either transmitter are direct, persisting in the presence of tetrodotoxin. Together with our previous electrophysiological results, we describe for the first time the neurochemical modulators of the critical clock neurons, the LNds (Yao, 2016).

Time of day specific physiological effects of the cholinergic agonist nicotine is mediated by light and the molecular clock. Our results demonstrate that the LNds are more depolarized by acetylcholine during the day and more hyperpolarized by GABA during the night in standard equinox light cycles (LD). In mammals and *Drosophila* alike, these transmitters have opposing functions in sleep-wake behavior, and physiology of the LNvs (Chung et al., 2009; Lelito and Shafer, 2012; Muraro and Ceriani, 2015; Wu et al., 2014; Yang et al., 2010). Our findings suggest a physiological underpinning for their disparate behavioral roles. GABA receptivity prevails during the nighttime to promote sleep, while nicotinic receptivity dominates during the day to promote wakefulness. We found that time-of-day dependent responses to nicotine do not persist under constant darkness suggesting that they are at least partially light-mediated. Using a per^{01} background fly, we found that cholinergic receptivity in LD is partially controlled by the molecular clock. RNA-

sequencing from isolated clock populations suggests that *nAChR* mRNA in the LNds do not undergo clock-mediated oscillations across the day (Abruzzi et al., 2017). Though it remains to be tested molecularly, this correlates with and may explain our findings that cholinergic excitation through nAChRs is strongly coupled to cycles in environmental light. However, it does not limit the possibility that nAChRs undergo clock-mediated post-translational turnover during LD cycles offering an explanation of our observations in per^{01} flies. Alternatively, our observations in LD with per^{01} LNds may reflect a disruption of rhythms in molecular regulators of basal membrane potential, and therefore receptivity to nicotinic excitation downstream of nAChRs themselves.

In contrast to acetylcholine, responses to GABA persist independently of light inputs and are controlled by the molecular clock. Interestingly, not only does the molecular clock control GABAergic response magnitude during the day and night, but also the polarity of response. We have observed LNd depolarization to GABA in three independent experiments. First, during the daytime in wildtype cells at lower GABA doses (0.75mM), in per^{01} LNds, and in *Rdl* knockdown cells at nighttime (see Chapter 4). We speculate that the clocks in per^{01} LNds in DD are each "stopped", heterogeneously at physiological states that represent "day" and "night." In fully functioning clock neurons, the molecular clock controls these states by gating the receptivity of LNds to GABA and perhaps other transmitter types. Our *Rdl* knockdown experiments suggest that the molecular clock controls GABA receptivity at least in part through RDL receptor levels, though there are certainly other methods to control GABA receptivity in the *Drosophila* brain (Chapter 4). Our experiments cannot discriminate between the possibilities that the molecular clock controls post-translational levels of RDL, or other channels and receptors directing

membrane excitability to GABA transmission. In the mammalian SCN, responses to GABA in equinox entrainment conditions are more excitatory during the day than night due to rhythms in the concentration of Cl^- present inside the cell upon GABA-AR channel activation (Albers et al., 2017; Wagner et al., 2001). Though it remains to be tested, given that the LNds express the chloride transporter *kcc*, it is formally possible that Cl^- potential in the LNds is under the control of the molecular clock and may explain our physiological observations with both GABA and nicotine (Abruzzi et al., 2017).

Materials and Methods

Drosophila Strains. Flies were reared on cornmeal-sucrose-yeast media under a 12:12 light:dark cycle at 25°C. The following fly lines were used: per^{01} (Konopka and Benzer, 1971), *w;CLK856-GAL4;* (Gummadova et al., 2009), *w;UAS-ASAP2f;* BSN: 65414 (Yang et al., 2016), and *w;CLK856-GAL4*, *UAS-ASAP2f*; (stably recombined for the purposes of these studies).

ASAP2f Live Imaging. Male flies expressing the ASAP2f construct under the control of the *CLK856-GAL4* were entrained to 12:12 LD cycles and aged 5-7 days. Flies were anesthetized on ice in daytime or nighttime as specified in text and figure legends. Daytime dissections were performed in the presence of dim ambient environmental light. Flies dissected for nighttime applications were in kept under aluminum foil in complete darkness until dissection and all environmental light in, or to the room was off. For experiments in constant darkness, constant temperature flies were removed from incubators on the first full day of DD and kept in foiled vials until dissection. Fresh HL3 was prepared to the following specifications in 1mL of milliQ water: 70mM NaCl, 5mM KCl, 1.5mM $CaCl_2$, 20mM $MgCl_2$ hexhydrate, 10mM $NaHCO_3$, 5mM trehalose dihydrate,

115mM sucrose, 5mM HEPES. The solution was titrated to pH 7.1 and vacuum filtered. All solutions for imaging experiments herein were prepared in HL3, pH 7.1. Brains were dissected in room temperature HL3, placed in the bottom of a 35mm petri dish with a perfusion insert and adhesive layer (PDI, Bioscience Tools) and allowed to equilibrate for 2min prior to imaging with constant flow of room temperature HL3 with 2uM tetrodotoxin with the exception of experiments in Figures 2, 3 with *acute* application of 2uM tetrodotoxin. Preparations were visualized using an Olympus Fluoview FV1000 confocal equipped with an Olympus LUMPlanFI 40×/0.8 W water-immersion objective (Olympus, Center Valley, PA). The LNds were identified by their anatomical locations and expression of fluorescent ASAP2f proteins. We used a magnetic microscope adapter appropriate for the Olympus Fluoview confocal microscope to hold the petri dish in place on the stage (MA-110, Bioscience Tools). We used an 8-channel pinch-value perfusion system calibrated to deliver each solution at the same flow rate, without cross-talk between solutions and manually controlled the delivery of each solution for the appropriate duration of the imaging session (PS-8H, Bioscience Tools). An 8-channel perfusion manifold delivered solutions to the Petri dish from the pinch-valve system, while a magnetic holder equipped with suction tubing controlled the liquid outflow (MTH-P and MTH-S, Bioscience Tools). Each brain was imaged for 90sec total with a 488nm laser between 5-10% power and a frame rate of 2 frames/second (2Hz). Sessions were structured as follows: 15-second pre-stimulus, 30-sec stimulus with vehicle (HL3) containing 2uM tetrodotoxin, XmM nicotine with 2uM TTX, or XmM GABA with 2uM TTX, followed by 30-second HL3 wash out. Brains were imaged only once, and received only one stimulus or vehicle application.

ASAP2f Imaging Analysis. ROIs were drawn around imaged LNds using Olympus Fluoview software. Each ROI per brain represents a single LNd in either hemisphere identified by anatomical position and expression of the ASAP2f fluorescence construct. Raw ASAP2f fluorescence intensities were exported for all time points of the 90-second imaging time course and then normalized to percent fluorescence changes (deltaF/F_0) where F_0 is calculated as the average of raw intensity values in the frames before stimulus or vehicle application. Brains which moved significantly due to poor mounting were excluded from further analyses. We used Prism to transform percent fluorescence values for each ROI using a centered, 6^{th}-order polynomial (GraphPad, Prism version 8.0.2 for Mac, GraphPad Software, San Diego, California USA). Centering converts each X-value collection bin to XC = X - MeanX. X-values represent imaging "time," do not vary between experiments, and therefore are not a parameter that requires fitting. Only the fluorescence values are fitted to the 6^{th}-order polynomial. Individual ROIs best-fit curves (light grey lines on trace plots), the mean of all fitted curves (black solid lines), and 95% prediction bands (black dashed lines surrounding the solid line) that enclose the area representing 95% of "future" data points interpolated from the curve were calculated. Prediction bands represent the uncertainty in the true position of the curve (enclosed by the confidence bands), and account for scatter of data around the curve. We automatically removed outliers from trace data using ROUT method with False-discovery rate (FDR) less than 1% (GraphPad, Prism version 8.0.2 for Mac, GraphPad Software, San Diego, California USA). We also tested experiments for normality with a D'Agostino-Pearson normality test that assumes that the spread of points for each X-value collection bin is normally distributed between replicates (GraphPad, Prism version 8.0.2 for Mac, GraphPad

Software, San Diego, California USA). R^2 values were calculated for all experiments and included on graph title to measure goodness of fit of the 6^{th}-order fitting method. Mean Maximum (inhibition) and Minimum (excitation) Fluorescence values were calculated by selecting the maximum or minimum intensities in fitted frames following vehicle stimulus and represented in histograms with the mean and SEM for each stimulus. The Total Response Area and Net Response Area were quantified using Prism software's AUC analysis over the fitted data considering "peaks" that both above and below the baseline (GraphPad, Prism version 8.0.2 for Mac, GraphPad Software, San Diego, California USA). Outliers were identified by Prism using the ROUT method with Q (False-discovery rate) = 1% and excluded from analysis (GraphPad, Prism version 8.0.2 for Mac, GraphPad Software, San Diego, California USA). For analyses where LNd responses to a single bath-application, responding cells had a maximum positive ("hyperpolarized") or negative ("depolarized") fluorescence that was at least 2X the vehicle mean fluorescence values for the relevant daytime or nighttime control. All other cells were called "non-responders." Non-responders were excluded from quantification and indicated in grey on trace plots and percentage graphs. Each LNd was sorted in to only a single category (hyperpolarized, depolarized, no response) based on their greatest positive or negative peak relative to the vehicle control. Significance between mean maximum or minimum ASAP2f fluorescence (delta F/F0) and total and net response areas of traces ($P<0.05$) was calculated using One-way ANOVA with Sidak correction for multiple comparisons between all groups (GraphPad, Prism version 8.0.2 for Mac, GraphPad Software, San Diego, California USA). Where fewer than three groups were being analyzed, we determined significance using an unpaired t-test with Welch's correction between each

pair (GraphPad, Prism version 8.0.2 for Mac, GraphPad Software, San Diego, California USA). Significance ($p<0.05$) is reported with actual values when P-value is <0.05. Significant values are bolded.

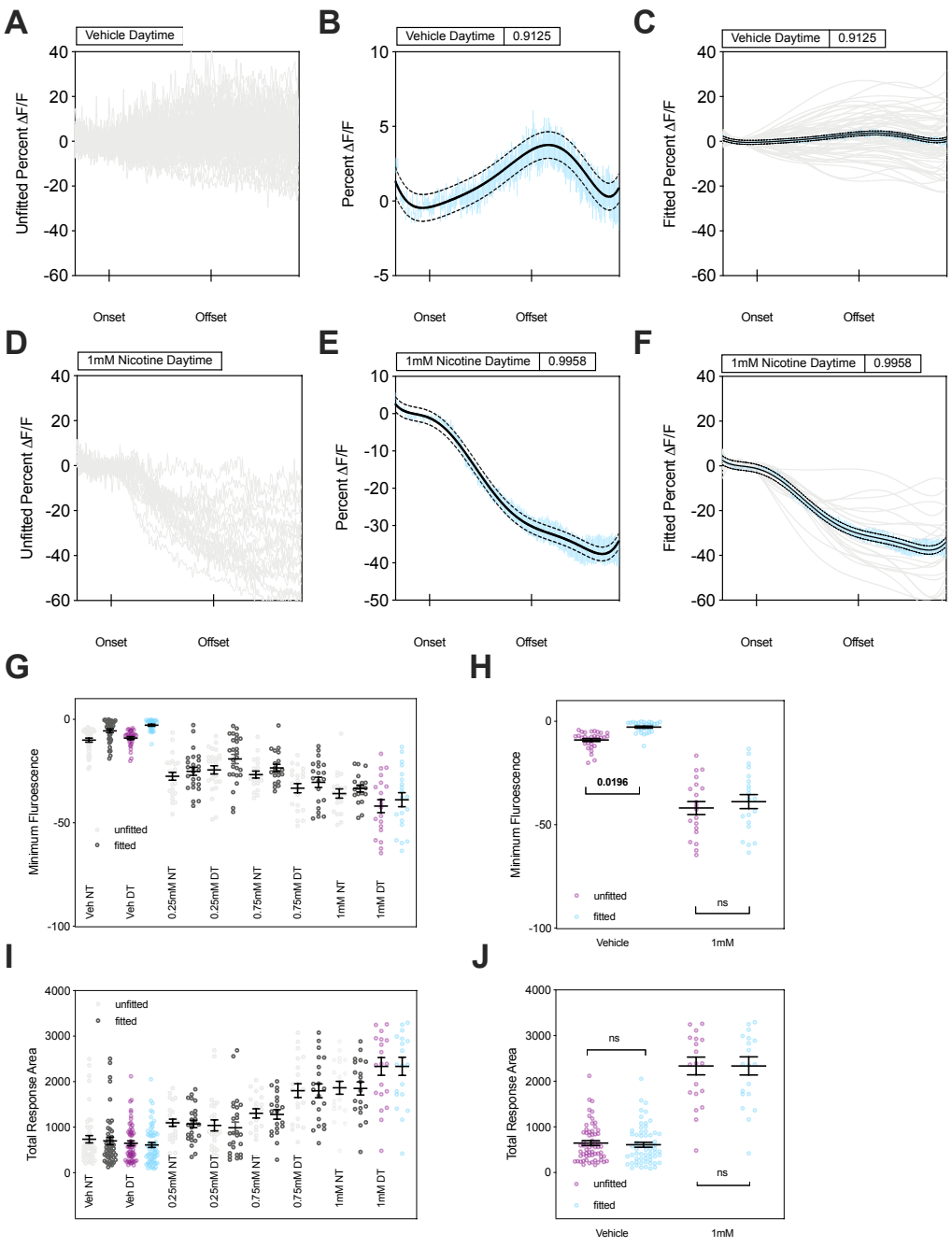

Figure 2.1. Comparison of raw and centered, sixth-order polynomial fitting of ASAP2f fluorescence time course data from LNd clock neurons applied vehicle or nicotine.

A-J. Data was gathered from sessions in which vehicle with 2uM TTX, or XmM nicotine + 2uM TTX was presented for 30sec (Onset and Offset on X-axis) preceded by 15sec and followed by 30sec HL3 wash. Results presented are collected from males of 4 independent crosses imaged across 4 separate days in which DT and NT flies were imaged alternately. Only one nicotine concentration was presented per brain. See Materials and Methods for complete fly rearing and imaging methodology. A, C. Percent deltaF/F LNd responses to vehicle (HL3) with 2uM TTX in day. Each light grey line represents one LNd with no fitting (A) or polynomial fitting (C). B. The SEM of raw traces (light blue) in A with fitted mean (solid black) and 95% confidence prediction bands (dashed black). C. Fitted individual LNd responses superimposed by the SEM and mean fitted line shown in B. D, F. Percent deltaF/F LNd responses to 1mM nicotine with 2uM TTX in day. Each light grey line represents one LNd with no fitting (A) or polynomial fitting (C). E. The SEM of raw traces (light blue) in A with fitted mean (solid black) and 95% confidence prediction bands (dashed black). F. Fitted individual LNd responses superimposed by the SEM and mean fitted line shown in E. G. The minimum fluorescence for nicotine dose response experiment from raw (dark grey) or fitted (light grey) traces. Each dot represents a single LNd's minimum fluorescence following vehicle or nicotine application. H. Minimum fluorescence values from vehicle and 1mM day experiments with fitted (blue) or raw (pink) source data. I. The total response area for nicotine dose response experiments from raw (dark grey) or fitted (light grey) traces. Each dot represents a single LNd's total response area. J. Total response area values from vehicle and 1mM day experiments with fitted (blue) or raw (pink) source data. All statistics are calculated using One-way ANOVA with Sidak correction for multiple comparisons between all groups. Significance ($p<0.05$) is reported with actual values when P-value is <0.05. Significant values are bolded. Error bars represent SEM.

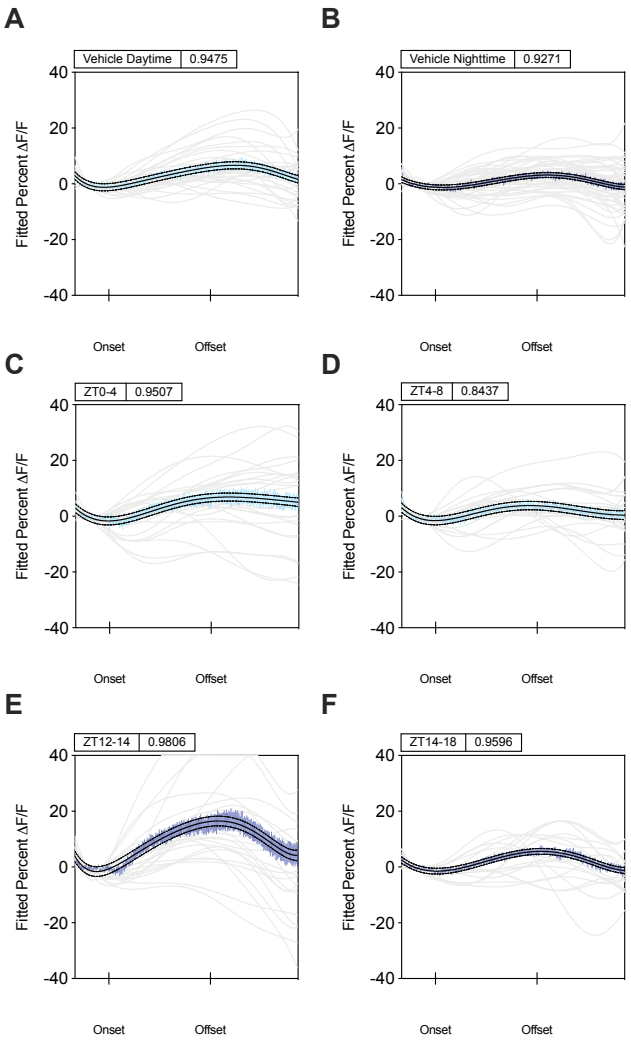

Figure 2.2. LNd responses to vehicle or 2uM TTX in day (ZT0-4, ZT4-8) and night (ZT12-14, 14-18) windows in 12:12LD.

Plots show fitted LNd responses to application of 30-seconds of HL3 vehicle or 2uM TTX from 2 days of imaging, and at least 2 independent crosses. Data was collected from each treatment group (A-F) on both days of imaging. Percent deltaF/F LNd responses to vehicle (HL3) or 2uM TTX in day (light blue, A, C, D) or night (dark blue, B, E, F). Each light grey line represents one LNd with polynomial fitting. The SEM of raw traces (blue) with fitted mean (solid black) and 95% confidence prediction bands (dashed black) is superimposed on each plot. The R^2 for the fitted mean is included on the title of each plot. Brains, LNds for each plot: A. 12, 29, B. 14, 50, C. 10,29, D. 11,29, E. 11, 30, F. 16, 30.

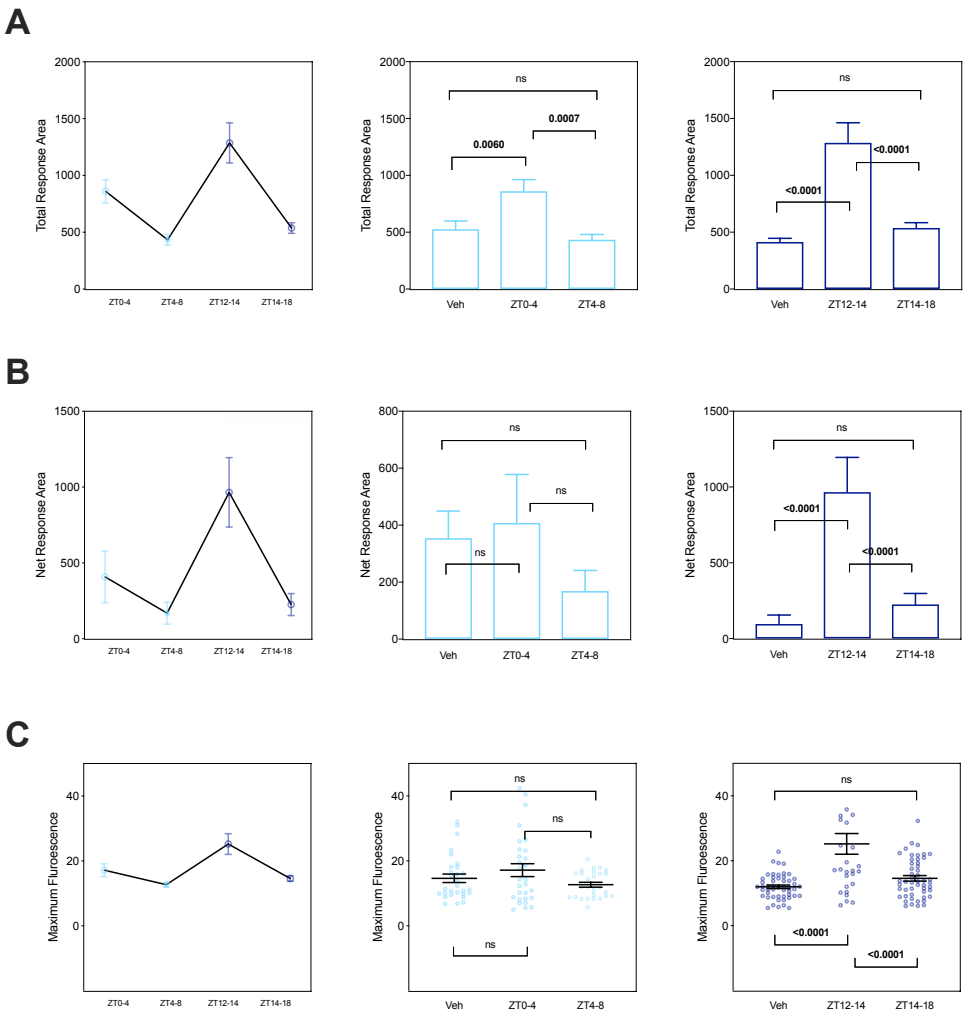

Figure 2.3. Quantification of LNd responses to vehicle, or 2uM TTX application.
A. Total response area from day (center) and night (right) experiments with fitted source data from Figure 2. The trends of all 2uM TTX application experiments are summarized in line graphs at the far left panel. B. Net response area from entire day (left), day (center), and night (right). C. Mean minimum fluorescence of fitted traces from the entire day (left), day (center) and night (right). Each dot represents a single LNd's minimum fluorescence response after vehicle or 2uM TTX application. All statistics are calculated using One-way ANOVA with Sidak correction for multiple comparisons between all groups. Significance ($p<0.05$) is reported with actual values when P-value is <0.05. Significant values are bolded. Error bars represent SEM.

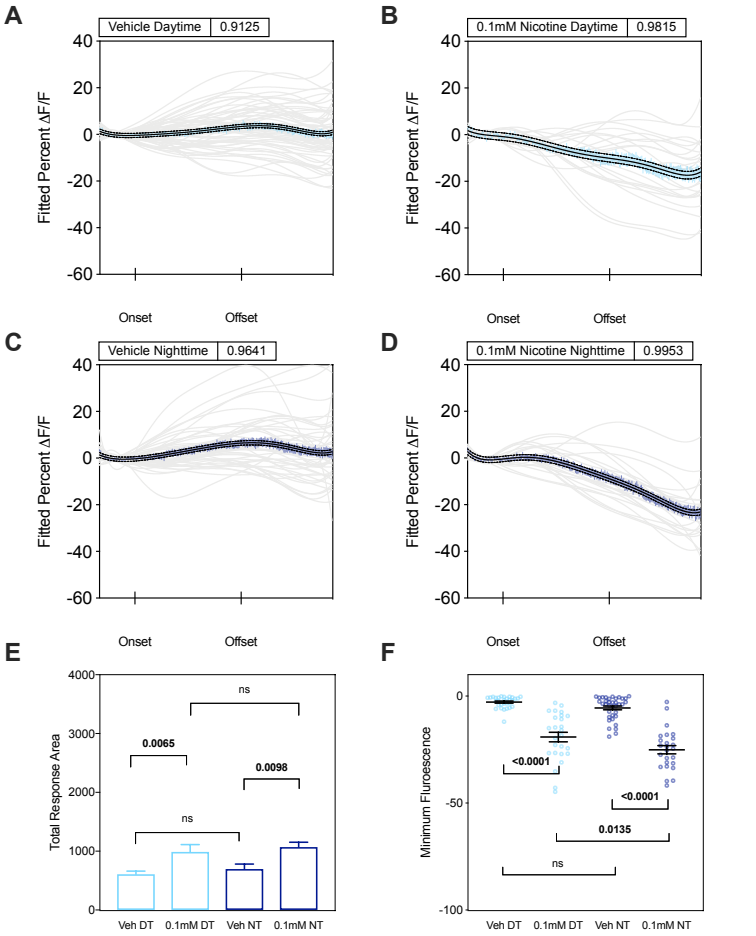

Figure 2.4. LNd responses to 0.1mM nicotine in the presence of vehicle or 2uM TTX in day (ZT4-8) and night (ZT14-18).

Each light grey line represents one LNd with polynomial fitting. The SEM of raw traces (blue) with fitted mean (solid black) and 95% confidence prediction bands (dashed black) is superimposed on each plot. The R^2 for the fitted mean is included on the title of each plot. A, C. Percent deltaF/F LNd responses to vehicle (HL3) with 2uM TTX in day (A) or night (C). B, D. Percent deltaF/F LNd responses to 0.1mM nicotine with 2uM TTX in day (B) or night (D). E. Total response area from day and night vehicle and 0.1mM nicotine experiments with fitted source data. F. Mean minimum fluorescence for nicotine dose response experiments from fitted traces. Each dot represents a single LNd's minimum fluorescence. All statistics are calculated using One-way ANOVA with Sidak correction for multiple comparisons between all groups. Significance ($p<0.05$) is reported with actual values when P-value is <0.05. Significant values are bolded. Error bars represent SEM. Brains, LNds for each plot: A. 21, 62, B. 20, 44, C. 10, 24, D. 8, 25.

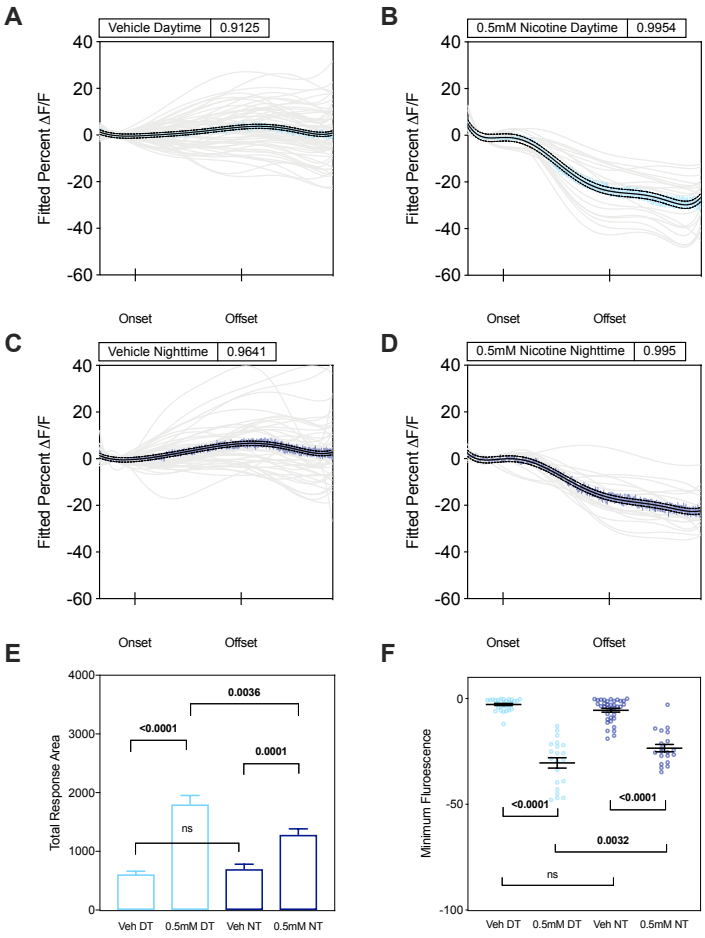

Figure 2.5. LNd responses to 0.5mM nicotine in the presence of 2uM TTX in day (ZT4-8) and night (ZT14-18).

Each light grey line represents one LNd with polynomial fitting. The SEM of raw traces (blue) with fitted mean (solid black) and 95% confidence prediction bands (dashed black) is superimposed on each plot. The R^2 for the fitted mean is included on the title of each plot. A, C. Percent deltaF/F LNd responses to vehicle (HL3) with 2uM TTX in day (A) or night (C). B, D. Percent deltaF/F LNd responses to 0.5mM nicotine with 2uM TTX in day (B) or night (D). E. Total response area from day and night vehicle and 0.5mM nicotine experiments with fitted source data. F. Mean minimum fluorescence for nicotine dose response experiments from fitted traces. Each dot represents a single LNd's minimum fluorescence. All statistics are calculated using One-way ANOVA with Sidak correction for multiple comparisons between all groups. Significance ($p<0.05$) is reported with actual values when P-value is <0.05. Significant values are bolded. Error bars represent SEM. Brains, LNds for each plot: A. 21, 62, B. 20, 44, C. 7, 22, D. 8, 20.

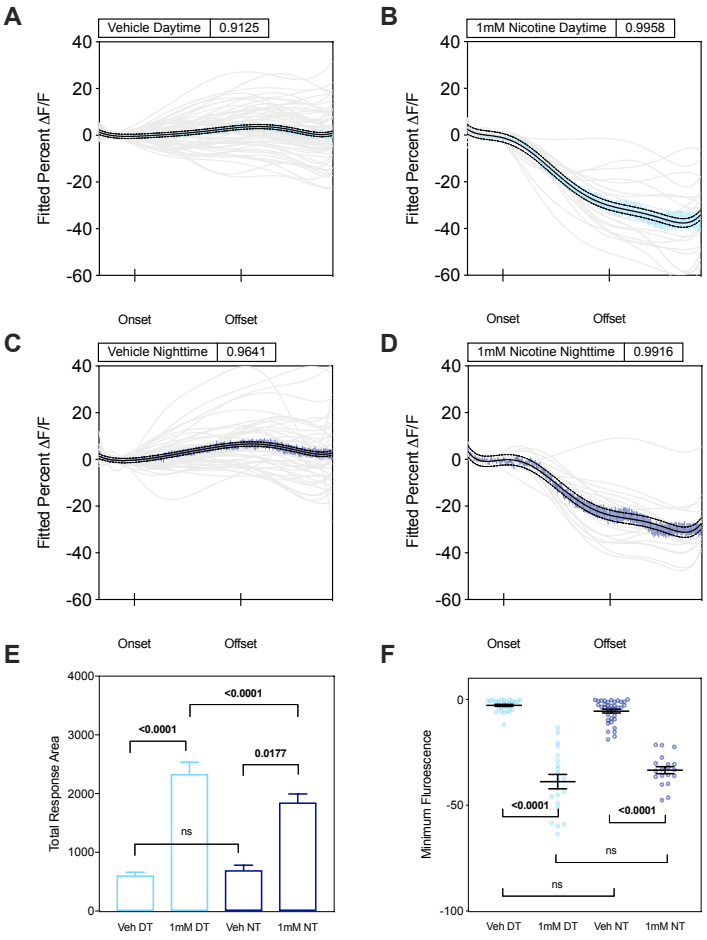

Figure 2.6. LNd responses to 1mM nicotine, 2uM TTX in day (ZT4-8) and night (ZT14-18).

Each light grey line represents one LNd with polynomial fitting. The SEM of raw traces (blue) with fitted mean (solid black) and 95% confidence prediction bands (dashed black) is superimposed on each plot. A, C. Percent deltaF/F LNd responses to vehicle (HL3) with 2uM TTX in day (A) or night (C). The R^2 for the fitted mean is included on the title of each plot. B, D. Percent deltaF/F LNd responses to 1mM nicotine with 2uM TTX in day (B) or night (D). E. Total response area from day and night vehicle and 1mM nicotine application using fitted source data. F. Mean minimum fluorescence for nicotine dose response experiments from fitted traces. Each dot represents a single LNd's minimum fluorescence. All statistics are calculated using One-way ANOVA with Sidak correction for multiple comparisons between all groups. Significance ($p<0.05$) is reported with actual values when P-value is <0.05. Significant values are bolded. Error bars represent SEM. Brains, LNds for each plot: A. 21, 62, B. 20, 44, C. 8, 20, D. 7, 20.

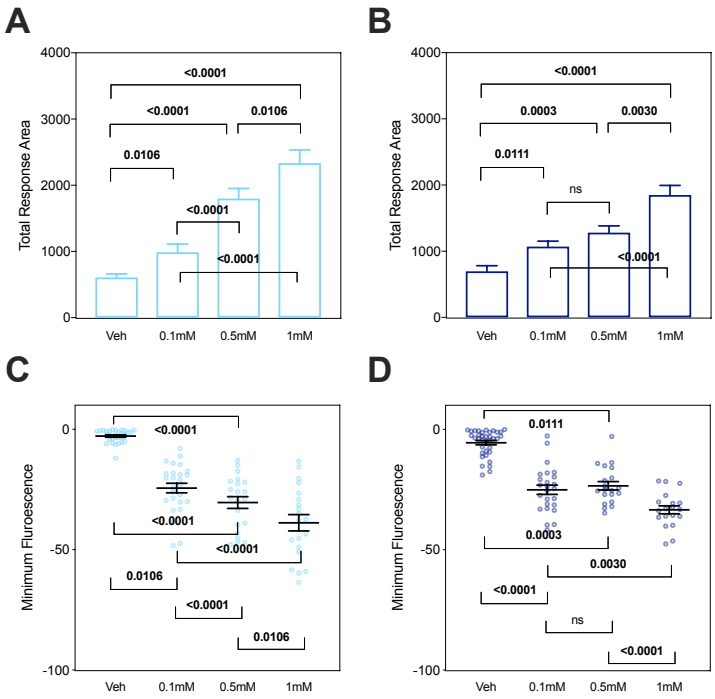

Figure 2.7. Quantification of LNd responses to 0.1mM, 0.5mM and 1mM nicotine in the presence of 2uM TTX in day (ZT4-8) and night (ZT14-18).
A, B. Total response area from day (A) and night (B) experiments with fitted source data. C, D. Mean minimum fluorescence for nicotine dose response experiments from fitted traces in day (C) or night (D). Each dot represents a single LNd's minimum fluorescence. All statistics are calculated using One-way ANOVA with Sidak correction for multiple comparisons between all groups. Significance ($p<0.05$) is reported with actual values when P-value is <0.05. Significant values are bolded. Error bars represent SEM.

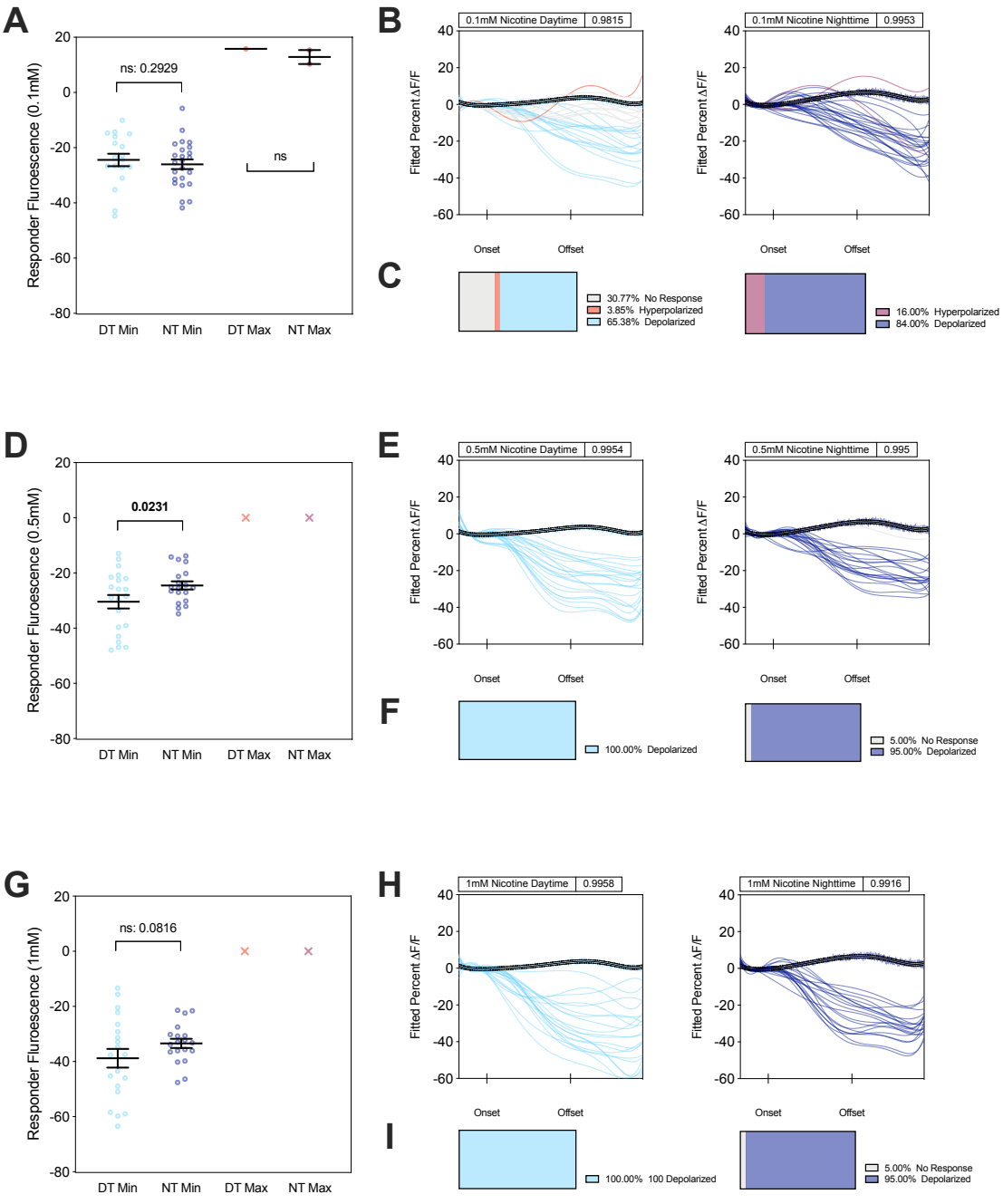

Figure 2.8. Analysis of LNd responses to nicotine application after sorting.

See Materials and Methods for sorting methodology. A, D, G. Quantification of maximum and minimum fluorescence values of LNd responses to 0.1mM, 0.5mM and 1mM nicotine with 2uM TTX in day (ZT4-8) and night (ZT14-18) excluding non-responding cells (grey, “no response”). Each dot represents a single LNd’s minimum or maximum fluorescence, E, H. Visual depiction of sorted responses to 0.1, 0.5 and 1mM nicotine in the day (left) and night (right). Non-responding cells are in grey, depolarized cells are in blue, and hyperpolarized cells in red. The relevant day or night vehicle control fitted mean and SEM is superimposed with the LNd traces. C, F, I. The percentages of cells in each category and the number of LNds, and brains used in each quantification for all nicotine dose response experiments. All statistics are calculated using an unpaired t-test with Welch’s correction between each pair. P-values are reported with actual values. Significant P-values (<0.05) are bolded.

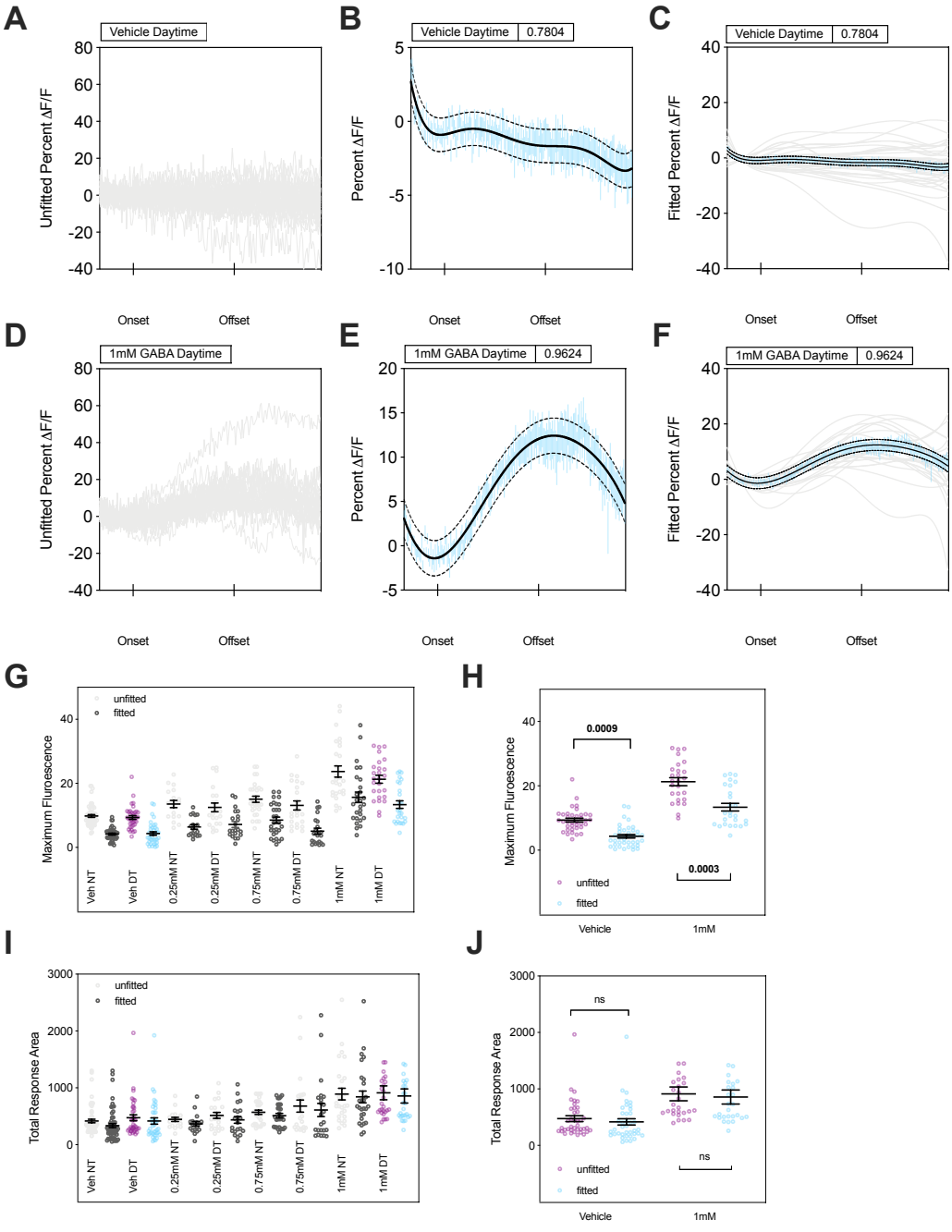

Figure 2.9. Comparison of raw and centered, sixth-order polynomial fitting of ASAP2f fluorescence time course data from LNd clock neurons applied vehicle or GABA.

A-J. Data was gathered from time courses in which vehicle with 2uM TTX, or XmM GABA + 2uM TTX was presented for 30-sec preceded (Onset and Offset on X-axis) and followed by 30sec HL3 wash. Results presented are collected from males of 4 crosses imaged across 4 separate days in which DT and NT flies were imaged alternately. Only one GABA concentration was presented per brain. See Materials and Methods for complete fly rearing and imaging methodology. A, C. Percent deltaF/F LNd responses to vehicle (HL3) with 2uM TTX in day. Each light grey line represents one LNd with no fitting (A) or polynomial fitting (C). B. The SEM of raw traces (light blue) in A with fitted mean (solid black) and 95% confidence prediction bands (dashed black). C. Fitted individual LNd responses superimposed by the SEM and mean fitted line shown in B. D, F. Percent deltaF/F LNd responses to 1mM GABA with 2uM TTX in day. Each light grey line represents one LNd with no fitting (A) or polynomial fitting (C). E. The SEM of raw traces (light blue) in A with fitted mean (solid black) and 95% confidence prediction bands (dashed black). F. Fitted individual LNd responses superimposed by the SEM and mean fitted line shown in E. G. The mean minimum fluorescence for GABA dose response experiment from raw (dark grey) or fitted (light grey) traces. Each dot represents a single LNd's minimum fluorescence. H. Mean minimum fluorescence values from vehicle and 1mM day experiments with fitted (blue) or raw (pink) source data. I. The total response area for GABA dose response experiments from raw (dark grey) or fitted (light grey) traces. Each dot represents a single LNd's total response area. J. Total response area values from vehicle and 1mM day experiments with fitted (blue) or raw (pink) source data. All statistics are calculated using One-way ANOVA with Sidak correction for multiple comparisons between all groups. Significance ($p<0.05$) is reported with actual values when P-value is <0.05. Significant values are bolded. Error bars represent SEM.

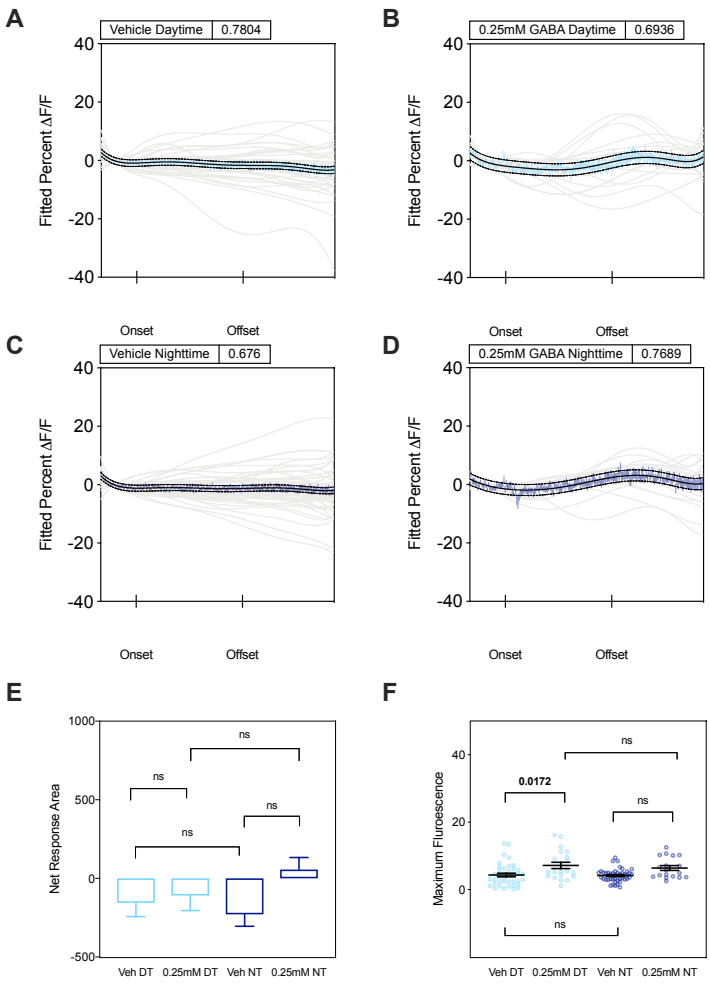

Figure 2.10. LNd responses to 0.25mM GABA in the presence of 2uM TTX in day (ZT4-8) and night (ZT14-18).

Each light grey line represents one LNd with polynomial fitting. The SEM of raw traces (blue) with fitted mean (solid black) and 95% confidence prediction bands (dashed black) is superimposed on each plot. The R^2 for the fitted mean is included on the title of each plot. A, C. Percent deltaF/F LNd responses to vehicle (HL3) with 2uM TTX in day (A) or night (C). B, D. Percent deltaF/F LNd responses to 0.25mM GABA with 2uM TTX in day (B) or night (D). E. Net response area from day and night vehicle and 0.25mM GABA experiments with fitted source data. F. Mean minimum fluorescence for GABA dose response experiments from fitted traces. Each dot represents a single LNd's minimum fluorescence. All statistics are calculated using One-way ANOVA with Sidak correction for multiple comparisons between all groups. Significance ($p<0.05$) is reported with actual values when P-value is <0.05. Significant values are bolded. Error bars represent SEM. Brains, LNds for each plot: A. 16, 39, B. 19, 66, C. 9, 21, D. 7,19.

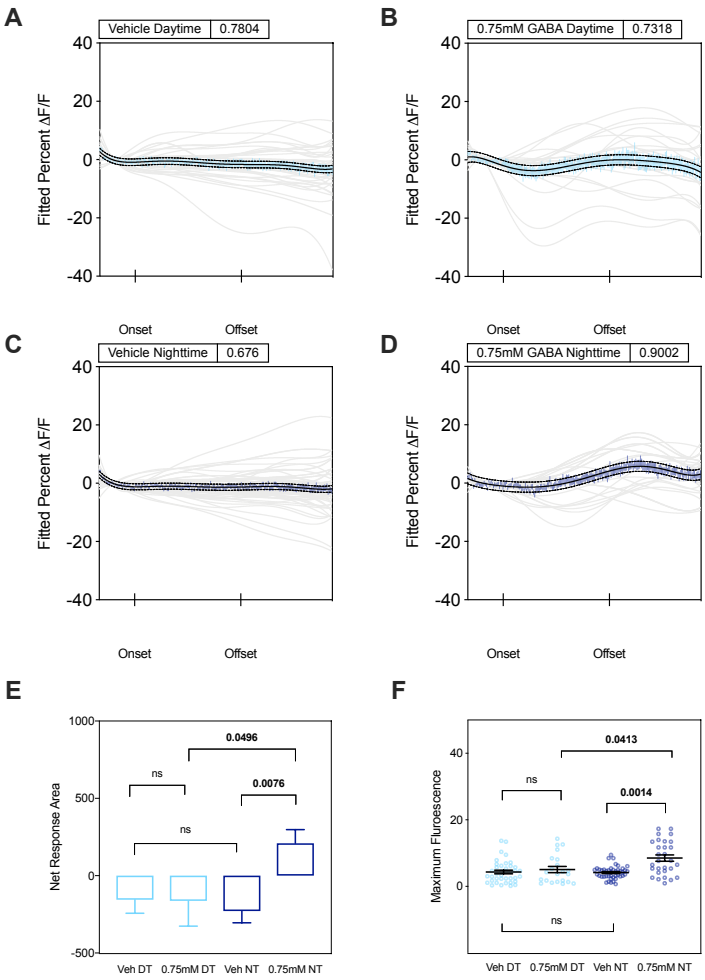

Figure 2.11. LNd responses to 0.75mM GABA, 2uM TTX in day (ZT4-8) and night (ZT14-18).

Each light grey line represents one LNd with polynomial fitting. The SEM of raw traces (blue) with fitted mean (solid black) and 95% confidence prediction bands (dashed black) is superimposed on each plot. The R^2 for the fitted mean is included on the title of each plot. A, C. Percent deltaF/F LNd responses to vehicle (HL3) with 2uM TTX in day (A) or night (C). B, D. Percent deltaF/F LNd responses to 0.75mM GABA with 2uM TTX in day (B) or night (D). E. Net response area from day and night vehicle and 0.75mM GABA experiments with fitted source data. F. Mean minimum fluorescence for GABA dose response experiments from fitted traces. Each dot represents a single LNd's minimum fluorescence. All statistics are calculated using One-way ANOVA with Sidak correction for multiple comparisons between all groups. Significance ($p<0.05$) is reported with actual values when P-value is <0.05. Significant values are bolded. Error bars represent SEM. Brains, LNds for each plot: A. 16, 39, B. 19, 66, C. 10, 23, D. 10, 29.

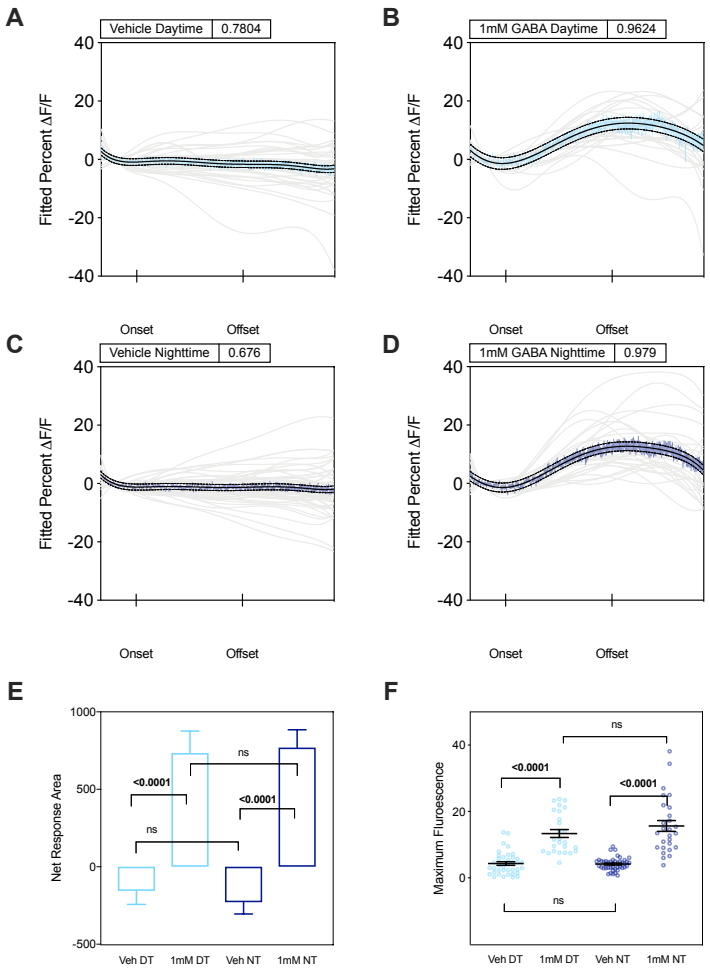

Figure 2.12. LNd responses to 1mM GABA, 2uM TTX in day (ZT4-8) and night (ZT14-18).

Each light grey line represents one LNd with polynomial fitting. The SEM of raw traces (blue) with fitted mean (solid black) and 95% confidence prediction bands (dashed black) is superimposed on each plot. The R^2 for the fitted mean is included on the title of each plot. A, C. Percent deltaF/F LNd responses to vehicle (HL3) with 2uM TTX in day (A) or night (C). B, D. Percent deltaF/F LNd responses to 1mM GABA with 2uM TTX in day (B) or night (D). E. Net response area from day and night vehicle and 1mM GABA experiments with fitted source data. F. Minimum fluorescence for GABA dose response experiments from fitted traces. Each dot represents a single LNd's minimum fluorescence. All statistics are calculated using One-way ANOVA with Sidak correction for multiple comparisons between all groups. Significance ($p<0.05$) is reported with actual values when P-value is <0.05. Significant values are bolded. Error bars represent SEM. Brains, LNds for each plot: A. 16, 39, B. 19, 66, C. 9, 27, D. 9, 27.

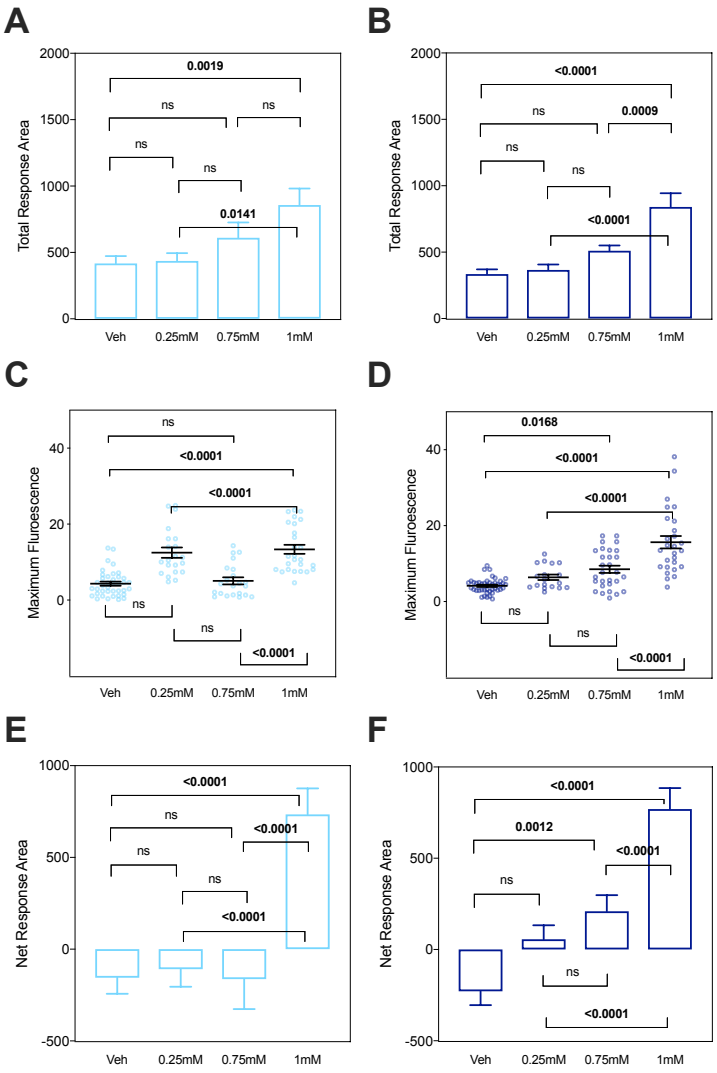

Figure 2.13. Quantification of LNd responses to 0.25mM, 0.75mM and 1mM GABA with 2uM TTX in day (ZT4-8) and night (ZT14-18).

A, B. Total response area from day (A) and night (B) experiments with fitted source data. C, D. Mean minimum fluorescence for GABA dose response experiments from fitted traces in day (C) or night (D). Each dot represents a single LNd's minimum fluorescence. E, F. Net response area from day (E) and night (F) experiments with fitted source data. All statistics are calculated using One-way ANOVA with Sidak correction for multiple comparisons between all groups. Significance ($p<0.05$) is reported with actual values when P-value is <0.05. Significant values are bolded.

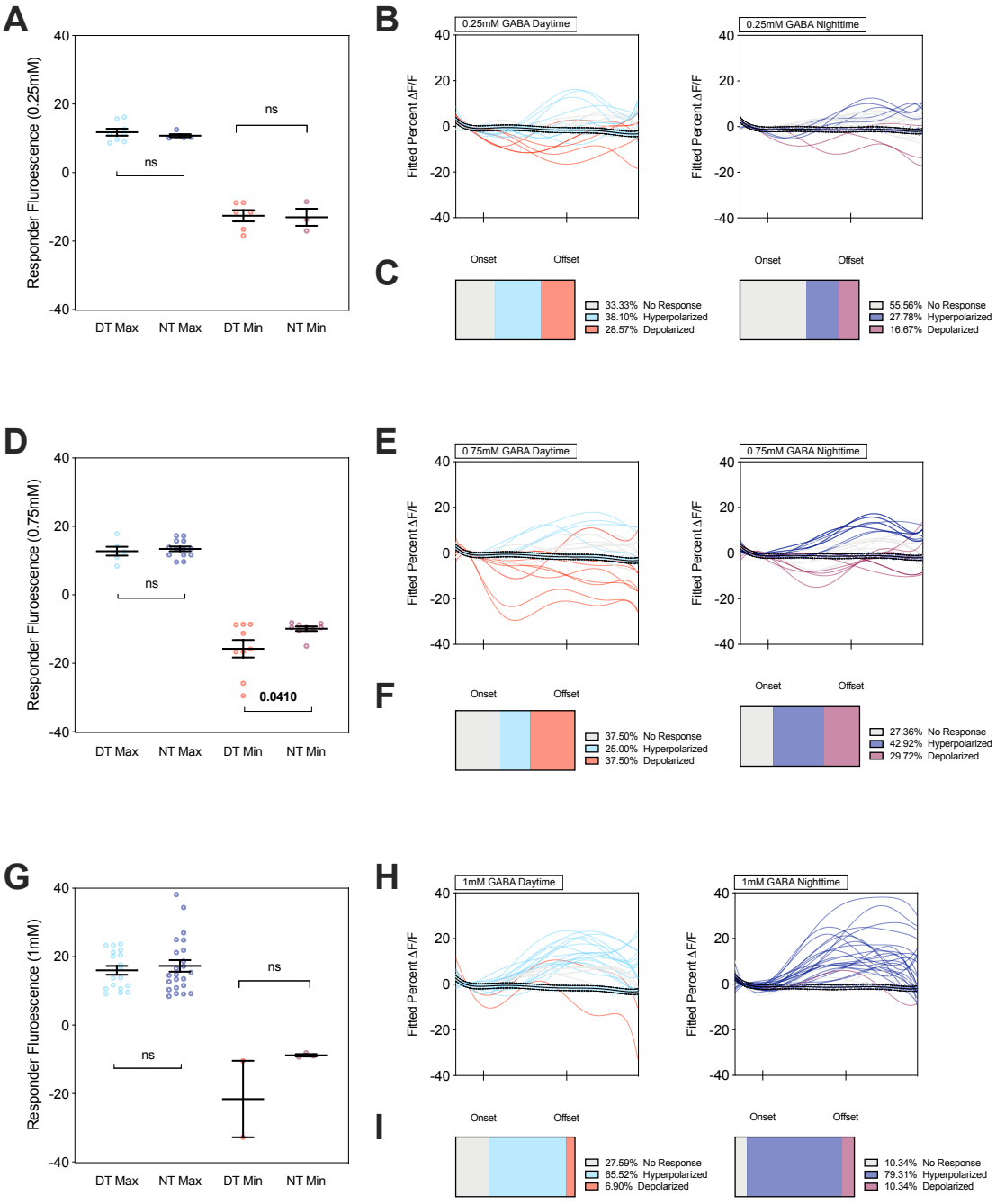

Figure 2.14. Sorting of LNd responses to GABA.

See Materials and Methods for sorting methodology. A. D. G. Quantification of mean maximum and minimum fluorescence values of LNd responses to 0.25mM, 0.75mM and 1mM GABA with 2uM TTX in day (ZT4-8) and night (ZT14-18) excluding non-responding cells (grey, “no response”). Each dot represents a single LNd’s minimum or maximum fluorescence. E, H. Visual depiction of sorted responses to 0.25mM, 0.75mM and 1mM GABA in the day (left) and night (right). Non-responding cells are in grey, depolarized cells are in red, and hyperpolarized cells in blue. The relevant day or night vehicle control fitted mean and SEM is superimposed with the LNd traces. C, F, I. The percentages of cells in each category and the number of LNds, and brains used in each quantification for all GABA dose response experiments. All statistics are calculated using an unpaired t-test with Welch’s correction between each pair. P-values are reported with actual values. Significant P-values (<0.05) are bolded.

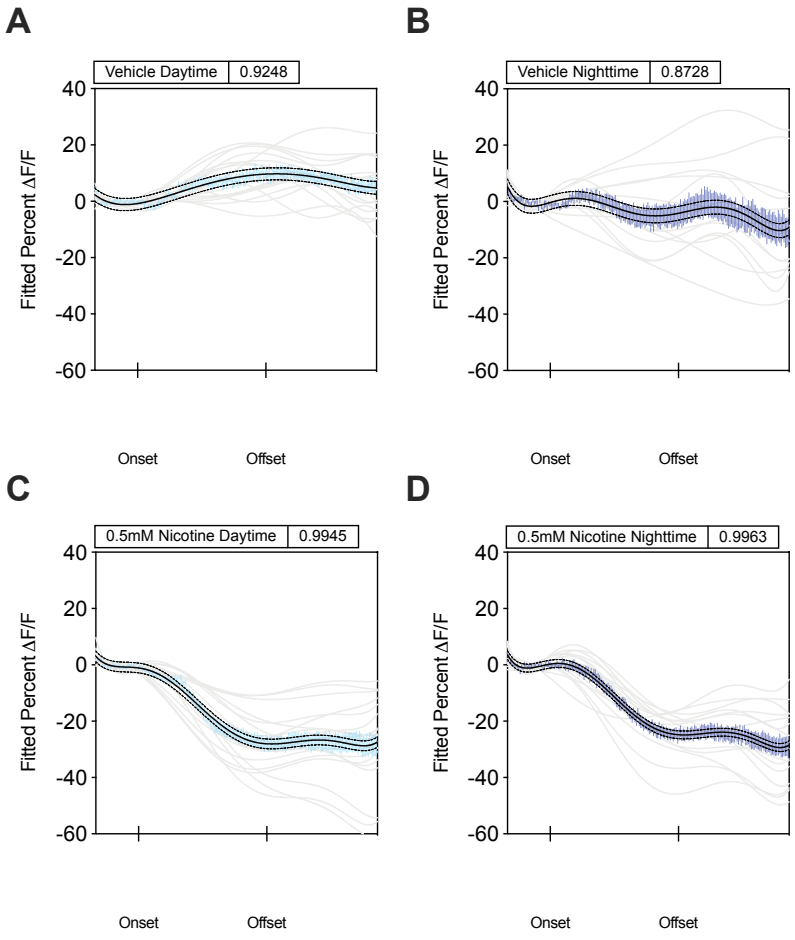

Figure 2.15. LNd responses to 0.5mM nicotine in the presence of 2uM TTX in subjective day (CT4-8) and night (CT14-18) on the first full day of constant temperature, and darkness (DD1).

Data was collected from a minimum of 2 independent crosses. Each light grey line represents one LNd with polynomial fitting. The SEM of raw traces (blue) with fitted mean (solid black) and 95% confidence prediction bands (dashed black) is superimposed on each plot. The R^2 for the fitted mean is included on the title of each plot. Error bars represent SEM. A, B. Percent deltaF/F LNd responses to vehicle (HL3) with 2uM TTX in subjective day (A) or night (B). B, D. Percent deltaF/F LNd responses to 0.5mM nicotine with 2uM TTX in subjective day (C) or night (D). Brains, LNds for each plot: A. 6, 19, B. 5, 19, C. 6, 14, D. 6, 16.

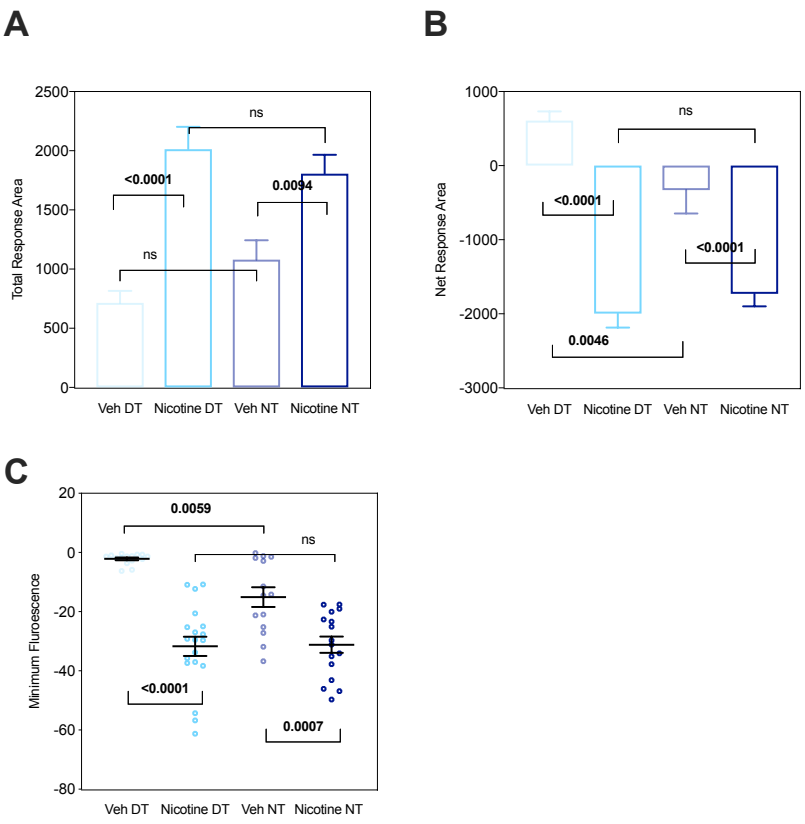

Figure 2.16. Quantification of LNd responses to 0.5mM nicotine, 2uM TTX in subjective day (light blue, CT4-8) and night (dark blue, CT14-18) on DD1.
All data is quantified from traces in Figure 15. A. Total response area from subjective day (A) and night (B) experiments with fitted source data. B. Net response area from subjective day and night vehicle and 0.5mM nicotine experiments with fitted source data. C. Mean minimum fluorescence from fitted traces. Each dot represents a single LNd's minimum fluorescence. All statistics are calculated using One-way ANOVA with Sidak correction for multiple comparisons between all groups. Significance ($p<0.05$) is reported with actual values when P-value is <0.05. Significant values are bolded.

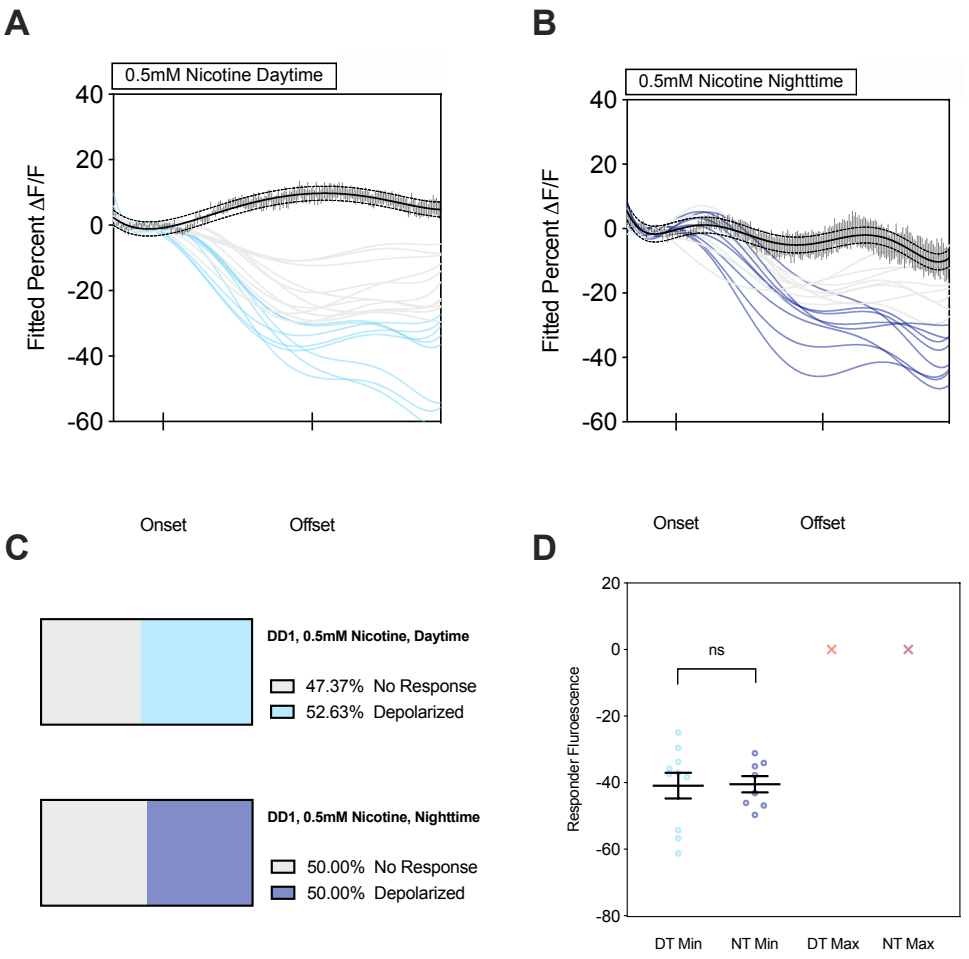

Figure 2.17. Sorted LNd responses to 0.5mM nicotine in subjective day and night on DD1. See Materials and Methods for sorting methodology. A, B. Visual depiction of sorted responses to 0.5mM nicotine in the subjective day (left) and night (right). Non-responding cells are in grey, depolarized cells are in blue, and hyperpolarized cells in red. The relevant day or night vehicle control fitted mean and SEM is superimposed with the LNd traces. C. The percentages of cells in each category and the number of LNds, and brains used in each quantification for each experiment. D. Quantification of maximum and minimum fluorescence values of LNd responses excluding non-responding cells (grey, "no response"). All statistics are calculated using an unpaired t-test with Welch's correction between each pair. P-values are reported with actual values. Significant P-values (<0.05) are bolded.

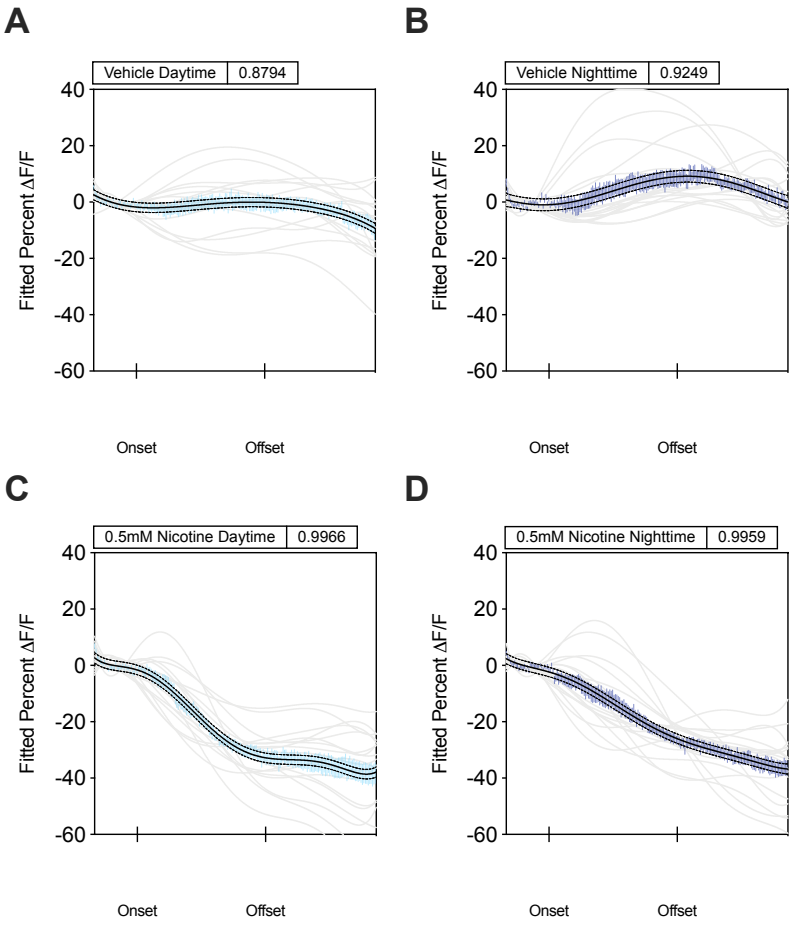

Figure 2.18. per^{01}, LNd responses to 0.5mM nicotine in the presence of 2uM TTX in day (ZT4-8) and night (ZT14-18) in 12:12 LD.

Data collected from a minimum of 2 independent crosses. Each light grey line represents one LNd with polynomial fitting. The SEM of raw traces (blue) with fitted mean (solid black) and 95% confidence prediction bands (dashed black) is superimposed on each plot. The R^2 for the fitted mean is included on the title of each plot. A, B. Percent deltaF/F LNd responses to vehicle (HL3) with 2uM TTX in day (A) or night (B). B, D. Percent deltaF/F LNd responses to 0.5mM nicotine with 2uM TTX in day (C) or night (D). Brains, LNds for each plot: A. 6, 19, B. 6, 20, C. 6, 17, D. 6, 18.

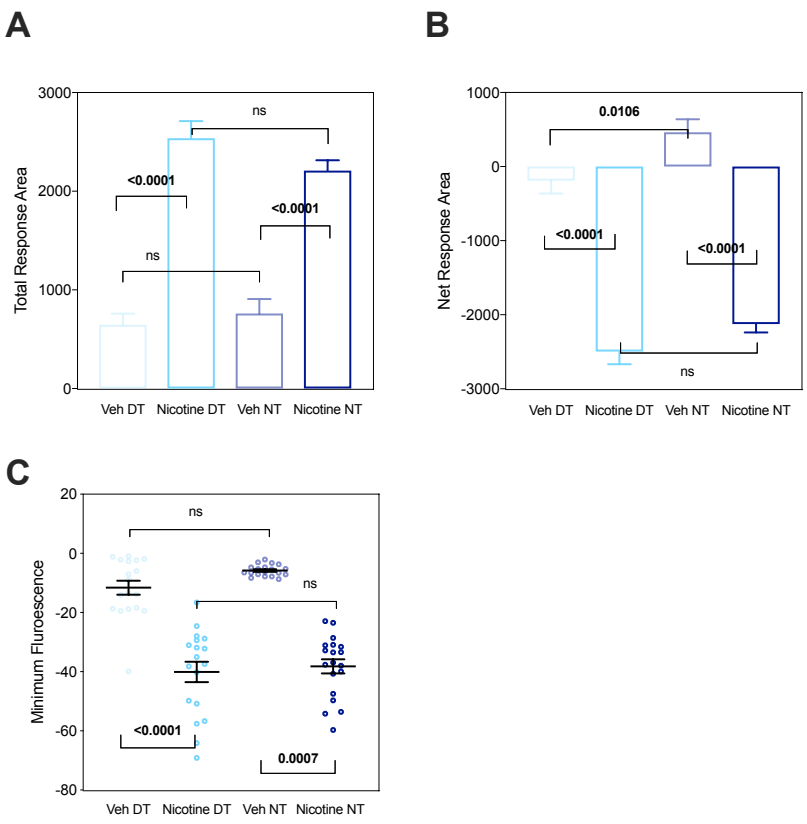

Figure 2.19. Quantification of per01, LNd responses to 0.5mM nicotine, 2uM TTX in day (light blue, ZT4-8) and night (dark blue, ZT14-18) in LD.
All data is quantified from traces in Figure 18. A. Total response area from day (A) and night (B) experiments with fitted source data. B. Net response area from day and night vehicle and 0.5mM nicotine experiments with fitted source data. C. Mean minimum fluorescence from fitted traces. Each dot represents a single LNd's minimum fluorescence. All statistics are calculated using One-way ANOVA with Sidak correction for multiple comparisons between all groups. Significance ($p<0.05$) is reported with actual values when P-value is <0.05. Significant values are bolded.

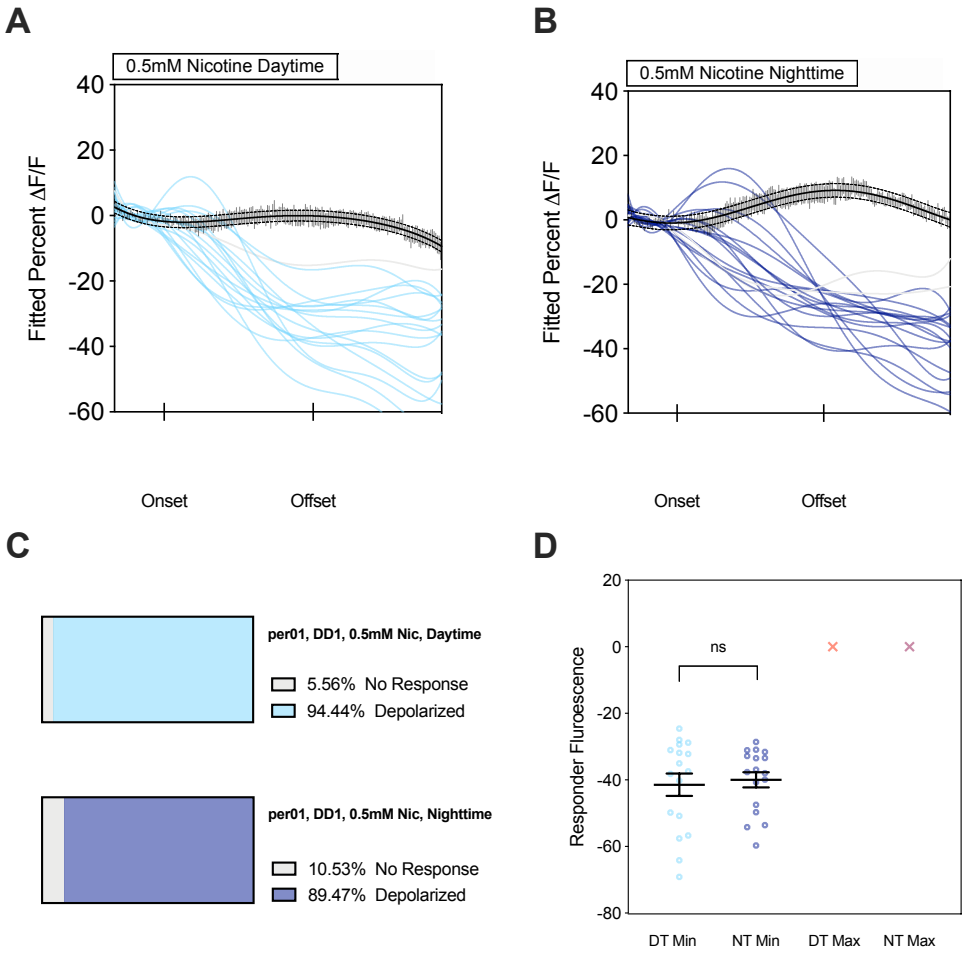

Figure 2.20. Sorting of per^{01}, LNd responses to 0.5mM nicotine in LD.
See Materials and Methods for sorting methodology. A, B. Visual depiction of sorted responses to 0.5mM nicotine in the day (left) and night (right). Non-responding cells are in grey, depolarized cells are in blue, and hyperpolarized cells in red. The relevant day or night vehicle control fitted mean and SEM is superimposed with the LNd traces. C. The percentages of cells in each category and the number of LNds, and brains used in each quantification for each experiment. D. Quantification of maximum and minimum fluorescence values of LNd responses excluding non-responding cells (grey, "no response"). All statistics are calculated using an unpaired t-test with Welch's correction between each pair. P-values are reported with actual values. Significant P-values (<0.05) are bolded.

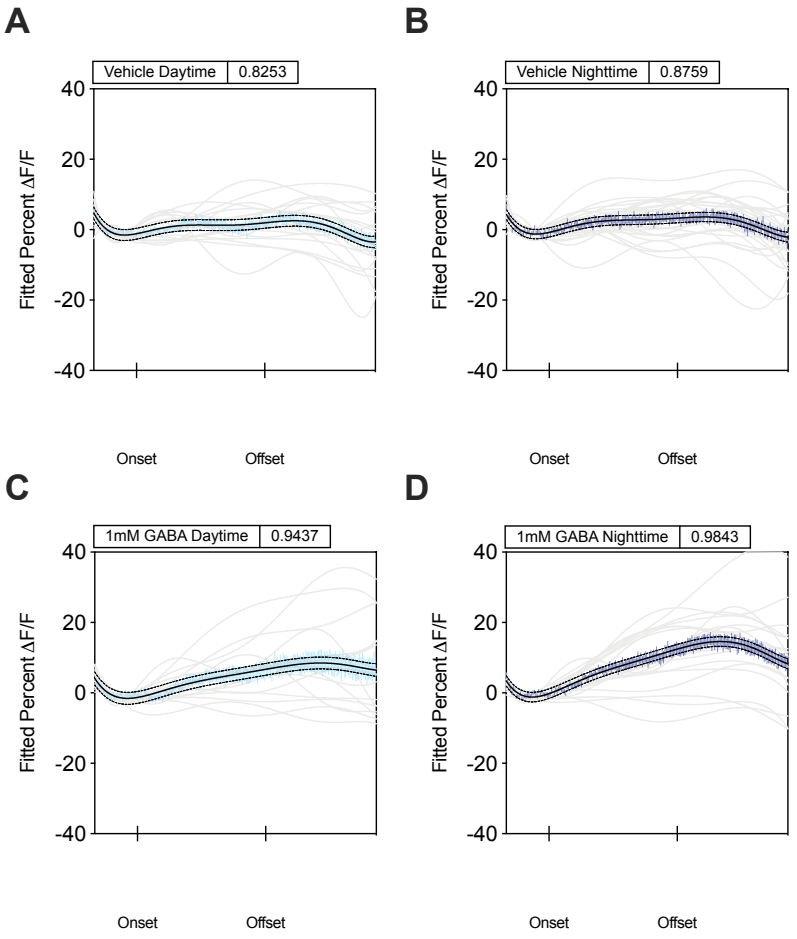

Figure 2.21. LNd responses to 1mM GABA, 2uM TTX in subjective day (CT4-8) and night (CT14-18) on the first full day of constant temperature, and darkness (DD1).
Data was collected from at least 2 independent crosses on two days of imaging. Data was collected from each treatment group (A-D) on both days of imaging. Each light grey line represents one LNd with polynomial fitting. The SEM of raw traces (blue) with fitted mean (solid black) and 95% confidence prediction bands (dashed black) is superimposed on each plot. The R^2 for the fitted mean is included on the title of each plot. A, B. Percent deltaF/F LNd responses to vehicle (HL3) with 2uM TTX in subjective day (A) or night (B). B, D. Percent deltaF/F LNd responses to 1mM GABA with 2uM TTX in subjective day (C) or night (D). Brains, LNds for each plot: A. 8, 21, B. 8, 20, C. 8, 17, D. 9, 32.

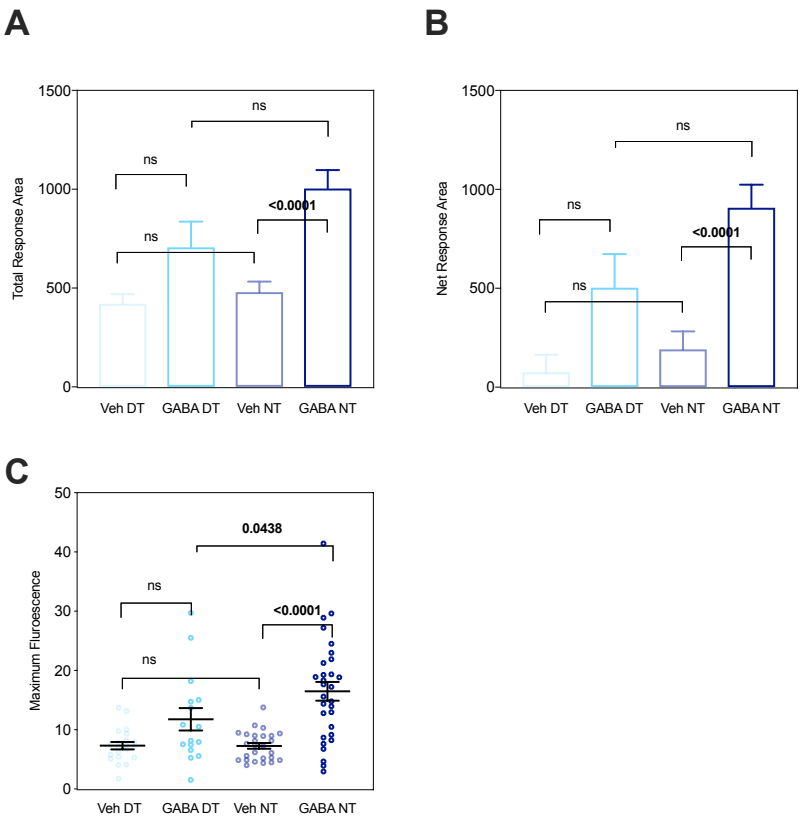

Figure 2.22. Quantification of LNd responses to 1mM GABA, 2uM TTX in subjective day (light blue, CT4-8) and night (dark blue, CT14-18) on DD1.
All data is quantified from traces in Figure 21. A. Total response area from subjective day (A) and night (B) experiments with fitted source data. B. Net response area from subjective day and night vehicle and 1mM GABA experiments with fitted source data. C. Mean minimum fluorescence from fitted traces. Each dot represents a single LNd's minimum fluorescence. All statistics are calculated using One-way ANOVA with Sidak correction for multiple comparisons between all groups. Significance ($p<0.05$) is reported with actual values when P-value is <0.05. Significant values are bolded.

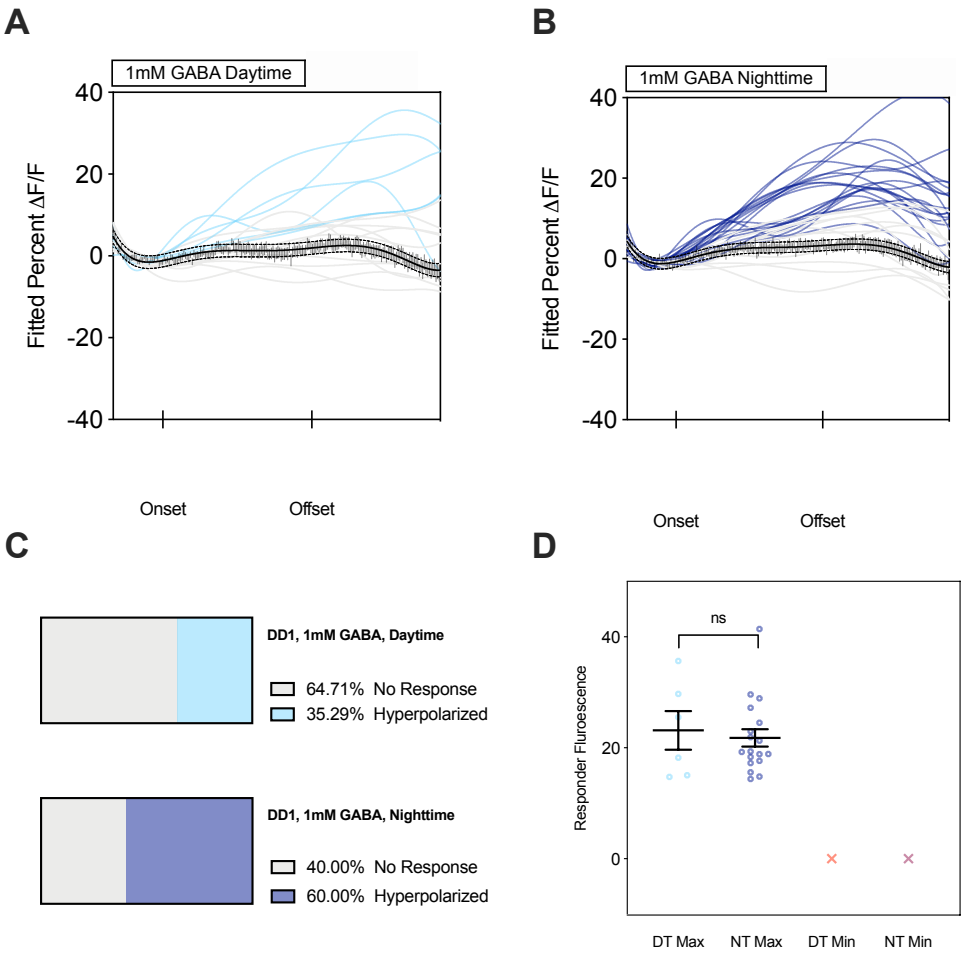

Figure 2.23. Sorted LNd responses to 1mM GABA on DD1.
See Materials and Methods for sorting methodology. A, B. Visual depiction of sorted responses to 0.5mM nicotine in the subjective day (left) and night (right). Non-responding cells are in grey, depolarized cells are in red, and hyperpolarized cells in blue. The relevant day or night vehicle control fitted mean and SEM is superimposed with the LNd traces. C. The percentages of cells in each category and the number of LNds, and brains used in each quantification for each experiment. D. Quantification of mean maximum and minimum fluorescence values of LNd responses excluding non-responding cells (grey, “no response”). All statistics are calculated using an unpaired t-test with Welch’s correction between each pair. P-values are reported with actual values. Significant P-values (<0.05) are bolded.

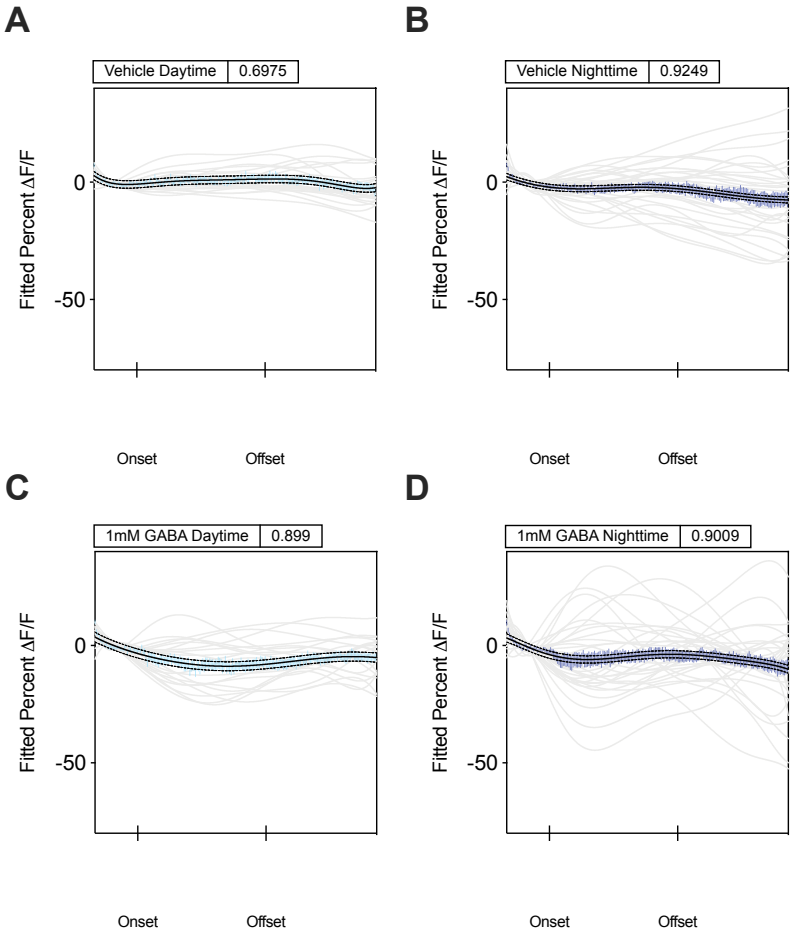

Figure 2.24. per^{01}, LNd responses to 1mM GABA, 2uM TTX in subjective day (CT4-8) and night (CT14-18) on the first full day of constant temperature, and darkness (DD1). Data was collected from at least two independent crosses over two days of imaging. Data was collected from each treatment group (A-D) on both days of imaging. Each light grey line represents one LNd with polynomial fitting. The SEM of raw traces (blue) with fitted mean (solid black) and 95% confidence prediction bands (dashed black) is superimposed on each plot. The R^2 for the fitted mean is included on the title of each plot. A, B. Percent deltaF/F LNd responses to vehicle (HL3) with 2uM TTX in subjective day (A) or night (B). B, D. Percent deltaF/F LNd responses to 1mM GABA with 2uM TTX in subjective day (C) or night (D). Brains, LNds for each plot: A. 8, 25, B. 9, 23, C. 8, 25, D. 10, 34.

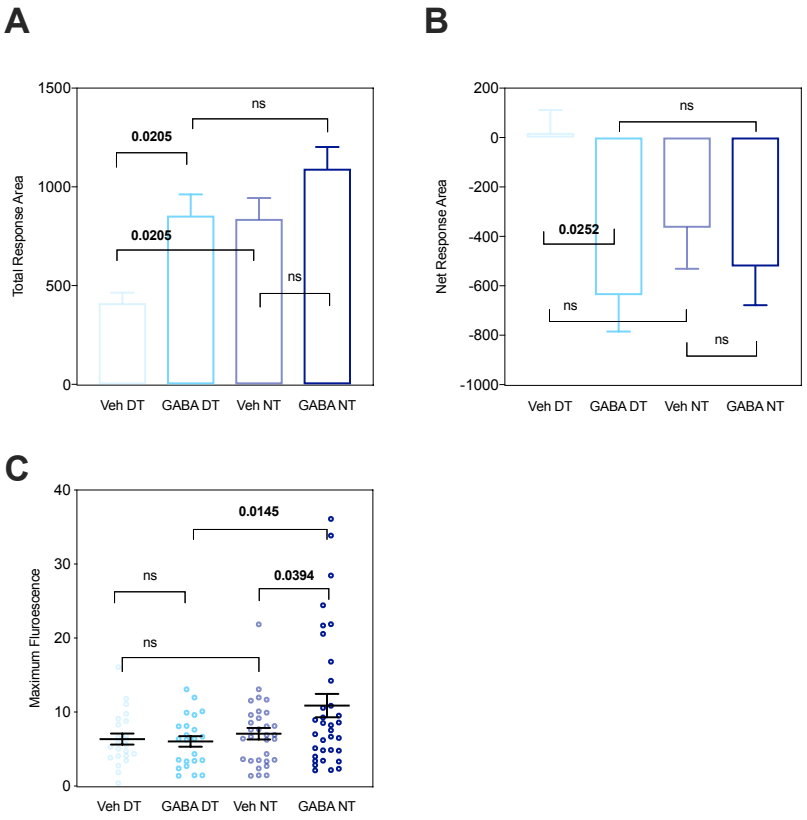

Figure 2.25. Quantification of per^{01}, LNd responses to 1mM GABA with 2uM TTX in subjective day (light blue, CT4-8) and night (dark blue, CT14-18) on DD1.
All data is quantified from traces in Figure 24. A. Total response area from subjective day (A) and night (B) experiments with fitted source data. B. Net response area from subjective day and night vehicle and 1mM GABA experiments with fitted source data. C. Minimum fluorescence from fitted traces. Each dot represents a single LNd's minimum fluorescence. All statistics are calculated using One-way ANOVA with Sidak correction for multiple comparisons between all groups. Significance ($p<0.05$) is reported with actual values when P-value is <0.05. Significant values are bolded.

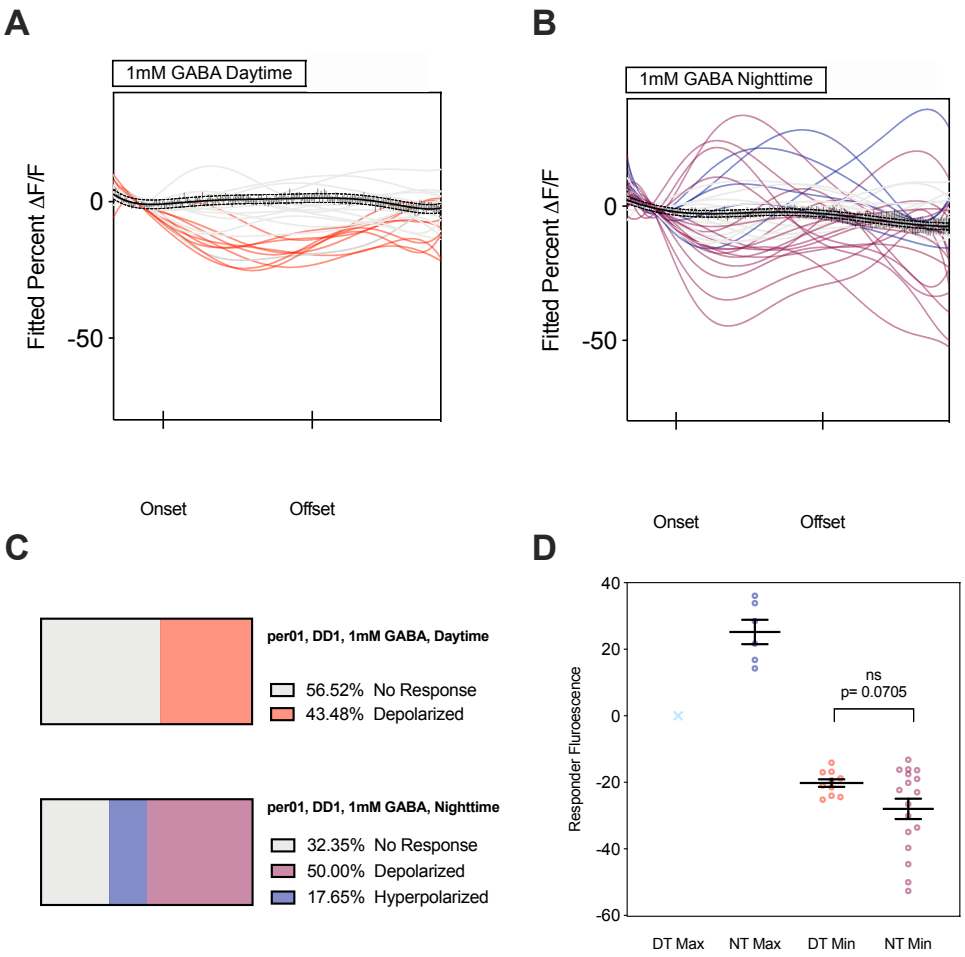

Figure 2.26. Sorted per^{01}, LNd responses to 1mM GABA on DD1.
See Materials and Methods for sorting methodology. A, B. Visual depiction of sorted responses to 1mM GABA in the subjective day (left) and night (right). Non-responding cells are in grey, depolarized cells are in red, and hyperpolarized cells in blue. The relevant day or night vehicle control fitted mean and SEM is superimposed with the LNd traces. C. The percentages of cells in each category and the number of LNds, and brains used in each quantification for each experiment. D. All statistics are calculated using an unpaired t-test with Welch's correction between each pair. P-values are reported with actual values. Significant P-values (<0.05) are bolded.

References

Abruzzi, K.C., Zadina, A., Luo, W., Wiyanto, E., Rahman, R., Guo, F., Shafer, O., and Rosbash, M. (2017). RNA-seq analysis of *Drosophila* clock and non-clock neurons reveals neuron-specific cycling and novel candidate neuropeptides. PLoS Genet. 13.

Agosto, J., Choi, J.C., Parisky, K.M., Stilwell, G., Rosbash, M., and Griffith, L.C. (2008). Modulation of GABAA receptor desensitization uncouples sleep onset and maintenance in *Drosophila*. Nat. Neurosci. 11, 354–359.

Albers, H.E., Walton, J.C., Gamble, K.L., McNeill, J.K., and Hummer, D.L. (2017). The dynamics of GABA signaling: Revelations from the circadian pacemaker in the suprachiasmatic nucleus. Front. Neuroendocrinol. 44, 35–82.

Allada, R., and Chung, B.Y. (2010). Circadian organization of behavior and physiology in *Drosophila*. Annu. Rev. Physiol. 72, 605–624.

An, S., Harang, R., Meeker, K., Granados-Fuentes, D., Tsai, C.A., Mazuski, C., Kim, J., Doyle, F.J., Petzold, L.R., and Herzog, E.D. (2013). A neuropeptide speeds circadian entrainment by reducing intercellular synchrony. Proc. Natl. Acad. Sci.

Aton, S.J., Colwell, C.S., Harmar, A.J., Waschek, J., and Herzog, E.D. (2005). Vasoactive intestinal polypeptide mediates circadian rhythmicity and synchrony in mammalian clock neurons. Nat. Neurosci. 8, 476–483.

Aton, S.J., Huettner, J.E., Straume, M., and Herzog, E.D. (2006). GABA and Gi/o differentially control circadian rhythms and synchrony in clock neurons. Proc. Natl. Acad. Sci. U. S. A. 103, 19188–19193.

Buhr, E.D., Yoo, S.H., and Takahashi, J.S. (2010). Temperature as a universal resetting cue for mammalian circadian oscillators. Science. 330, 379–385.

Cao, G., and Nitabach, M.N. (2008). Circadian Control of Membrane Excitability in *Drosophila melanogaster* Lateral Ventral Clock Neurons. J. Neurosci.

Challet, E., Caldelas, I., Graff, C., and Pévet, P. (2003). Synchronization of the molecular clockwork by light- and food-related cues in mammals. Biol. Chem.

Chen, T.W., Wardill, T.J., Sun, Y., Pulver, S.R., Renninger, S.L., Baohan, A., Schreiter, E.R., Kerr, R.A., Orger, M.B., Jayaraman, V., et al. (2013). Ultrasensitive fluorescent proteins for imaging neuronal activity. Nature.

Choi, H.J., Lee, C.J., Schroeder, A., Kim, Y.S., Jung, S.H., Kim, J.S., Kim, D.Y., Son, E.J., Han, H.C., Hong, S.K., et al. (2008). Excitatory Actions of GABA in the Suprachiasmatic Nucleus. J. Neurosci. 28, 5450–5459.

Chung, B.Y., Kilman, V.L., Keath, J.R., Pitman, J.L., and Allada, R. (2009). The GABAA Receptor RDL Acts in Peptidergic PDF Neurons to Promote Sleep in *Drosophila*. Curr. Biol. 19, 386–390.

Cusumano, P., Klarsfeld, A., Chélot, E., Picot, M., Richier, B., and Rouyer, F. (2009). PDF-modulated visual inputs and cryptochrome define diurnal behavior in *Drosophila*. Nat. Neurosci.

DeWoskin, D., Myung, J., Belle, M.D.C., Piggins, H.D., Takumi, T., and Forger, D.B. (2015). Distinct roles for GABA across multiple timescales in mammalian circadian timekeeping. Proc. Natl. Acad. Sci. 112, E3911–E3919.

Dissel, S., Hansen, C.N., Özkaya, Ö., Hemsley, M., Kyriacou, C.P., and Rosato, E. (2014). The logic of circadian organization in *Drosophila*. Curr. Biol.

Dunlap, J.C. (1999). Molecular Bases for Circadian Clocks Review review word for the late 80s and early 90s would have. Cell.

Enoki, R., Oda, Y., Mieda, M., Ono, D., Honma, S., and Honma, K. (2017). Synchronous circadian voltage rhythms with asynchronous calcium rhythms in the suprachiasmatic nucleus. Proc. Natl. Acad. Sci. 114, E2476–E2485.

Evans, J.A., Leise, T.L., Castanon-Cervantes, O., and Davidson, A.J. (2013). Dynamic Interactions Mediated by Nonredundant Signaling Mechanisms Couple Circadian Clock Neurons. Neuron 80, 973–983.

Evans, J.A., Suen, T.C., Callif, B.L., Mitchell, A.S., Castanon-Cervantes, O., Baker, K.M., Kloehn, I., Baba, K., Teubner, B.J.W., Ehlen, J.C., et al. (2015). Shell neurons of the master circadian clock coordinate the phase of tissue clocks throughout the brain and body. BMC Biol.

Flourakis, M., and Allada, R. (2015). Patch-clamp electrophysiology in *Drosophila* circadian pacemaker neurons. Methods Enzymol.

Freeman, G.M., Krock, R.M., Aton, S.J., Thaben, P., and Herzog, E.D. (2013). GABA networks destabilize genetic oscillations in the circadian pacemaker. Neuron 78, 799–806.

Gmeiner, F., Kolodziejczyk, A., Yoshii, T., Rieger, D., Nassel, D.R., and Helfrich-Forster, C. (2013). GABAB receptors play an essential role in maintaining sleep during the second half of the night in *Drosophila melanogaster*. J. Exp. Biol. 216, 3837–3843.

Golombek, D.A., and Rosenstein, R.E. (2010). Physiology of Circadian Entrainment. Physiol. Rev.

Grima, B., Chélot, E., Xia, R., and Rouyer, F. (2004). Morning and evening peaks of activity rely on different clock neurons of the *Drosophila* brain. Nature.

Gummadova, J.O., Coutts, G.A., and Glossop, N.R.J. (2009). Analysis of the *Drosophila* clock promoter reveals heterogeneity in expression between subgroups of central oscillator cells and identifies a novel enhancer region. J. Biol. Rhythms.

Guo, F., Cerullo, I., Chen, X., and Rosbash, M. (2014). PDF neuron firing phase-shifts key circadian activity neurons in *Drosophila*. Elife.

Guo, F., Yu, J., Jung, H.J., Abruzzi, K.C., Luo, W., Griffith, L.C., and Rosbash, M. (2016). Circadian neuron feedback controls the *Drosophila* sleep-activity profile. Nature.

Hamasaka, Y., Wegener, C., and Nässel, D.R. (2005). GABA modulates *Drosophila* circadian clock neurons via GABAB receptors and decreases in calcium. J. Neurobiol. 65, 225–240.

Helfrich-Förster, C. (2001). The locomotor activity rhythm of *Drosophila melanogaster* is controlled by a dual oscillator system. J. Insect Physiol.

Helfrich-Förster, C. (2003). The neuroarchitecture of the circadian clock in the brain of *Drosophila melanogaster*. Microsc. Res. Tech.

Helfrich-Förster, C., Yoshii, T., Wülbeck, C., Grieshaber, E., Rieger, D., Bachleitner, W., Cusumano, P., and Rouyer, F. (2007). The lateral and dorsal neurons of *Drosophila melanogaster*: New insights about their morphology and function. In Cold Spring Harbor Symposia on Quantitative Biology.

Hendricks, J.C., and Sehgal, A. (2004). Why a fly? Using *Drosophila* to understand the genetics of circadian rhythms and sleep. Sleep.

Hermann-Luibl, C., and Helfrich-Förster, C. (2015). Clock network in *Drosophila*. Curr. Opin. Insect Sci.

Hermann-Luibl, C., Yoshii, T., Senthilan, P.R., Dircksen, H., and Helfrich-Forster, C. (2014). The Ion Transport Peptide Is a New Functional Clock Neuropeptide in the Fruit Fly *Drosophila melanogaster*. J. Neurosci.

Hermann, C., Dircksen, H., Helfrich-Forster, C., and Yoshii, T. (2010). The neuropeptides PDF, NPF and ITP operate synergistically in the endogenous clock of *Drosophila melanogaster*. J. Neurogenet.

Herzog, E.D. (2007). Neurons and networks in daily rhythms. Nat. Rev. Neurosci. 8, 790 802.

Herzog, E.D., Aton, S.J., Numano, R., Sakaki, Y., and Tei, H. (2004). Temporal Precision in the Mammalian Circadian System: A Reliable Clock from Less Reliable Neurons. J. Biol. Rhythms.

Houben, T., Coomans, C.P., and Meijer, J.H. (2014). Regulation of circadian and acute activity levels by the murine suprachiasmatic nuclei. PLoS One.

Im, S.H., Li, W., and Taghert, P.H. (2011). PDFR and CRY Signaling Converge in a Subset of Clock Neurons to Modulate the Amplitude and Phase of Circadian Behavior in *Drosophila*. PLoS One 6, e18974.

Itri, J. (2004). Circadian Rhythm in Inhibitory Synaptic Transmission in the Mouse Suprachiasmatic Nucleus. J. Neurophysiol.

Johard, H.A.D., Yoishii, T., Dircksen, H., Cusumano, P., Rouyer, F., Helfrich-Förster, C., and Nässel, D.R. (2009). Peptidergic clock neurons in *Drosophila*: Ion transport peptide and short neuropeptide F in subsets of dorsal and ventral lateral neurons. J. Comp. Neurol.

Jones, A.K., Brown, L.A., and Sattelle, D.B. (2007). Insect nicotinic acetylcholine receptor gene families: From genetic model organism to vector, pest and beneficial species. In Invertebrate Neuroscience.

Kingsbury, N.J., Taylor, S.R., and Henson, M.A. (2016). Inhibitory and excitatory networks balance cell coupling in the suprachiasmatic nucleus: A modeling approach. J. Theor. Biol. 397, 135–144.

Kolodziejczyk, A., Sun, X., Meinertzhagen, I.A., and Nässel, D.R. (2008). Glutamate, GABA and acetylcholine signaling components in the lamina of the *Drosophila* visual system. PLoS One.

Konopka, R.J., and Benzer, S. (1971). Clock mutants of *Drosophila melanogaster*. Proc. Natl. Acad. Sci. U. S. A.

Lelito, K.R., and Shafer, O.T. (2012). Reciprocal cholinergic and GABAergic modulation of the small ventrolateral pacemaker neurons of *Drosophila*'s circadian clock neuron network. J. Neurophysiol.

Liang, X., Holy, T.E., Taghert, P.H., Lim, C., Allada, R., Partch, C.L., Green, C.B., Takahashi, J.S., Welsh, D.K., Takahashi, J.S., et al. (2016). Synchronous *Drosophila* circadian pacemakers display nonsynchronous Ca2+ rhythms in vivo. Science.

Macdonald, R.L., and Olsen, R.W. (1994). GABAA receptor channels. Annu. Rev. Neurosci.

McCarthy, E. v., Wu, Y., DeCarvalho, T., Brandt, C., Cao, G., and Nitabach, M.N. (2011). Synchronized Bilateral Synaptic Inputs to *Drosophila melanogaster* Neuropeptidergic Rest/Arousal Neurons. J. Neurosci.

Muraro, N.I., and Ceriani, M.F. (2015). Acetylcholine from Visual Circuits Modulates the

Activity of Arousal Neurons in *Drosophila*. J. Neurosci.
Nitabach, M.N. (2006). Electrical Hyperexcitation of Lateral Ventral Pacemaker Neurons Desynchronizes Downstream Circadian Oscillators in the Fly Circadian Circuit and Induces Multiple Behavioral Periods. J. Neurosci. 26, 479–489.
Nitabach, M.N., and Taghert, P.H. (2008). Organization of the *Drosophila* Circadian Control Circuit. Curr. Biol. 18.
Nitabach, M.N., Blau, J., and Holmes, T.C. (2002). Electrical silencing of *Drosophila* pacemaker neurons stops the free-running circadian clock. Cell.
Parisky, K.M., Agosto, J., Pulver, S.R., Shang, Y., Kuklin, E., Hodge, J.J.L., Kang, K., Liu, X., Garrity, P.A., Rosbash, M., et al. (2008). PDF Cells Are a GABA-Responsive Wake-Promoting Component of the *Drosophila* Sleep Circuit. Neuron 60, 672–682.
Park, D., and Griffith, L.C. (2006). Electrophysiological and Anatomical Characterization of PDF-Positive Clock Neurons in the Intact Adult *Drosophila* Brain. J. Neurophysiol.
Pittendrigh, C.S., and Daan, S. (1976). A functional analysis of circadian pacemakers in nocturnal rodents. J. Comp. Physiol. A 106, 333–355.
Reghunandanan, V., and Reghunandanan, R. (2006). Neurotransmitters of the suprachiasmatic nuclei. J. Circadian Rhythms.
Renn, S.C.P., Park, J.H., Rosbash, M., Hall, J.C., and Taghert, P.H. (1999). A pdf neuropeptide gene mutation and ablation of PDF neurons each cause severe abnormalities of behavioral circadian rhythms in *Drosophila*. Cell.
Restifo, L.L., and White, K. (1990). Molecular and genetic approaches to neurotransmitter and neuromodulator systems in *Drosophila*. Adv. In Insect Phys.
Rohling, J.H.T., vanderLeest, H.T., Michel, S., Vansteensel, M.J., and Meijer, J.H. (2011). Phase resetting of the mammalian circadian clock relies on a rapid shift of a small population of pacemaker neurons. PLoS One 6.
Rosbash, M. (2009). The implications of multiple circadian clock origins. PLoS Biol.
Schlichting, M., Menegazzi, P., Lelito, K.R., Yao, Z., Buhl, E., Dalla Benetta, E., Bahle, A., Denike, J., Hodge, J.J., Helfrich-Forster, C., et al. (2016). A Neural Network Underlying Circadian Entrainment and Photoperiodic Adjustment of Sleep and Activity in *Drosophila*. J. Neurosci.
Schubert, F.K., Hagedorn, N., Yoshii, T., Helfrich-Förster, C., and Rieger, D. (2018). Neuroanatomical details of the lateral neurons of *Drosophila melanogaster* support their functional role in the circadian system. J. Comp. Neurol.
Sehadova, H., Glaser, F.T., Gentile, C., Simoni, A., Giesecke, A., Albert, J.T., and Stanewsky, R. (2009). Temperature Entrainment of *Drosophila*'s Circadian Clock Involves the Gene nocte and Signaling from Peripheral Sensory Tissues to the Brain. Neuron 64, 251–266.
Seluzicki, A., Flourakis, M., Kula-Eversole, E., Zhang, L., Kilman, V., and Allada, R. (2014). Dual PDF Signaling Pathways Reset Clocks Via TIMELESS and Acutely Excite Target Neurons to Control Circadian Behavior. PLoS Biol. 12.
Shafer, O.T., and Yao, Z. (2014). Pigment-dispersing factor signaling and circadian rhythms in insect locomotor activity. Curr. Opin. Insect Sci.
Sheeba, V., Fogle, K.J., Kaneko, M., Rashid, S., Chou, Y.T., Sharma, V.K., and Holmes, T.C. (2008). Large Ventral Lateral Neurons Modulate Arousal and Sleep in

Drosophila. Curr. Biol. 18, 1537–1545.
Stoleru, D., Peng, Y., Agosto, J., and Rosbash, M. (2004). Coupled oscillators control morning and evening locomotor behaviour of *Drosophila*. Nature.
Stoleru, D., Peng, Y., Nawathean, P., and Rosbash, M. (2005). A resetting signal between *Drosophila* pacemakers synchronizes morning and evening activity. Nature.
Stoleru, D., Nawathean, P., Fernández, M. de la P., Menet, J.S., Ceriani, M.F., and Rosbash, M. (2007). The *Drosophila* Circadian Network Is a Seasonal Timer. Cell.
Tataroglu, O., and Emery, P. (2014). Studying circadian rhythms in *Drosophila melanogaster*. Methods.
Tataroglu, O., and Emery, P. (2015). The molecular ticks of the *Drosophila* circadian clock. Curr. Opin. Insect Sci. 7, 51–57.
Vansteensel, M.J., Michel, S., and Meijer, J.H. (2008). Organization of cell and tissue circadian pacemakers: A comparison among species. Brain Res. Rev. 58, 18–47.
Wagner, S., Sagiv, N., and Yarom, Y. (2001). GABA-induced current and circadian regulation of chloride in neurones of the rat suprachiasmatic nucleus. J. Physiol.
Wang, T.A., Yu, Y. V., Govindaiah, G., Ye, X., Artinian, L., Coleman, T.P., Sweedler, J. V., Cox, C.L., and Gillette, M.U. (2012). Circadian rhythm of redox state regulates excitability in suprachiasmatic nucleus neurons. Science.
Welsh, D.K., Takahashi, J.S., and Kay, S.A. (2010). Suprachiasmatic Nucleus: Cell Autonomy and Network Properties. Annu. Rev. Physiol. 72, 551–577.
Wu, M., Robinson, J.E., and Joiner, W.J. (2014). SLEEPLESS is a bifunctional regulator of excitability and cholinergic synaptic transmission. Curr. Biol.
Yan, L., Karatsoreos, I., LeSauter, J., Welsh, D.K., Kay, S., Foley, D., and Silver, R. (2007). Exploring spatiotemporal organization of SCN circuits. In Cold Spring Harbor Symposia on Quantitative Biology.
Yang, H.H.H., St-Pierre, F., Sun, X., Ding, X., Lin, M.Z.Z., and Clandinin, T.R.R. (2016). Subcellular Imaging of Voltage and Calcium Signals Reveals Neural Processing In Vivo. Cell.
Yang, J.-J., Wang, Y.-T., Cheng, P.-C., Kuo, Y.-J., and Huang, R.-C. (2010). Cholinergic modulation of neuronal excitability in the rat suprachiasmatic nucleus. J. Neurophysiol. 103, 1397–1409.
Yao, Z. (2016). Connectivity , Organization , and Network Coordination of the *Drosophila* Central Circadian Clock.
Yao, Z., and Shafer, O.T. (2014). The *Drosophila* circadian clock is a variably coupled network of multiple peptidergic units. Science.
Yao, Z., Macara, A.M., Lelito, K.R., Minosyan, T.Y., and Shafer, O.T. (2012). Analysis of functional neuronal connectivity in the *Drosophila* brain. J. Neurophysiol.
Yao, Z., Bennett, A.J., Clem, J.L., and Shafer, O.T. (2016). The *Drosophila* Clock Neuron Network Features Diverse Coupling Modes and Requires Network-wide Coherence for Robust Circadian Rhythms. Cell Rep.
Yoshii, T., Todo, T., Wülbeck, C., Stanewsky, R., and Helfrich-Förster, C. (2008). Cryptochrome is present in the compound eyes and a subset of *Drosophila*'s clock neurons. J. Comp. Neurol.
Yoshii, T., Wulbeck, C., Sehadova, H., Veleri, S., Bichler, D., Stanewsky, R., and Helfrich Forster, C. (2009). The Neuropeptide Pigment-Dispersing Factor Adjusts Period and Phase of *Drosophila*'s Clock. J. Neurosci. 29, 2597–2610.

Yoshii, T., Rieger, D., and Förster, C.H. (2012). Two clocks in the brain: An update of the morning and evening oscillator model in *Drosophila*. Prog. Brain Res.

Yoshii, T., Hermann-Luibl, C., and Helfrich-Föorster, C. (2016). Circadian light-input pathways in *Drosophila*. Commun. Integr. Biol.

Zheng, X., and Sehgal, A. (2008). Probing the relative importance of molecular oscillations in the circadian clock. Genetics 178, 1147–1155.

Chapter 3. PHASE: A MATLAB Program for *Drosophila* Activity, Sleep and Entrainment Analysis

Jenna L Persons[1*], Abbey Roelofs[2*], Alyssa Kalsbeek[1], Deepika Pandian[1], Maria P Fernandez[1], and Orie T Shafer[1]

*authors contributed equally to this work.

[1]Department of Molecular, Cellular, and Developmental Biology, University of Michigan, Ann Arbor, MI 48109, [2]Department of Information Technology, Advocacy and Research Support, University of Michigan, Ann Arbor, MI 48109

Author Contributions

JLP, conception and design, PHASE design, data acquisition, analysis and interpretation of data, drafting and revising the manuscript; AR, conception and design, PHASE programming, revising the manuscript; DP and AK, data acquisition and analysis; MPF and OTS, conception and design, interpretation of data, and revising the manuscript.

Abstract

Circadian clocks allow organisms to anticipate rhythms in the environment and organize rhythms in behavior over a range of entraining light and temperature durations and intensities. Understanding the molecular and neural basis for entrainment is central to understanding circadian clocks. *Drosophila melanogaster* has proved an indispensable

model for studying the molecular basis of circadian timekeeping, sleep and activity behavior. The *Drosophila* Activity Monitor (DAM) system (TriKinetics, Waltham, MA) and programs to analyze activity, periodicity and sleep from DAM-collected behavioral data are widely used by fly researchers. Standardized methodology has greatly improved our understanding of the molecular and genetic contributions of circadian clocks to behavior. However, a consensus on methods to quantitatively assess entrainment properties of flies in equinox conditions, non-equinox days, or to different period lengths has not been reached. We developed a free MATLAB software suite, PHASE, with an intuitive user interface that analyzes DAM-acquired data and measures Activity, Sleep, and Entrainment with flexibility to Zeitgeber duration and period length. To highlight the functions of PHASE, we describe the activity, sleep and entrainment behavior of wildtype flies and clock mutants and demonstrate that PHASE can provide key insight into the basis for circadian entrainment and the temporal organization of activity and sleep behavior.

Introduction

Circadian systems provide organisms with an internal sense of time. Biological clocks are present in nearly every organism on earth subject to daily oscillations in the environment from the earth's rotation (Moore, 1982). All known clocks have a cellular and molecular basis; commonly taking the form of a feedback loop whose approximately 24-hour transcription-translation rhythm tracks and anticipates changes in light and temperature to produce rhythms in physiological processes underlying daily bouts of wake, sleep, feeding and mating behavior (Allada and Chung, 2010b; Ko and Takahashi, 2006). While circadian clocks are present in a diversity of tissues, in many animals the

“master pacemakers" organizing behavior are housed in dedicated neuronal circuits in the central brain (Vansteensel et al., 2008). In mammals and invertebrates alike these central clock neuron networks are indispensable for daily behavior coordinated with environmental rhythms (Herzog, 2007). Without environmental input, neuronal clocks deviate slightly from the actual 24-hour day. This property requires that they be reset daily and “entrain” to a range of time-giving cues, or “Zeitgebers”, to synchronize behavior and physiology with rhythms in the environment (Challet et al., 2003; Yadlapalli et al., 2018; Yoshii et al., 2016).

Understanding entrainment is central to our understanding of circadian clocks and is an active, growing area of research (Rémi et al., 2010; Roenneberg et al., 2003). These efforts are made all the more important since human health has deteriorated in our modern environment bathed in around-the-clock light, food availability, and activity (Lunn et al., 2017). The absence of reliable, rhythmic entrainment cues that correctly correspond to human chronotype may be causal to increases in obesity, heart disease and other chronic illnesses (McKenna et al., 2018). Entrainment is facilitated by the combined efforts of the molecular clock itself, intrinsic sensory mechanisms, central to peripheral communication, and neuronal clock-to-clock communication (Golombek and Rosenstein, 2010; Schlichting et al., 2016; Sehadova et al., 2009). A disturbance in these physiological mechanisms or in the environment itself may contribute to poor entrainment which typically indicated by behavior that fails to anticipation or deviates significantly in timing relative to Zeitgebers. Mammalian models have provided critical insight into the neurophysiological basis of circadian entrainment and behavior, while our understanding of central circadian clocks' molecular and genetic basis is credited in large part to studies

in *Drosophila melanogaster.*

The *Drosophila* network exhibits remarkable similarity to the 20,000 neurons of the suprachiasmatic nuclei (SCN) that comprise the mammalian central circadian network (Hermann-Luibl and Helfrich-Förster, 2015). In both, daily oscillations of core clock proteins drive rhythms of neuronal activity in anatomically distinct dorsal and ventral (lateral, in *Drosophila*) populations (Helfrich-Förster et al., 2007). The *Drosophila* central circadian neuron network (CCNN) is composed of approximately 75 pairs of neurons that coordinate daily bouts in behavior by communicating with each other and relevant output centers in the central brain and peripheral tissues (Nitabach and Taghert, 2008). These populations are diverse in intrinsic excitability, receptivity to primary sensory information, and expression of neuropeptides and transmitters (Hermann et al., 2010; Johard et al., 2009; Picot et al., 2007). Neuronal communication is essential to produce coherent behavioral rhythms though it's molecular basis, and their combined contributions to activity, entrainment and sleep remain largely unknown (Guo et al., 2014; Nitabach, 2006; Nitabach et al., 2002, 2005).

The conservation of circadian architecture and function, when brought to bear with *Drosophila*'s molecular malleability and short-generation time is ideal for defining circadian inputs, outputs, and regulators. Often, single gene manipulations within remarkably few cells have dramatic effects on fly behavior due to the reduced genetic redundancy and neural scale of flies relative to mammals and fish (Renn et al., 1999). For many years, the behavioral effects of manipulations to the fly circadian system have been assessed quantitatively using recording mechanisms like the *Drosophila* Activity Monitor (DAM)-system (TriKinetics, Waltham, MA; Rosato and Kyriacou, 2006). By

collecting the number of infrared (IR) beam crosses of individually housed *Drosophila* in environmentally controlled incubators over the course of many weeks, the DAM-system records two major behavioral outputs of circadian systems, locomotor activity and sleep. Programs like ClockLab, Counting Macro, ActogramJ and ShinyR-DAM use DAM-collected behavior to quantitatively define rhythmicity and periodicity, overall activity and sleep (Cichewicz and Hirsh, 2018; Pfeiffenberger et al., 2010b, 2010c; Schmid et al., 2011). The latter measure, sleep, is defined as any period of *in*activity (no IR beam crosses) greater than or equal to 5-minutes (Hendricks and Sehgal, 2004; Huber et al., 2004). The field's near-universal use of DAM systems and programs to analyze DAM data allow researchers to make direct comparisons between experimental manipulations from different labs and from different eras and this has been of great benefit to the field. Although some studies have assessed the entrainment of the *Drosophila* sleep/activity rhythm to light:dark cycles of different day lengths, the overwhelming majority of studies have focused on entrainment to 12:12 light:dark (LD) cycles (i.e., equinox) and few have examined the entrainment of the fly clock to non-24 hour LD cycles, conditions that reveal important features of circadian entrainment (Green et al., 2015; Rieger et al., 2003; Schlichting et al., 2016). Previously developed analysis programs are therefore best suited for analyzing endogenous time keeping in free-running conditions without environmental cues and entrainment behavior in 12:12 equinox light or temperature paradigms. To understand the roles of neurons and molecular clocks in entrainment however, circadian systems must be pushed outside of their entrainment ranges using a variety of periods, Zeitgeber durations, and modalities (Rémi et al., 2010; Roenneberg et al., 2003). Although some studies have quantified aspects of circadian entrainment in

individual flies the field has typically relied on the visual assessment of averaged population profiles to gauge entrainment to environmental cycles (Helfrich-Förster, 2000; Potdar and Vasu, 2012; Rieger et al., 2012; Schlichting and Helfrich-Förster, 2015; Schlichting et al., 2016; Yao et al., 2016). Thus, unlike the analysis of free-running circadian rhythms, there is no consensus for the quantification of entrainment. Presently, the field lacks a) standardized, quantitative measurements of entrainment and b) simple methods to extract this information from DAM-data.

We developed a free MATLAB-based program, PHASE, as a potential solution to quantify and standardize measures of entrainment behavior from DAM-collected *Drosophila* behavior data. PHASE has a user-friendly interface, measures Activity, Sleep and Entrainment in behavior paradigms with any Zeitgeber duration and period length, and creates statistics and graphical exports for population averages and individual flies. In addition to widely used measures of sleep and activity, our program provides measurements of phase and anticipation for individual flies from which the strength of entrainment may be inferred.

Herein, we describe PHASE's experimental accommodations, new analysis metrics to quantify entrainment in in individual flies, and use our application to analyze activity, sleep, and entrainment of wildtype flies and canonical circadian clock mutants under 24h equinox LD cycles, under long days, and under long and short LD periods. We show that PHASE quantifies important aspects sleep and activity behavior, throughout diurnal cycles, and within specific time windows across the day in standard 12:12 LD, 14:10 long LD, and 23- and 25-hour period equinox paradigms. In addition, PHASE defines sleep latency and activity anticipation and makes accurate measurements of

behavioral phase under a wide range of entrainment conditions in a flexible manner. We hope that PHASE, in combination with free programs like the browser-based ShinyR-DAM, will provide researchers with user-friendly, accessible analysis tools to explore circadian entrainment under a wide range of paradigms (Cichewicz and Hirsh, 2018). When leveraged with the advantages of the *Drosophila* model, PHASE may provide key insights into the molecular and neuronal basis of circadian entrainment. The PHASE software, a full protocol and all associated materials are available for download from Google Drive.

Results

Program Requirements. To use the full-version, users will need a MATLAB R2017b or later, the PHASE application and xlwrite toolbox downloaded from Google Drive, and installed into the MATLAB program. Alternatively, users without access to MATLAB may download PHASE installers for PC or MAC that use the free version of MATLAB, Runtime. We developed an extensive user manual that describes the purpose and calculations behind each of PHASE's components and includes a step-by-step protocol to analyze activity, sleep and entrainment behavior. PHASE accepts DAM-system monitor data processed by DAMFileScan into 1-minute bins by "channel counts" representing individual flies (Trikinetics, Waltham, MA). Data collected from the same set of consecutive days can be processed by PHASE from the same file directory; however, independent behavioral experiments must be processed by PHASE from a separate folder.

User Interface. PHASE's graphical interface (Figure 1A) prompts users to select the folder containing monitor data, the monitor boards and channels to be analyzed, and

experimental parameters in the “Data Settings” box (Figure 1B). When data is successfully uploaded PHASE will automatically display the first recorded bin date and time; thus, users must specify the date and 24-hour time (HH:MM) on which they wish to start analysis. We built PHASE with flexibility for period length, duration and time of Zeitgeber onset. The relationships between the indicated period and Zeitgeber parameters specified in Data Settings define the “day” and “night.” This feature allows users to easily analyze sleep and wake behavior in non-equinox paradigms and in specific windows of the day or night.

Completion of the Data Settings box (Figure 1B) is required for all subsequent analyses tabs: Activity or Sleep (Figure 1C), Phase Analysis (Figure 1D), or Anticipation or Latency (Figure 1E). Each analysis may be performed independently for activity or sleep by checking the “Include … Analysis” box under each analysis tab, specifying an output file directory, and clicking the “… Activity” or “Sleep Analysis” buttons at the bottom of PHASE. A unique file directory must be indicated for PHASE’s Excel outputs and graphs.

Activity or Sleep Analysis. PHASE offers two activity analysis types in the Activity or Sleep Analysis tab of the PHASE GUI: “Normalized Activity Analysis” and “Averaged Activity Analysis” (Figure 2A). PHASE may process 1-minute binned IR-beam cross activity data for a selection of “Days to Use” by “Normalizing” activity by the total IR beam crosses in the day, or average of days (Figure 2B). Alternatively, users may “Average” behavior data, which divides each bin’s total IR counts by the “Bin Size” specified in “Activity or Sleep” parameters (Figure 2C). Normalization preserves the temporal properties of behavior and is the standard for visualizing *Drosophila* behavior data. Averaging preserves both the

temporal qualities and true measurements of overall activity. Averaged activity may be useful when comparing not only when, but also how much activity occurs at a given time of day. PHASE's Excel outputs measure individual fly activity in raw IR (Figure 2D), bin averaged (Figure 2E) or normalized (Figure 2F) counts across the period, day, and night relative to the Zeitgeber parameters in Data Settings for all days and independent days included in "Days to Use" (Figure 2A, PHASE GUI set up for activity analysis, Figure 2B,C graph exports, Figure 2D-F, quantifications).

Standard sleep graphs and calculations are also available in the Activity or Sleep Analysis tab of the PHASE GUI by clicking the "Sleep Analysis" button (Figure 3A). PHASE converts 1-minute IR activity data to "sleep" using a binary function where sleep equals "1" for any 1-minute bin part of a 5-minute (or more) series of bins without IR beam crosses, and no sleep equals "0". Therefore, there is an effective 5-minute minimum for 1 "bout" of sleep as previously described (Hendricks and Sehgal, 2004; Huber et al., 2004). PHASE exports sleep graphs (Figure 3B) and calculates individual fly total and average minutes of sleep (Figure 2C), bout number (Figure 3D) and duration (Figure 3E) for the day, night and period indicated in Data Settings (Figure 3A, PHASE GUI set up for sleep analysis, Figure 3B sleep graphs, Figure 3C-E, sleep quantifications).

Activity or sleep graphs may be created for entire populations or individual flies on a single day, average of days (Figure 4A-C, F) or continuously plotted selection of days (Figure4D-E) by manipulating the entries in the Activity or Sleep analysis tab (Figure 5A, B, PHASE GUI settings for Figure 4). Graphs for sleep or activity are available in traditional binned bars (Figure 4A-C), or lines (Figure4D-F) that are easily manipulated in MATLAB and exported for publication as .pdf, .jpg, or .tiff formats. We anticipate that the

ability to create individual plots for hundreds of individuals at once will be particularly useful for analyzing behavior in non-standard conditions, with uncharacterized Zeitgebers or genetic manipulations that create complex, diverse phenotypes.

Quantifying Entrainment Behavior. Circadian clocks help organisms predict daily oscillations in Zeitgebers like light and temperature, and coordinate sleep and activity behavior with these environmental rhythms. *Drosophila* clocks entrain within a particular range to periods shorter and longer than 24-hours, various day lengths and are sensitive to inputs from multiple Zeitgebers (Bywalez et al., 2012; Yoshii et al., 2009). As researchers investigate new entrainment paradigms, it's critical that measuring a fly's ability to entrain to Zeitgebers, and infer the strength of entrainment, be made simple and high-throughput. The strength of entrainment may be quantified by measuring how accurately (with respect to time) the phase of activity or sleep behavior corresponds to a Zeitgeber transition, as well as how much activity or sleep behavior correctly anticipates a Zeitgeber transition. A deviation in the behavior's phase and minimal anticipation of a Zeitgeber reflects weak resetting by that cue, and consequently, weak entrainment. Current methods to quantify entrainment behavior in flies are low throughput and qualitative. Many researchers smooth behavioral data using digital filters to minimize the acute, sensory "startle effect" to Zeitgeber transitions and other environmental anomalies that obscure analysis before manually selecting peaks that correspond to the entrainment paradigm (Helfrich-Förster, 2000; Potdar and Vasu, 2012; Rieger et al., 2012; Schlichting and Helfrich-Förster, 2015; Schlichting et al., 2016; Yao et al., 2016). The lack of standardized methodology to quantitate circadian phase of entrainment, activity anticipation, sleep latency and duration makes metrics difficult to compare between

experiments. In addition, smoothing behavioral data may also obscure the “startle effect” in instances where it is useful to quantify the response (or lack thereof) to incoming sensory stimuli (Riemensperger et al., 2018; Vaccaro et al., 2016).

To address these methodological challenges, we equipped PHASE with methodology to quantitatively measure the phase and amount and duration of activity anticipation and sleep latency behavior relative to a given Zeitgeber. PHASE’s Phase Analysis defines the precise ZT and area of sleep and behavior peaks. Additionally, Anticipation or Latency Analysis quantifies the length of time, and amount of sleep or activity behavior that occurs leading (activity anticipation) or following (sleep latency) a Zeitgeber transition. PHASE uses two mathematical representations of anticipation and latency that exclude or include acute sensory responses, respectively: 1) area under the curve (AUC) and duration (minutes) between *smoothed* maxima and minima, and 2) the slope of a linear regression through *unsmoothed* data. We acknowledge that any one measure of Anticipation of Latency alone may fail to discriminate between relevant experimental groups. Together, however, we expect PHASE’s entrainment analyses will allow researchers to find the best representation of their data and entrainment paradigm with increased visual, statistical power.

PHASE employs a Savitzky-Golay filter that smooths 1-minute binned data prior to performing Phase Analysis and Anticipation or Latency Analysis. Savitzky-Golay filters, also known as least squares smoothing filters, fit an unweighted linear least-squares fit polynomial of a given degree across a given frame of data (Orfanidis, 1995, Section 8.3.5). Higher order polynomials (3^{rd} or 5^{th} order) generally allow for a high-level of smoothing while preserving narrow data features often attenuated by moving-average

and bandpass filtering. Lower order polynomials (1st order) are better for smoothing wider peaks but often minimize narrow features' height and width. An odd-numbered filter frame width (in minutes) determines the window of data over which the polynomial is fitted to replace subsequent central points by the best approximation of the in-frame data. Larger filter frame widths will reduce noise by effectively "averaging" over more data points, while smaller frame widths better preserve the original data. The result is a filter that adjusts to a user's desired level of smoothing; dialing in signal-to-noise to reduce or maximize small features.

PHASE's smoothing functions are entirely modifiable in the Phase Analysis and Anticipation or Latency Analysis tabs. Users design filters by specifying a polynomial order and filter frame length that best fits their data and their intended use. It is imperative that users view this as an iterative process, since varying polynomial order and filter frame length produces significantly different measures of sleep and activity quantity (AUC) and durations for Anticipation and Latency analysis (Figure 6A-H). To facilitate this process, we have prefilled the PHASE GUI with filter parameters that were used successfully in this manuscript to gather anticipation, latency and phase measurements. PHASE also creates individual fly plots that display the 1-minute raw activity, overlaid by the smoothed Savitzky-Golay curve to allow users to visually select the best smoothing for their behavioral paradigm.

Anticipation or Latency Analyses. PHASE calculates the quantity (AUC), duration and slope of sleep or activity behavior according to parameters indicated in the Anticipation or Latency analysis box. Users specify the Savitzky-Golay filter parameters, the days and Zeitgeber time(s) of interest, and a window (minutes) in which behavior prior to (activity

anticipation) or after (sleep latency) the ZT should be considered. Within the window, activity functions move negatively along the x-axis (time) from a ZT to grab the maxima/greatest activity and then the minimum/least activity from smoothed data. Conversely, sleep functions move positively along the x-axis (time) from a ZT to derive the first minima/least amount of sleep and the maxima/greatest amount of sleep from smoothed data. Sleep or activity quantity (AUC) and duration calculations *exclude* the "startle effect" by gathering maxima and minima from the first bin after or before a given ZT, respectively. The AUC and the duration (minutes) of activity anticipation or sleep latency are calculated subsequently from the smoothed maxima and minima and exported to an Excel file for each fly included in the analysis.

PHASE creates individual fly anticipation and latency plots that display the original 1-minute activity or sleep data, Savitzky-Golay smoothed curve (blue line), maximum and minimum bins (indicated with blue carrots), and duration (annotated above carrots) within the user's specified window from the given ZT (grey shaded region) (Figures 7A,B, activity and 8A,B, sleep). At the individual fly level, 1^{st} -order (Figures 7A, 8A) and 3^{rd} -order polynomials (Figures 7B, 8B) applied to original 1-minute data over the same 4-hour filter frame length visibly changes the smoothed curve to more accurately fit the original behavior data's peaks and troughs. However, excluding evening sleep latency quantity (Figure 7D) these changes are non-significant at the quantitative level for morning and evening activity or sleep quantity (AUC) and duration metrics (Figures 7C and 8C, D). Nevertheless, we believe that users should visually inspect filtering to ensure that it smooths 1-minute behavior data without significantly broadening (lower order polynomials) or narrowing (higher order polynomials) activity or sleep features.

Smoothed data is useful to minimize noise from the “startle effect” to Zeitgeber transitions, or unwanted environmental disturbances. Acute activity responses to light or temperature changes may be important indications of sensory function that feed in to circadian clocks and facilitate entrainment. Thus, PHASE’s Anticipation or Latency analysis also calculates the slope of a liner-regression for unsmoothed data within the user’s specified window from a given ZT that *includes* the 1-minute bin of the indicated ZT to preserve responses to Zeitgeber transitions. PHASE graphs the slopes of the linear regressions for individual flies and entire populations (light grey, individuals and dark grey, population average) to visually depict the intensity of behavior relative to a ZT for a single day or average of days (Figures 7E, 8E). More positive activity slopes indicate greater anticipation, and acute response to Zeitgeber transitions (Figure 7E). Slope measurements may also be useful for assessing sleep following a Zeitgeber transition (Figure 8E). More positive sleep slopes visually represent less time to reach maximum sleep depth. The activity and sleep slopes for each fly are exported to the Anticipation or Latency output Excel file for statistical analysis. Using these quantitative measurements to compare wildtype population slopes, we found that evening activity slope (Figure 7F) and night sleep slope (Figure 8F) were significantly greater than their respective morning slopes. The entries in to the PHASE GUI used for Figures 7 and 8 are visualized in Figure 9.

Phase Analysis. PHASE also utilizes Savitzky-Golay filtering to smooth activity or sleep data and make phase calls unbiasedly across the entire period, or with respect to a user’s ZT of interest. In the Phase Analysis tab, users may average days of 1-minute sleep or activity data, smooth data using adjustable Savitzky-Golay frame and polynomial

parameters, and finds maxima/peak bins using a user defined minimum peak distance. Peak distance (minutes) determines if PHASE includes “shoulder” peaks as part of a single peak or excludes these adjacent peaks as part of a separate, unrelated peak of behavior. When no ZT of interest is indicated in the Phase Analysis tab, all peak calls are plotted, and the Excel export summarizes the AUC and ZT of every possible peak within the smoothed data. When a ZT, or set of ZTs is specified, PHASE plots and exports values for only those peaks closest to the given ZTs (Figure 10A, ZTs 0, 12).

Filter design like for Anticipation or Latency is a visual process and can be adapted to keep, or washout small behavior features as needed. 1^{st} -order polynomial filters (10A, 11A) create broader activity and sleep peaks than 3^{rd} -order (10B, 11B) polynomial filters of the same 4-hour frame length, and 4-hour peak separation for the same w^{1118} flies (Figure 10A,B activity and 11A,B, sleep). Qualitative changes due to polynomial order change the activity and sleep peak maximums and therefore, cause statistically significant changes in the apparent distance of morning and evening peaks from the ZT of interest (left, Figure 10C, activity, 11C, sleep). Polynomial order of the smoothing filter also significantly alters the AUC and height of peak calls (middle and right, Figure 10C, activity, 11C, sleep). The flexibility of filter smoothing for Phase Analysis and Anticipation or Latency are strengths of PHASE. We encourage users to produce a few iterations of their data using various filter orders, frame lengths and peak separation (Phase Analysis only), visually inspecting the fit, and then applying the final filter design to all comparable behavior data. Entries in to the PHASE GUI for the analyses in Figures 10 and 11 are described in Figures 12A, B.

Analysis of Wildtype Flies and Clock Mutants. To demonstrate the functionality of PHASE

and highlight it's use across entrainment paradigms, we used PHASE to describe the activity and sleep features of Canton-s wild type and w^{1118} control flies, and canonical *Drosophila* clock mutants, per^{01} and *cyc*, and *pdf* in equinox, long day, and short and long period conditions. *Period* and *cycle* are key components of the negative and positive-limbs of the *Drosophila* cellular molecular clock, respectively. PERIOD (PER) and its heterodimer TIMELESS (TIM) exhibit near perfect endogenous 24-hour transcriptional-translational oscillations that persist in the absence of environmental cues (reviewed in Allada and Chung, 2010). *Per* and *tim* mRNA transcription is positively activated by CLOCK/CYCLE (CLK/CYC) transcription factors and reaches a peak in the middle of the night. PER/TIM proteins accumulate in the cytoplasm, heterodimerize, and enter the nucleus to block CLK/CYC- mediated transcription at their own loci and other genes within the circadian transcriptional program. When too few PER/TIM dimers are produced as a consequence of their own negative regulation, CLK/CYC repression is relieved and the cycle begins again. These transcriptional rhythms are coincident with 24-hour rhythms in physiology underlying activity and sleep behavior (Yang and Sehgal, 2001).

Though there are molecular clocks throughout the body, the timekeeping and neuronal activity of 150 master clock neurons in the central brain are essential for *Drosophila*'s diurnal, bimodal behavioral rhythms, and their persistence in constant conditions without light or temperature cues (reviewed in Helfrich-Förster et al., 2007). The approximate nature of the molecular clock (endogenously running 23.5 hours in *Drosophila*) necessitates that it be reset daily by environmental inputs to maintain rhythms that properly track and anticipate the day length (reviewed in Tataroglu and Emery, 2014). Light and temperature information enters the *Drosophila* central circadian clock network

(CCNN) through a combination of parallel visual inputs from the retina, HB-eyelet, ocelli and peripheral sensory organs including the chordotonal organs and aristae (Rieger et al., 2003; Schlichting et al., 2016; Yadlapalli et al., 2018; Yoshii et al., 2016). CCNN neurons communicate time-of-day information received through these centers to one-another and relevant output centers using peptidergic signaling and neurotransmission at direct synaptic connections (Yoshii et al., 2016). Pigment Dispersing Factor (PDF) neuropeptide release from a small subset of ventral clock neurons is critical for generating neuronal activity rhythms that coordinate behavior across the day and predicts and adapts to Zeitgebers (Yoshii et al., 2009). *Drosophila* mutants for proteins of the molecular clock and the critical coupling neuropeptide PDF are well characterized (Allada et al., 1998; Konopka and Benzer, 1971; Rutila et al., 1998; Yoshii et al., 2009). Their stereotyped behavior, when coupled with the genetic tools available in the fly, has helped define the roles of the molecular clock in directing the behavioral outputs of specific CCNN populations, and in clock-to-clock neuronal communication.

Activity and Sleep Analysis. Canton-s (cs) and w^{1118}, are strongly rhythmic in equinox light conditions, at constant temperature (12:12 LD). Male flies exhibit bimodal increases in activity that anticipate the transitions to lights-on (ZT0) and lights-off (ZT12), and consolidated bouts of sleep during mid-day and throughout the night (Figure 13A,B, right). Rhythms in activity and sleep persist through 14-days of constant darkness, and constant temperature (DD) though running shorter than 24-hours without resetting light cues (Figure 13A,B, left). Null mutations in *per* and *cyc* render flies' molecular clock "broken," however their mutations manifest different behaviorally, likely owing to their roles in the negative- and positive-limb of the molecular clock, respectively. per^{01} flies are arrhythmic

in constant conditions, and exhibit little to no morning or evening anticipatory bouts of activity excepting the “startle effect” to light transitions in entrained conditions (Figure 13E) (Konopka and Benzer, 1971). The percent of total activity *per*^{01} flies exhibit during the day is significantly less than wildtype strain cs, and correlated with increases in significant increases in daytime sleep (left, Figure 13F,G). *cyc* mutants are also arrhythmic in constant conditions, however under entrained conditions they’re essentially “nocturnal” with visibly and statistically more activity during the nighttime than daytime than both control strains (Figure 13D, F) (Kempinger et al., 2009; Rutila et al., 1998). Consequently, *cyc* flies sleep significantly less than Canton-s or w^{1118} control strains during the nighttime (right, Figure 13G).

In line with previous reports, *pdf* mutants have no morning anticipation, are less rhythmic in constant conditions, and have phase-advanced evening activity (Figure 13C) (Renn et al., 1999; Tomioka et al., 2008). To quantify the amount of activity occurring from ZT8-12 and statistically compare changes in evening peak activity across genotypes, we took advantage of the fact that the parameters in PHASE Data Settings allow users to adjust the “day” onset and duration, and therefore any activity or sleep quantifications derived from that window. We changed the “Zeitgeber On” to ZT “8” and the “Hours of Zeitgeber” to “4.” All quantifications annotated with “day” in activity or sleep Excel outputs then represented a small region of behavior just before lights off. We found that *pdf* mutants have significantly more activity than w^{1118} flies during the hours leading up to the transition to lights-off (left, Figure 13H). Importantly, these increases in the *pdf* mutant were only visible when activity was normalized to total activity, and not averaged by the bin size (compare 13H, left and right). This indicates that while the overall levels

of activity during ZT8-12 are not greater in the *pdf* mutant, the percentage of their total active time during that window were indeed greater. We believe the ability to quantify activity and sleep metrics in defined windows is a strength of PHASE that will allow users to analyze features that were previously rather tricky to quantify, or only visually indicated. The free-running rhythmicity in DD for each genotype in Figure 13 is quantified in Table 1.

Activity Anticipation and Sleep Latency Analysis. Next, we used PHASE's Anticipation or Latency analysis to quantify the ability of Canton-s, w^{1118} and circadian mutants to predict the transitions to onset and offset of lights in equinox conditions. We filtered 3 days of entrained 12:12 LD data with a Savitzky-Golay filter of 3rd -order polynomial and 241-minute (4-hour) filter frame and quantified the amount (AUC) and duration (minutes) of behavior within a 3-hour window before (activity anticipation normalized to total activity) or after (sleep latency) ZT0 and ZT12 (Figure 14).

w^{1118} flies most robustly predict the transitions to lights-on with the longest duration and greatest quantity (AUC) of morning activity anticipation (Figure 14A,B). Cs wildtype, per^{01}, *cyc* and *pdf* mutant flies have significantly decreased morning activity quantity (AUC) and anticipation duration relative to w^{1118} (Figure 14A). Evening activity AUC in *cyc* and anticipation duration is decreased in *cyc* and per^{01}, while *pdf* mutants are significantly greater in evening anticipation AUC (Figure 14B). Male flies in equinox light have a well-described midday bout of sleep that begins shortly after lights-on. We find that though there is no difference among genotypes in daytime sleep AUC, all circadian mutants require significantly less time to coordinate their transition from morning activity to day sleep than w^{1118} flies (Figure 14C). Nighttime sleep latency and AUC is significantly

decreased only in *cyc* mutants, indicative of their nocturnal increases in activity behavior (Figure 14D).

PHASE also quantifies the slope of a best-fit linear regression through unsmoothed 1-minute data before (activity anticipation) or after (sleep latency) a given ZT. In one measurement, slope can capture the quantity and time of behavior. When analyzed in a restricted time window, steeper, more intense slopes represent more behavior over less time, while flatter slopes generally represent less behavior over more time. We compared each genotype's slope in the same 3-hour window and 3 days of 12:12 LD used for the aforementioned AUC and duration measures. Cs, per^{01}, *cyc* and *pdf* flies have significantly flatter, less robust normalized activity anticipation slopes leading up to lights-on relative to w^{1118} flies (Figure 15A). w^{1118} evening slopes are greater than all other genotypes (Figure 15B). *pdf* mutants, owing to their phase-advanced evening peak have significantly greater evening activity slope than cs flies but no more than w^{1118} (Figure 15B). Canton-s flies exhibit greater evening peak slopes than all mutant genotypes excepting *pdf*, and not greater than w^{1118} flies (Figure 15B). These data indicate that w^{1118} flies have the most robust anticipatory behavior to lights-on and lights-off, and that Canton-s flies better anticipate transitions than clock mutants per^{01} , and *cyc*. Finally, that true to previous findings, *pdf* mutants are advanced in evening peak behavior relative to controls.

We found the slope of latency to midday sleep to be similar across genotypes (Figure 16A). The exception are *cyc* flies, with a latency slope approaching zero that captures their binary transitions from nighttime activity to daytime sleep (Figure 16A). Compared to w^{1118}, all genotypes have significantly less intense transitions to nighttime

sleep following light offset (Figure 16B). Again, *cyc* mutant's sleep slope after lights-off is close to zero and in some flies, negative. This suggests that as a population they are not sleeping after lights-off, while negative slopes suggest that some flies are also becoming more active (Figure 16B). It is important to note, that slopes identify more significant differences among genotypes for sleep latency, particularly at nighttime (Compare Figures 15D, 16B). Activity anticipation metrics however remain predictive and significant regardless of method used (Compare Figures 15B and 16B). This is likely because sleep measures are far more discrete- a 1 or zero for any given bin- than 1-minute IR-beam crosses which may occupy any percentage of 1 for any given bin. It is imperative that users find the best method to discriminate between relevant groups in the context of a particular biological question. Concrete answers to activity and sleep behavior "time" and "quantity" relative to a Zeitgeber transition are best determined by AUC and duration, respectively. In contrast, slope is better suited to quantify and visually identify data trends as it combines the amount of behavior in a defined time in one measure.

Phase Analysis in Equinox and Long Days. PHASE's Phase Analysis smooths individual fly day-averaged 1-minute sleep and activity data with a user designed Savitzky-Golay filter. The phase (ZT) relative to the parameters specified in Data Settings, and area under the curve are defined for all peaks when no ZT is specified in the Phase Analysis tab. However, only those peaks closest to a specified ZT when indicated will be visualized on plots or reported in Excel outputs. We tested the software's ability to define phase metrics and determine how well flies entrain to non-equinox conditions particularly without the aid of a molecular clock or essential peptidergic clock-to-clock communication. We collected behavior data from wildtype and circadian mutant flies in 7 days of 12:12 equinox light,

and 7 days of 14:10 LD (Figure 17A-E). By visually inspecting and iteratively modifying filter parameters, we determined that for both LD conditions, a 3rd -order filter, 241-minute frame width and 3-hour peak separation (Figures 18A, 19A) was superior to a filter with either a) 1st -order filter (Figure 20A, 21A) or b) 4-hour peak separation (Figure 22A, 23A). Our final filter design preserved peak height and area better than 1st -order filters, and more precisely defined statistical differences between each genotype's peak phase ZT (the peak's maximum bin) than 4-hour separation filters.

We identified the closest activity peak to the on- and offset of lights in 3 days of entrained equinox and long day conditions, converted these to a phase (in hours) relative the Zeitgeber transition and compared the mean phases, their associated peak areas across genotypes. PHASE is able to distinguish statistically significant differences in activity peak phase in equinox and long days (Figure 18B, C and 19B, C). w^{1118} and cs flies, entrain strongly to equinox and long days with less than a 0.5 hour deviation from lights on- and lights-off transitions. Both strains have consolidated peaks of activity behavior that center around the transition to lights-on and lights-off in 12:12 LD and re-entrain precisely with little error in 14:10 LD (Figures 18B,C and 19B, C, left). *pdf* mutant flies are significantly delayed in phase, and per^{01} was delayed but not significantly in morning peak in 12:12 LD (Figure 18B, left). Because both genotypes lack anticipatory morning behavior and only wake with light onset, their peak phase ZT is slightly delayed relative to control Canton-s and w^{1118} strains. *Cyc* flies, in contrast are advanced during the morning and significantly delayed during the evening (Figures 18B,C and 19B, C, left). In either LD 12:12 or 14:10 conditions, *cyc* mutants peak activity bouts occur greater than 0.5 hours before lights-on and after lights-off. Finally, we determined that *pdf* mutants are

phase-advanced in evening activity under both 12:12 and 14:10 conditions (Figure 18C, 19C). *Pdf* mutants maintain their advance evening phenotype in 14:10 LD, however the advance loses significant relative to control strains (Figure 19C).

We also quantified the amount of activity in phase calls for each condition's morning and evening peaks. Morning or evening peak area under the smoothed curve (AUC) were reduced under 14:10 LD relative to those 12:12 LD when reported as averaged activity counts (right, Figures 18 B,C and 19B, C) but not when reported as activity normalized to total IR counts (center, Figures 18B, C and 19B, C). This indicates that while the percentage of the total period's activity that takes place in each peak phase is relatively stable across entrainment paradigms, the actual IR beam crosses do change, possibly to distribute behavior across a longer light-portion of the period. We also found that the AUC of morning peak activity when expressed as a percentage of total activity was similar between genotypes in 12:12 LD and 14:10 LD ("Normalized," center, 18B and 19B). However, when the AUC were calculated using averaged IR beam crosses, the results in 12:12LD showed significantly more morning and evening peak area in *cyc* mutants relative to controls and significantly less in cs and per^{01} relative to w^{1118} ("Averaged," right, 18B and 19B). These data stress the importance of choosing the best measurement to assess entrainment properties. While the phase (ZT) of peaks may be comparable between genotypes regardless of the values of activity data (averaged or normalized), the amount of activity that occurs in a given peak (AUC) may be more or less informative depending on the application.

Phase Analysis in 23-hour and 25-hour Periods. Flies and mammals can naturally entrain to periods within approximately 2-hours greater or lesser than the 24-hour period imposed

by the Earth's rotation, and even far beyond conventional limits when facilitated by light and food-cues (Gronfier et al., 2007; Harrison et al., 2016; Houben et al., 2014; Walbeek and Gorman, 2017). Beyond natural entrainment ranges, organisms are progressively delayed (periods >24-hours) or advanced (periods <24-hours) relative to the phase of Zeitgeber transitions (Aton et al., 2004; Tataroglu and Emery, 2014). It is hypothesized that in order to entrain, organisms must speed-up or slow-down their molecular clocks to compensate for the shorted, or lengthened periods, respectively (Pittendrigh and Daan, 1976). The molecular and neural mechanisms through which this coordination occurs remain unknown. Determination of entrainment limits and the phase angle of entrainment under various environmental periods are classic methods for understanding entrainment (Helfrich-Förster, 2000; Levine et al., 2002; Tang et al., 2010). We therefore built PHASE to track entrainment under non-24 hour environmental periods.

We examined w^{1118} and cs wildtype flies under 24-hour, 23-hour and 25-hour periods. Using Phase Analysis and the optimized filter with a 3rd -order polynomial, 241-minute frame width and 3-hour peak separation (see Figures 18 and 19), we identified the highest activity peak in a 3-hour window before or after the on- and offset of lights on the first, third and sixth day of each paradigm. We converted the ZTs of peak maximums to distance (hours) from Zeitgeber transition and statistically compared each genotype's entrainment on successive days. On the first full day in 24-hour 12:12 LD paradigms flies are beginning to reorganize their bimodal activity peaks to the new paradigm (Figure 24A left, B). Both genotypes are fully entrained and stably anticipate lights-on and lights-off starting on Day 3 of 12:12 LD (Figure 24A middle, B). Conversely, on day one flies in 23-hour 11.5:11.5 LD paradigms are able to track morning lights-on, but become

progressively delayed on days three and six (Figure 25A, B). Evening peak behavior fails to track or anticipate lights-off on days one, three or six and is greater than 1-hour delayed on all days of the 23-hour paradigm in either genotype (Figure 25A, B). In contrast, flies in long periods (25-hour 12.5:12.5 LD) are greater than 1-hour advanced on all days relative to morning lights-on, and increasingly more advanced relative to evening lights-off (Figure 25C, D).

Taken together, this suggests that flies are less able to speed-up or slow-down their circadian behavior on each successive day to adapt to non-24-hour periods. Interestingly, 23-hour periods appear to most robustly reorganize morning activity behavior, while 25-hour periods favor evening activity behavior (Compare Figure 25C and D). The *Drosophila* clock neuron network (CCNN) in 12:12 LD is divided into distinct "morning" and "evening" activity-promoting populations (Grima et al., 2004; Stoleru et al., 2005). Though the clock network is certainly more complex than a simple "morning" and "evening" population model, one possible explanation for the aforementioned observations is that these populations are differentially selected and temporally reconfigured in 23- and 25- hour paradigms (Dissel et al., 2014; Yoshii et al., 2012). Though it remains to be tested, this hypothesis and others dissecting the role of the neuronal populations and the molecular clock in circadian rearrangement to different entrainment paradigms, may be quantitatively analyzed using PHASE.

Discussion

Nearly every terrestrial organism has an internal sense of time to synchronize behavior and physiology to oscillations in environmental conditions imposed by the earth's rotation. The flexibility of the molecular clock allows organisms to entrain to a

range of time-giving light and temperature cues. Entrainment is central to our understanding of circadian clocks; how entrainment information is conveyed, and the roles of the molecular clock and particular specific neuronal populations in circadian behavior are active areas of research. The functional homology of mammalian and *Drosophila* circadian networks when coupled with advantages unique to the fly model system, namely their extensive genetic toolbox and widely-shared behavioral methodology, has enabled researchers to dissect the molecular and genetic contributions of endogenous timekeeping to behavior. Currently, the field lacks universal tools to quantitatively and flexibly analyze the entrainment of activity and sleep. Therefore, we developed PHASE to quantify and standardize the analysis of *Drosophila* entrainment using data collected by the nearly universally employed DAM-system (TriKinetics, Waltham, MA).

During the preparation of PHASE software and this manuscript, ShinyR-DAM was published by the Hirsh Lab (Cichewicz and Hirsh, 2018). ShinyR-DAM is a free, browser-based application that processes DAM behavior data and provides measures of activity, sleep, and circadian periodicity. Our application is a complement to ShinyR-DAM and ClockLab that performs the standard measures of sleep and activity available in the aforementioned programs, but distinguishes itself in its ability to accommodate, visually represent and quantitate circadian behavior under any entrainment paradigm. In addition, PHASE is equipped with a user-friendly graphical interface and statistical and graphical outputs that allows users to quantitatively characterize the entrainment of activity and sleep in individual flies. We expect this aspect of PHASE may be particularly useful in characterizing new entrainment modalities where relevant behaviors of individuals could

be washed-out in the population's mean activity or sleep. Herein, we've demonstrated the functionality of our application by describing the activity, sleep and entrainment behavior of wildtype and classical circadian mutants, per^{01}, *cyc*, and *pdf* in equinox LD, long-day LD, short and long periods, and in defined windows across entrainment paradigms. Finally, we show that PHASE's adjustable Savitzky-Golay polynomial filtered and non-filter entrainment features can provide quantitative measurements of activity anticipation, sleep latency and peak phase. In summary, we hope that PHASE and other free platforms like browser-based ShinyR-DAM will facilitate the characterization of the network's and molecular clock's functions in circadian activity, sleep and entrainment behavior. PHASE software downloads; code and a detailed user manual are available on the Google Drive.

Materials and Methods

PHASE Accessibility. The full version of the PHASE program functions on MATLAB versions R2017b or later and requires the xlwrite toolbox to create statistical workbooks. The PHASE program, xlwrite toolbox and associated materials, including PHASE code and a detailed protocol may be downloaded from the Google Drive. PHASE is also available in a stand-alone version, which requires only the free version of MATLAB, Runtime. We note that the standalone version has reduced access to code manipulation.

Drosophila Strains. Flies were reared on cornmeal-sucrose-yeast media under a 12:12light :dark cycle at 25°C. The following fly lines were used: w^{1118} (Bloomington stock: 3605), Canton-s (Bloomington stock: 9514), per^{01} (Konopka and Benzer, 1971), *cyc* (Rutila et al., 1998), *pdf* (Renn et al., 1999).

Behavior. Flies aged 5-7 days were placed individually in recording glass tubes containing 2% agar-4% sucrose food at one end. Tubes were loaded into DAM2 *Drosophila* Activity

Monitors (TriKinetics, Waltham, MA) for locomotor activity recording. Flies were maintained at a constant temperature of 25°C and activity counts were collected in 1-minute bin during 7 days of a 12:12 LD cycle and a subsequent week of constant darkness for equinox experiments or 7days of 12:12 LD followed by 7days of 14:10 LD for long-day experiments. In period experiments flies were maintained for 7 days in 12:12 LD, 11.5:11.5 LD or 12.5:12.5 LD at constant temperature of 25°C.

ClockLab Analysis. Rhythmicity and periodicity of individual flies in the last 4-days of DD were determined by χ–square analysis with a confidence level of 0.05 using ClockLab software from Actimetrics (Wilmette, IL, USA). Rhythmic Power, a measure of the strength of the free-running rhythm, was calculated by subtracting the periodogram amplitude from the χ–square value measured at a significance of 0.01. Rhythmic flies were those with Power values greater than 10. Rhythmic power, percent rhythmicity, free-running periodicity of rhythmic flies and N are summarized in Table 1.

Sleep and Activity Analysis. Activity and sleep qualities were calculated using PHASE. Activity data from the DAM-system was gathered in total beam crosses per 1-minute bin and averaged to the 30min bin-size specified in PHASE's graphical interface, or normalized to the total activity. PHASE defines sleep as uninterrupted inactivity lasting for five minutes or more, as previously described (Hendricks et al., 2000; Shaw et al., 2000; Huber et al., 2004). Activity or sleep across the entire day, in Zeitgeber-on or –off portions of the day, or between ZT8-12 were compared between genotypes using One-way ANOVA with a Tukey correction for multiple comparisons in Prism software (GraphPad, Prism version 8.0.2 for Mac, GraphPad Software, San Diego, California USA).

Anticipation and Latency Analysis. Activity anticipation or sleep latency area under the curve (AUC) and duration (minutes) measures are taken following the application of a Savitzky-Golay filter with a X-order polynomial to the original 1-minute binned data. The polynomial order, and filter frame length is specified in each figure legend that uses Anticipation or Latency analysis. Maximum and minimum activity or sleep bins were determined when anchored to the Zeitgeber on- and offset specified in the figure legend for each experiment. For each paradigm, standard equinox, long-day or natural, PHASE explored a 3-hour window to determine the maximum and minimum activity or sleep bins excluding the "startle effect" of Zeitgeber transitions. Sleep functions move positively along the x-axis (time) from a ZT to derive the first minima/least amount of sleep and the maxima/greatest amount of sleep from smoothed data. Activity functions move negatively along the x-axis (time) from a ZT to grab the maxima/greatest activity and then the minimum/least activity from smoothed data. Sleep or activity AUC and duration calculations exclude the "startle effect" by gathering maxima and minima from the first bin after or before a given ZT, respectively. The AUC between the two bins and the duration (minutes) of activity anticipation and sleep latency are calculated subsequently from these maxima and minima. Slopes are calculated by drawing a linear regression between unsmoothed behavioral data in the same analysis windows as those in AUC and duration measurements. Intensities include the first bin of a specified ZT. Activity anticipation AUC, duration, slopes and sleep latency AUC, duration, slopes were compared between genotypes using One-way ANOVA with a Tukey correction for multiple comparisons (GraphPad, Prism version 8.0.2 for Mac, GraphPad Software, San Diego, California USA).

Phase Analysis. Phase measures are taken following the application of a Savitzky-Golay filter with a X-order polynomial and X-hour minimum peak distance to the original 1-minute binned data averaged across the first three entrained days of 12:12 and 14:10 behavior or the first, third or sixth day of 23-, 24- and 25-hour period experiments. Order, minimum peak distance and filter frame length are specified in each figure legend for those figures using Phase Analysis. PHASE uses the MATLAB function *findpeaks* to smooth data across a day or average of indicated days, define peak height and width, and thereby calculates area. Shoulder peaks that fall within the peak separation window on either side of a major peak are summed together as a single peak. Phase calls were made for individual flies and converted to distance (in hours) from Zeitgeber onset or offset. The mean and SEM for each genotype's phase ZT and AUC was compared using One-way ANOVA with a Tukey correction for multiple comparisons (GraphPad, Prism version 8.0.2 for Mac, GraphPad Software, San Diego, California USA).

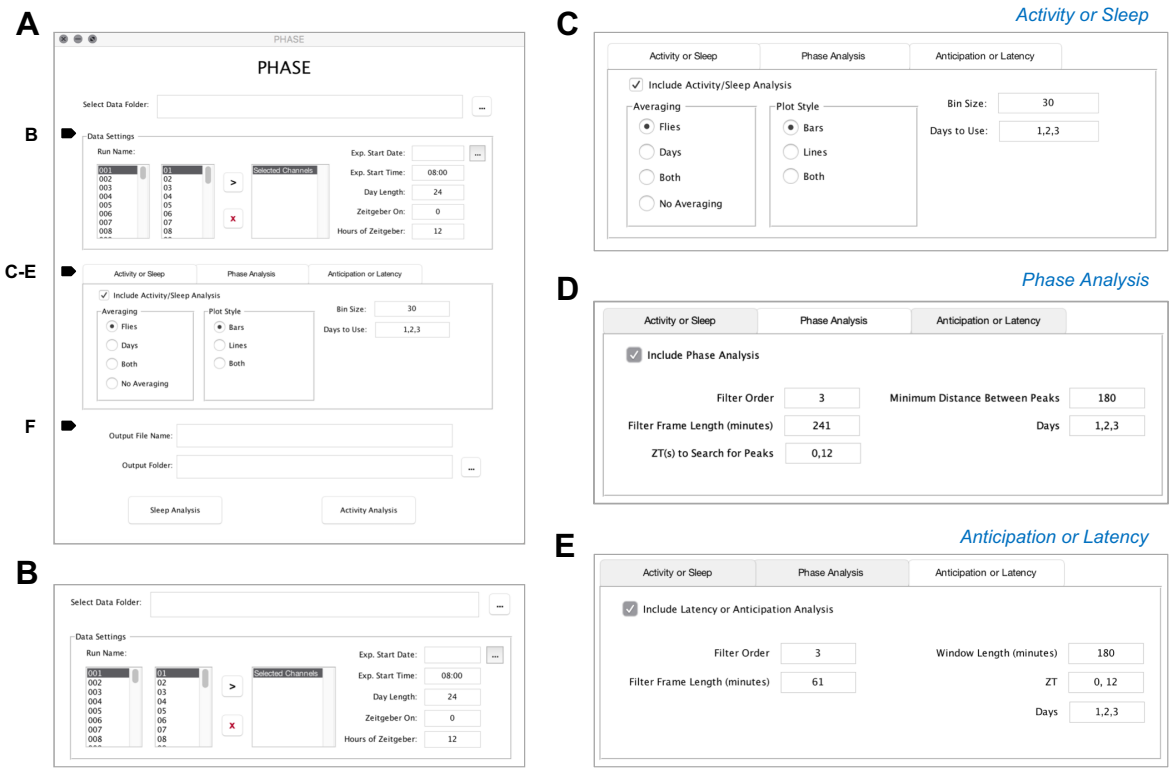

Figure 3.1. The PHASE user interface.
A. The PHASE GUI. Users upload behavior data in "Data Settings" (B), select one, or all of the independent analyses in C-E, specify a "Output File Name" and "Folder" and push the "Sleep" or "Activity Analysis" buttons. B. Completion of "Data Settings" is required for all subsequent analysis. Users select and upload the "Data Folder" containing 1-minute DAMFileScan processed behavior data from a continuous set of dates. PHASE automatically extracts the "Run Name," boards and "Exp. Start Date" and "Time" from the data. Users select the boards and flies to be analyzed, and set the experimental parameters including "Period Length," time of Zeitgeber onset and duration of Zeitgeber. C. PHASE performs "Activity or Sleep" analysis and creates bar or line plots for individual flies and populations over a selection of "Days to Use" with an adjustable "Bin Size". E. The "Phase Analysis" tab prompts users to specify the Savitzky-Golay filter polynomial "Order," and "Frame," the peak separation or "Minimum Distance" and the "Days" over which PHASE defines and finds peaks within smoothed behavior data closest to the user's "ZTs". E. Activity "Anticipation" and sleep "Latency" applies a Savitzky-Golay filter of an indicated polynomial "Order" and "Frame" to averaged "Days" of behavior data. Users specify the window size in minutes that PHASE looks before ("Activity Anticipation") or after ("Sleep Latency") a given "ZT" to determine peak size and duration within smoothed behavior data.

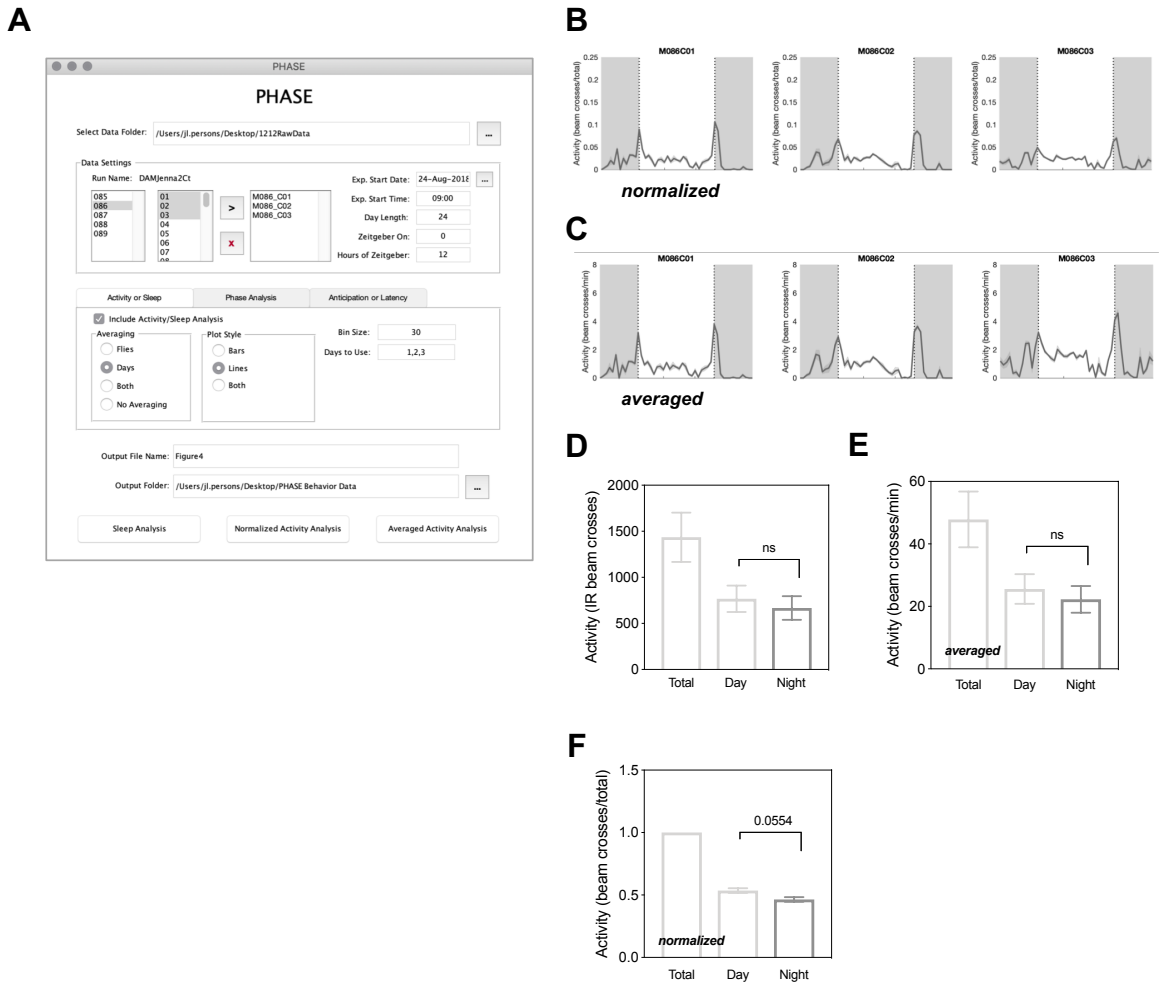

Figure 3.2. Fly activity analysis with PHASE.
A. Data entry for individual w^{1118} flies. B, C. Example activity plots showing 3 sample flies' 3 days of "Normalized" (B) or "Averaged" (C) activity for 3 averaged days of 12:12 LD. Individual plots are automatically titled with the monitor and channel numbers for quick identification and removal of dead, inactive flies. D. Total (across the 24-hour period), Day, and Night activity represented in raw IR beam crosses. E. Total, Day and Night activity represented in "Averaged Activity Analysis" (beam crosses/min) calculated by dividing each 30-minute binned raw IR beam crosses by 30 (or "Bin Size"). F. Total, Day and Night activity represented in "Normalized Activity Analysis" (beam crosses/total) calculated by dividing each 30-minute binned raw IR beam crosses by the total IR beam crosses. Error bar on histograms reflects SEM. P-values are determined by two-tailed unpaired t-test and considered significant if <0.05. N = 3 flies.

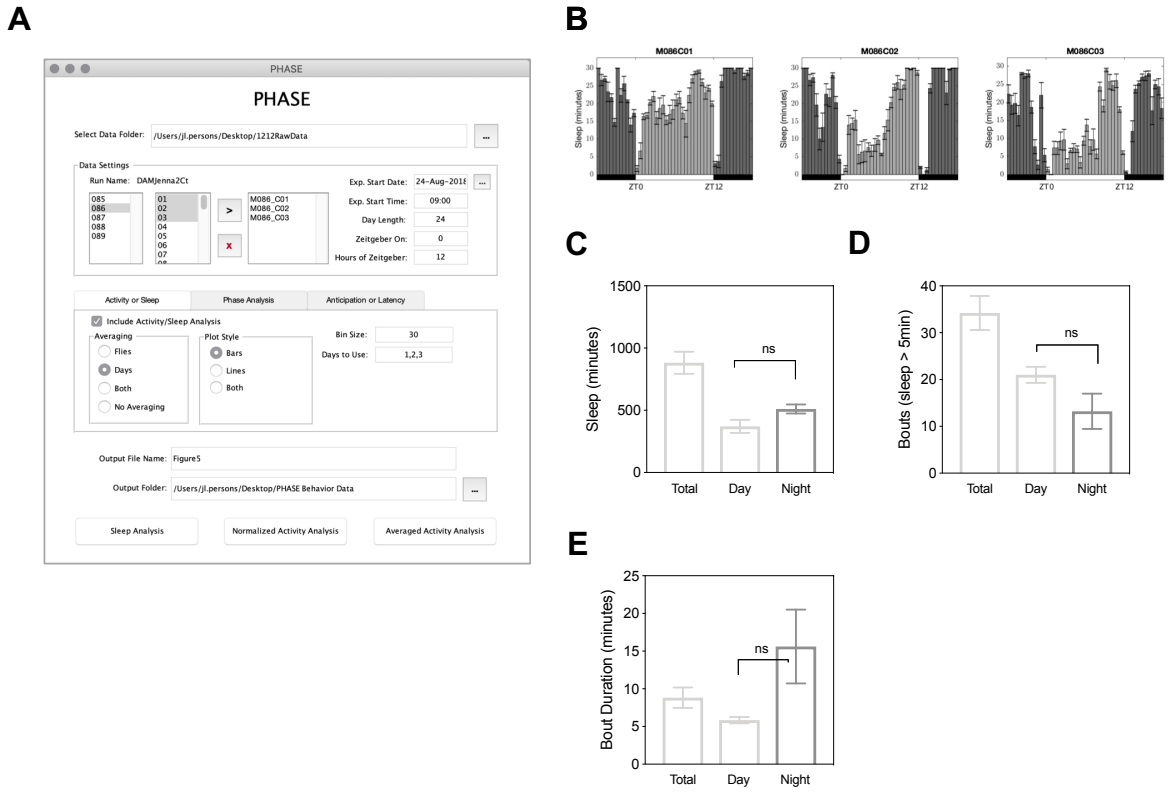

Figure 3.3. Fly sleep analysis with PHASE.
A. Data entry for individual w^{1118} flies. B. Example sleep plots showing 3 days of sleep averaged by "Days" for 3 sample flies. Far left plot shows a dead fly (red text). Individual plots are automatically titled with the monitor and channel numbers for quick identification and removal of dead, inactive flies. C. Total, Day, and Night minutes of sleep. D. Total number of bouts across the entire 24-hour period (Total), Day or Night. One bout of sleep is any 5-minute or greater bout of inactivity, where there were no IR beam crosses. The effective minimum for a bout is therefore, 5-minutes. E. The average bout duration across the 24-hour period, in the Day or Night. Error bar on histograms reflects SEM. P-values are determined by two-tailed unpaired t-test and considered significant if <0.05. N = 3 flies.

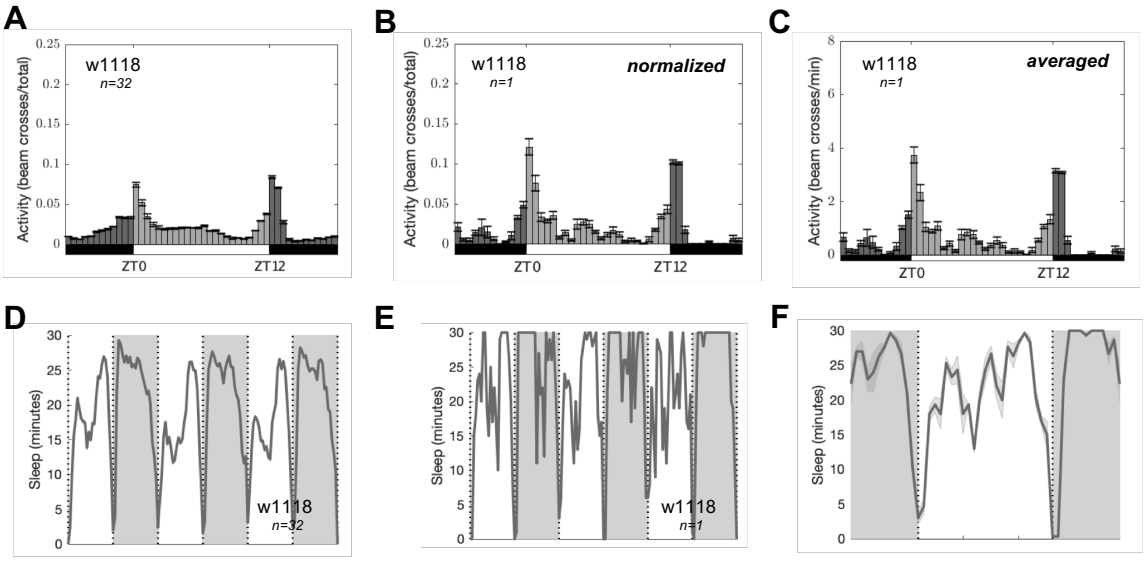

Figure 3.4. PHASE graph outputs.
A-F. Plotting options in the "Activity or Sleep" analysis tab allow users to create line (D-F) or bar graphs (A-C) of sleep and activity behavior averaged or separated by days for entire populations and individual flies. A-C. PHASE graphs of an average of 3 days of 12:12 LD activity data normalized to total activity for an entire population of w^{1118} flies (A) or individuals (B). PHASE also graphs activity averaged by the "Bin Size." Sleep plots for the same 3 days of 12:12 LD data as in A-C with *un*averaged consecutive days displayed for the population average (D) and single flies with 30-minute bins (E) and averaged days for single flies (F). Line graphs display the mean as a bold line, with the SEM shaded above and below the mean. Bars graphs display X-minute binned activity or sleep data and SEM. Graphs are saved as .fig files that are easily manipulated in MATLAB and exportable as .jpg, .tif, or .pdf formats for publications.

A

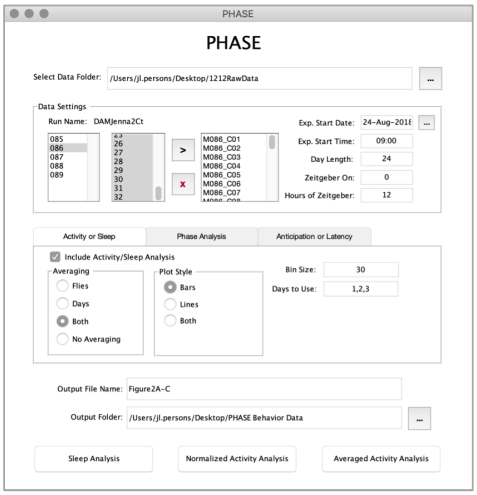

B

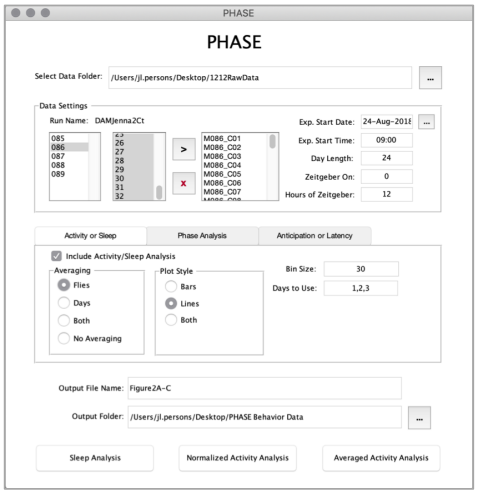

Figure 3.5. PHASE data settings for Figure 3.4.
A. Data entry for Figure 2A–C. 3-days (August 24th – August 26th) of activity averaged by "Both" flies and days for 32 Canton-s flies in 12:12 LD cycle 9:00am to 9:00pm. "Normalized Activity Analysis" was selected for A and B. "Averaged Activity Analysis" was selected for C. B. Data entry for Figure 2D-F. 3-days averaged (August 24th – August 26th) sleep analysis of 32 Canton-s flies in 12:12 LD cycle 9:00am to 9:00pm. Averaging was by "Flies" in D and E, and by "Both" in F.

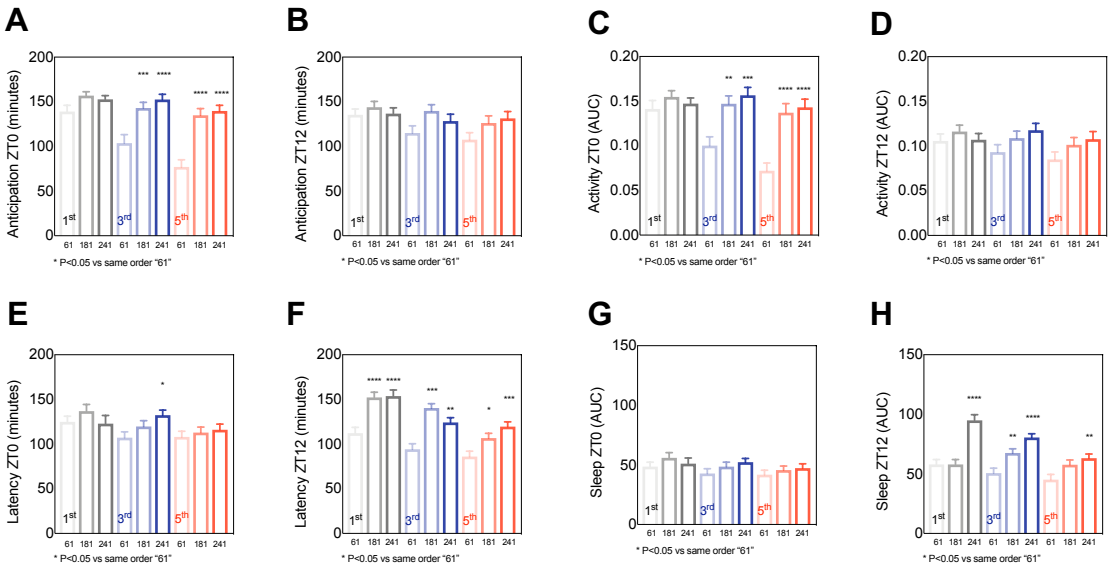

Figure 3.6. Comparison of activity anticipation and sleep latency measurements using iterative Savitzky-Golay filters.

Data in histograms represents w^{1118} (n=32) behavior collected from the first 3 days of entrained 12:12 LD conditions. A-H. 1-minute behavior data was first averaged by day for individual flies, then by population and fitted to a 1st, 3rd, or 5th -order polynomial with 1, 3, and 4-hour frame lengths (specified in minutes as they appear in PHASE's user interface on X-axis). All activity was processed using "Normalized Activity Analysis." 1-minute activity data was converted to sleep before application of polynomial filters. PHASE defined activity anticipation (A-D) and sleep latency (E-H) AUC and duration in minutes from the smoothed data's maximum and minimum bins within a 3-hour window before (activity anticipation) or after (sleep latency) lights-on (ZT0) and lights-off (Z12). Error bars on histograms reflect SEM. P-values are reported if >0.05 by One-way ANOVA with Tukey correction for multiple comparisons between all groups. * indicates significant difference from within order frame size 61, or 1-hour. ^ indicates significance from cs. P-value key: 0.033 (* or ^), 0.002 (** or ^^), <0.001 (*** or ^^^), <0.0001 (**** or ^^^^). N= 32 for all histograms.

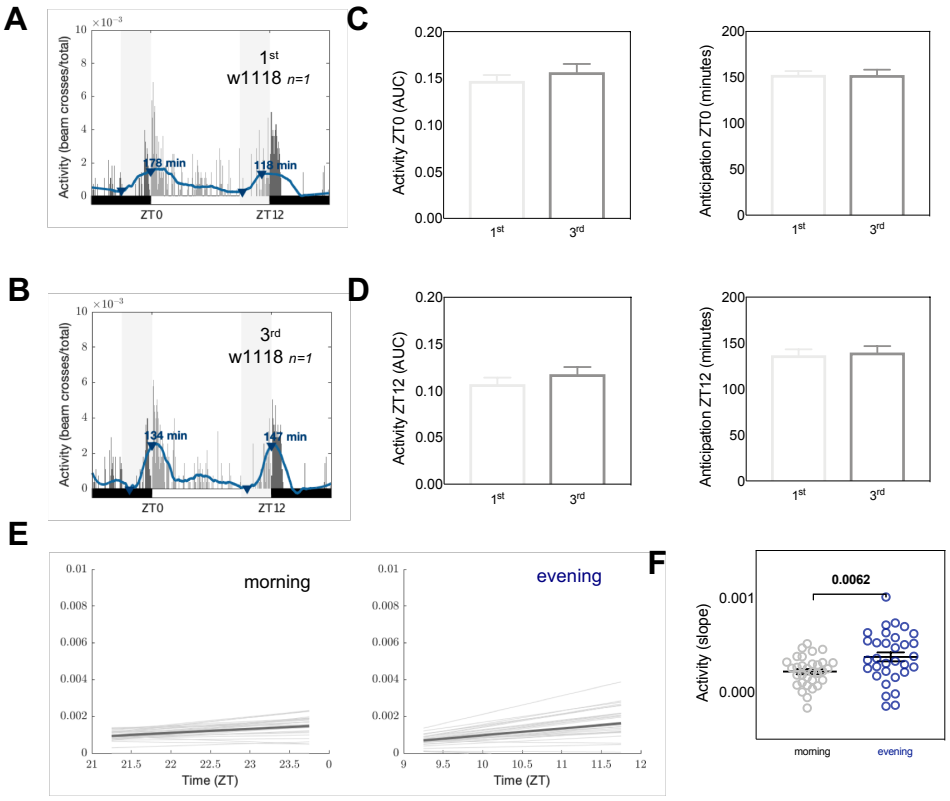

Figure 3.7. Measuring activity anticipation using Savitzky-Golay smoothing and unsmoothed linear-regression.

Data in anticipation graphs (individual flies), slope plots and histograms (population) represents w^{1118} behavior collected from the first 3 days of entrained 12:12 LD conditions. A-D. 1-minute behavior data was first averaged by day for individual flies, then by population and fitted to a 1st and 3rd- order polynomial with a 241-minute, or 4-hour frame length. PHASE defined activity anticipation measures from the smoothed data's maximum and minimum bins within a 3-hour window before lights-on (ZT0) and lights-off (Z12). A, B. Representative Savitzky-Golay fitting of a 1st (A) and 3rd –order polynomial (B) to activity data from the same cs fly. The blue line represents the smoothed data. Blue carrots mark the minimum and maximum within the grey-shaded analysis window before ZT0 and ZT12. Duration between min and max bins annotates the maximum carrot. C, D. The activity anticipation AUC (left) and duration in minutes (right) of smoothed data between maximums and minimums before ZT0 (C) and ZT12 (D). E. PHASE also defines individual fly's slope of a linear regression through *un*smoothed data in the same window as in A-D. Slope plots of unsmoothed 1-minute activity data for the 3-hour window before ZT0 (left, morning) and ZT12 (right, evening). The dark grey line plots the population's average linear-regression. F. Average morning and evening anticipation slopes. Error bar on histograms reflects SEM. P-values <0.05 are considered significant and are bolded. N= 32 for all histograms.

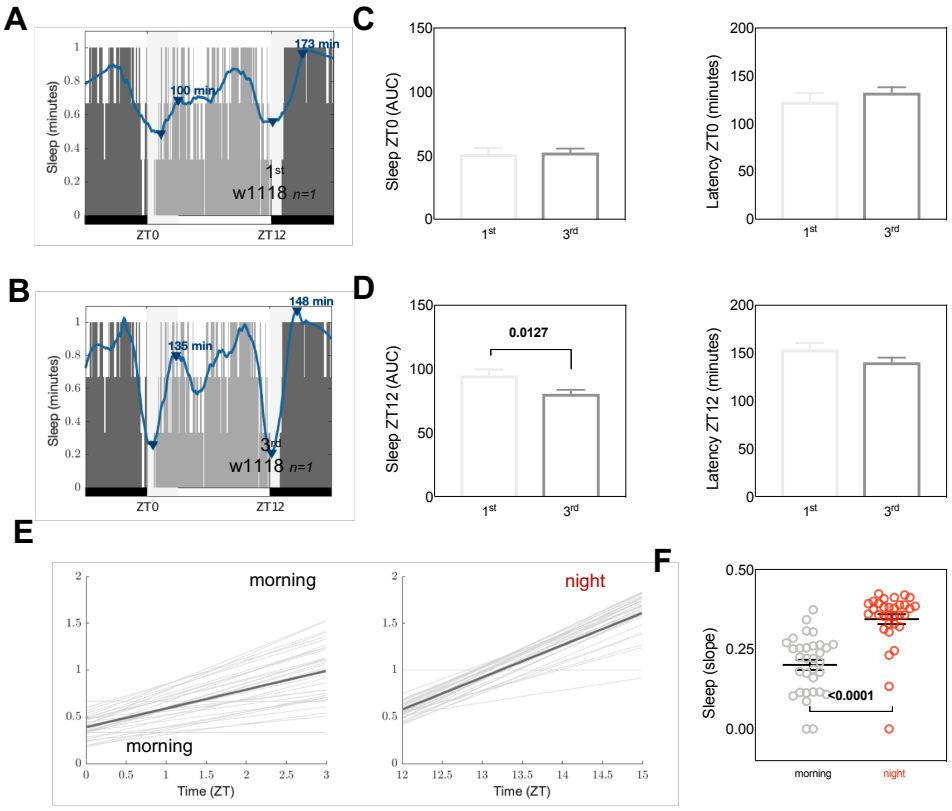

Figure 3.8. Measuring sleep latency using Savitzky-Golay smoothing and unsmoothed linear-regression.

Data in anticipation graphs (individual flies), slope plots and histograms (population) represents w^{1118} behavior collected from the first 3 days of entrained 12:12 LD conditions. PHASE converts 1-minute activity data to sleep using a binary function where sleep equals "1" for any 1-minute bin part of a 5-minute (or more) series of bins without IR beam crosses, and no sleep equals "0". Therefore, minutes are not true "minutes" as there is an effective 5-minute minimum. A-D. Sleep data was first averaged by day for individual flies, then by population and fitted to a 1st and 3rd- order polynomial with a 241-minute, or 4-hour frame length. PHASE defined sleep latency measures from the smoothed data's maximum and minimum bins within a 3-hour window after lights-on (ZT0) and lights-off (Z12). A, B. Representative Savitzky-Golay fitting of a 1st (A) and 3rd –order polynomial (B) to sleep data from the same cs fly. The blue line represents the smoothed data. Blue carrots mark the minimum and maximum within the grey-shaded analysis window after ZT0 and ZT12. Duration between min and max bins annotates the maximum carrot. C, D. The sleep latency AUC (left) and duration in minutes (right) of smoothed data between maximums and minimums after ZT0 (C) and ZT12 (D). E. PHASE also defines individual fly's sleep slope of a linear regression through *un*smoothed data in the same window as in A-D. Slope plots of unsmoothed sleep data for the 3-hour window after ZT0 (left, morning) and ZT12 (right, evening). The dark grey line plots the population's average linear-regression. F. Average morning and night sleep slopes. Error bar on histograms reflects SEM. P-values <0.05 are considered significant and are bolded. N= 32 for all histograms.

A

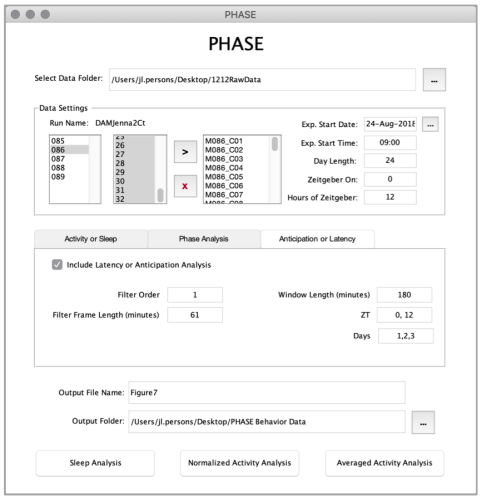

B

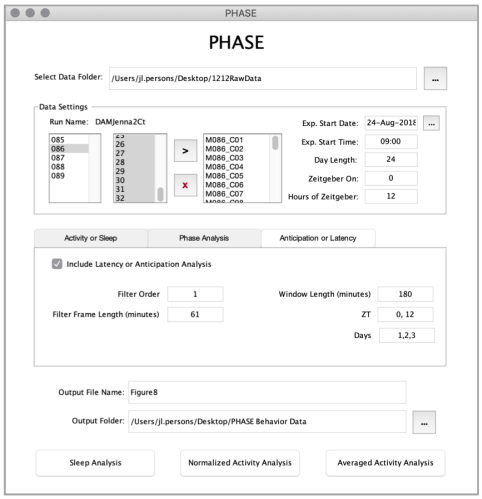

Figure 3.9. PHASE data settings for Figures 3.7 and 3.8.
A. Data entry for Figure 7A–F. 3-days (August 24th – August 26th) of averaged activity analyzed in the “180” -minutes before ZTs “0, 12” with a 1st or 3rd –order and ”241” –minute frame Savitzky-Golay filter. B. Data entry for Figure 8A–F. 3-days (August 24th – August 26th) of averaged sleep analyzed in the “180” -minutes after ZTs “0, 12” with a 1st or 3rd –order and ”241” –minute frame Savitzky-Golay filter.

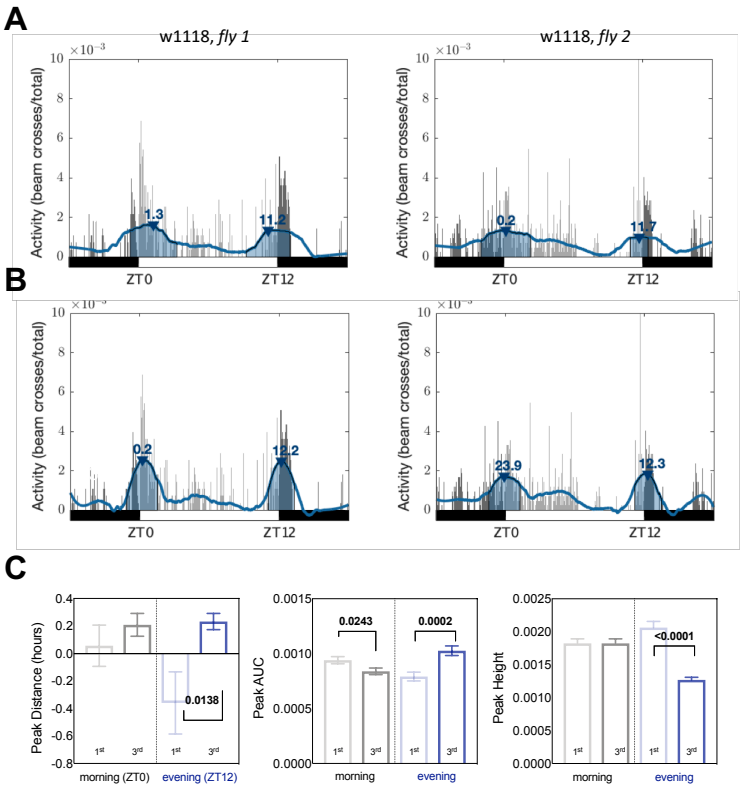

Figure 3.10. Activity phase calls using Savitzky-Golay smoothing functions.
A-C. The first 3 days of entrained 12:12 LD activity data was first averaged by day for individual flies, then by population, and fitted using Savitzky-Golay smoothing functions with a 1st or 3rd –order polynomial, 241-minute frame and a 180-minute or 3-hour distance peak separation. PHASE called peaks closest to ZT 0 and ZT 12. PHASE applies *findpeaks* to smoothed data to determine the peak maximum, height (1-minute beam crosses) and width (minutes). 1-minute peak maximums are converted to ZT relative to those specified in "Data Settings." We called peaks closest to ZT 0 and ZT 12. A, B. Two representative w^{1118} flies fitted with a 1st –order filter (A) or 3rd –order filter. Blue line over 1-minute activity data represents Savitzky-Golay smoothed data. Blue shading represents peak area, while blue carrots indicate peak maximums annotated with ZT. C. Average of 32 Canton-s flies' peak activity phase relative to ZT0 or ZT12 (left), area (middle) and height (right) for morning and evening peak calls with 1st and 3rd –order polynomials. Error bar on histograms reflects SEM. P-values are reported if <0.05 as determined by two-tailed unpaired t-test between 1st and 3rd polynomials within morning and evening peaks. P-values <0.05 are considered significant. N = 32 for histograms.

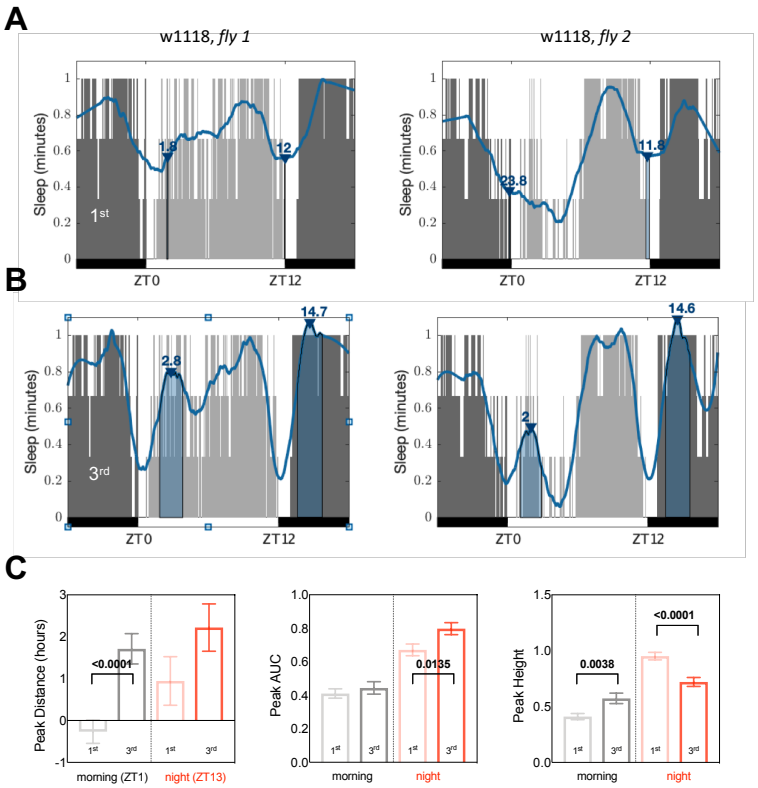

Figure 3.11. Sleep phase calls using Savitzky-Golay smoothing functions.
A-C. The first 3 days of entrained 12:12 LD sleep data was first averaged by day for individual flies, then by population, and fitted using Savitzky-Golay smoothing functions with a 1st or 3rd –order polynomial, 241-minute frame and a 180-minute or 3-hour distance peak separation. PHASE applies *findpeaks* to smoothed data to determine the peak maximum, height (1-minute beam crosses) and width (minutes). 1-minute peak maximums are converted to ZT relative to those specified in "Data Settings." We called peaks closest to ZT 1 and ZT13. A, B. Two representative w^{1118} flies fitted with a 1st –order filter (A) or 3rd –order filter. Blue line over 1-minute sleep data represents Savitzky-Golay smoothed data. Blue shading represents peak area, while blue carrots indicate peak maximums annotated with ZT. C. Average of 32 Canton-s flies' peak sleep phase relative to ZT1 and ZT13 (left), area (middle) and height (right) for early morning (ZT 18-24) and early night (ZT12-16) peak calls with 1st and 3rd –order polynomials. Error bar on histograms reflects SEM. P-values are reported if <0.05 as determined by two-tailed unpaired t-test between 1st and 3rd polynomials within morning and night peaks. P-values <0.05 are considered significant. N = 32 for histograms.

A

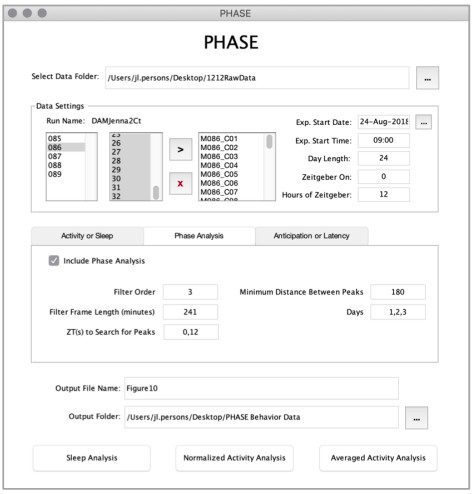

B

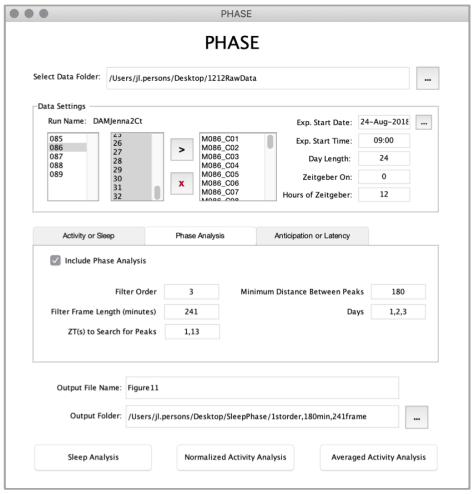

Figure 3.12. PHASE data settings for Figures 3.10 and 3.11.
A. Data entry for Figure 10A–C. 3-days (August 24th – August 26th) of averaged activity phase analyzed with a 1st or 3rd –order and ”241” –minute frame length Savitzky-Golay filter and ”180” –minute peak separation. B. Data entry for Figure 11A–C. 3-days (August 24th – August 26th) of averaged sleep phase analyzed with a 1st or 3rd –order and ”241” –minute frame length Savitzky-Golay filter and ”180” –minute peak separation.

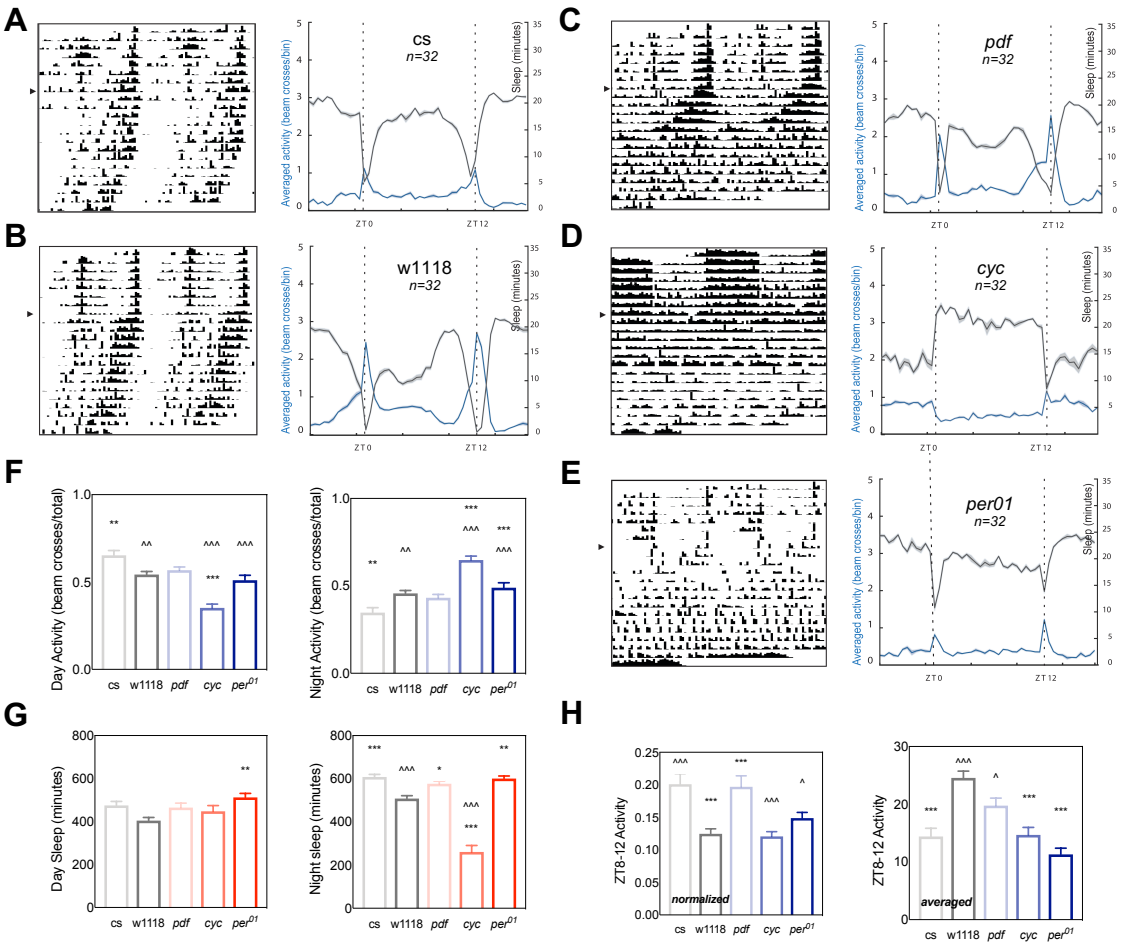

Figure 3.13. Activity and sleep analysis of wildtype Canton-s and w^{1118}, and circadian mutants, per^{01}, cyc and pdf in standard, equinox light.

A-E. Flies were entrained for 2 days and left in 12:12 LD conditions for 4 subsequent days before release into constant darkness, constant temperature for 14 days. Representative fly actograms (left) for the duration of the experiment for each genotype. Arrow represents first day of constant conditions. Graphs on right and data in histograms represent the genotype's average of the first 3 days of entrained 12:12 LD for sleep (grey) or 30-minute binned "Averaged" activity (blue). Quantities were first averaged for individual flies across the 3 days of LD, and then by genotype. F. Day (right) and night (left) "Normalized" activity. G. Day (left) and night (right) sleep (minutes). H. Activity quantities exclusively during ZT8-12, "Normalized" on left and "Averaged" on right. Error bars on histograms reflect SEM. P-values are reported if >0.05 by One-way ANOVA with Tukey correction for multiple comparisons between all groups. * indicates significant difference from w^{1118}. ^ indicates significance from cs. P-value key: 0.033 (* or ^), 0.002 (** or ^^), <0.001 (*** or ^^^), <0..0001 (**** or ^^^^). These flies are also used for data in Figures 14-17. N= 32 flies for all histograms, activity and sleep plots.

Genotype	n	Rhythmic Power	Percent Rhythmicity	Rhythmic N	Period (of Rhythmic n)
w1118	30	104.45 ± 10.20	100	30	23.57 ± 0.04
cs	26	30.65 ± 7.43	69.23	18	23.93 ± 0.13
pdf	25	16.64 ± 5.76	44.00	11	22.91 ± 0.42
cyc	27	-11.41 ± 2.38	0	0	N/A
per01	19	-3.18 ± 1.94	15.79	3	30.83 ± 0.60

Table 3.1. ClockLab analysis of flies in Figures 3.13-3.16.
See Materials and Methods for analysis details.

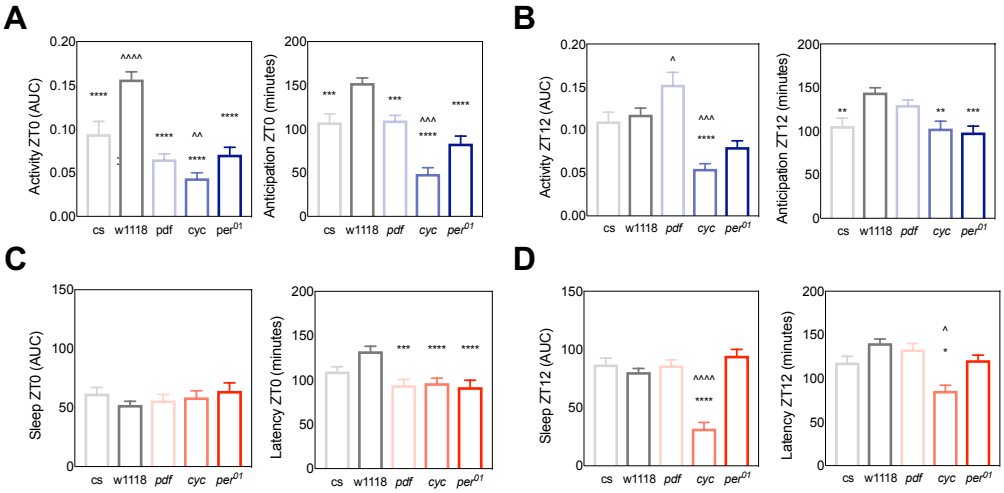

Figure 3.14. Activity anticipation and sleep latency analysis of wildtype Canton-s and w^{1118}, and circadian mutants, per^{01}, cyc and pdf.

A-D. Flies were entrained for 2 days and left in 12:12 LD conditions for 4 subsequent days before release into constant darkness, constant temperature for 14 days. Data in histograms represent the genotype's average for the first 3 days of entrained 12:12 LD for sleep (red) or 30-minute binned activity "Normalized" to the total activity (blue). 1-minute behavior data was first averaged by day for individual flies, then by population and fitted to a 3rd- order polynomial with a 241-minute, or 4-hour frame length. PHASE defined anticipation and latency measures from the smoothed data's maximum and minimum bins within a 3-hour window before or after lights-on (ZT0) and lights-off (Z12), respectively. A, B. Activity AUC (left) and anticipation duration (right) for 3-hours before morning (A) and evening (B) light transitions. C, D. Sleep AUC (left) and latency duration (right) for 3-hours after morning (C) and evening (D) light transitions. Error bars on histograms reflect SEM. P-values are reported if >0.05 by One-way ANOVA with Tukey correction for multiple comparisons between all groups. * indicates significant difference from w^{1118}. ^ indicates significance from cs. P-value key: 0.033 (* or ^), 0.002 (** or ^^), <0.001 (*** or ^^^), <0.0001 (**** or ^^^^). N = 32 for all genotypes.

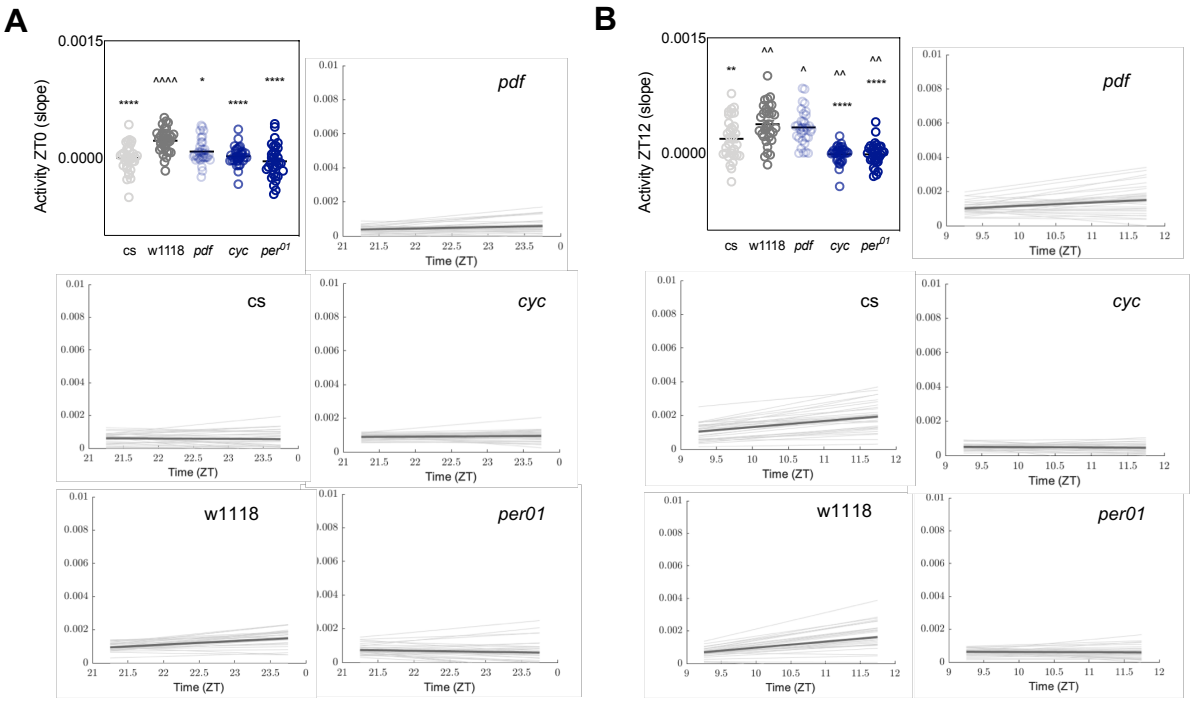

Figure 3.15. Morning and evening activity anticipation slopes.
A, B. Flies were entrained for 2 days and left in 12:12 LD conditions for 4 subsequent days. Data represent the genotype's average for the first 3 days of entrained 12:12 LD. PHASE calculated each individual fly's average activity slope of a linear regression through *un*smoothed data in the 3-hour window prior to ZT0 (A) or ZT12 (B). Slopes were first averaged by day for individual flies, then by genotype for histograms. Slope plots represent each genotypes' unsmoothed normalized activity data for the 3-hour window before ZT0 or ZT12. Open circles represent all selected flies unsmoothed behavior data. Light grey lines are individual fly linear regressions. The dark grey line plots the population's average linear-regression. Error bars on histograms reflect SEM. P-values are reported if >0.05 by One-way ANOVA with Tukey correction for multiple comparisons between all groups. * indicates significant difference from w^{1118}. ^ indicates significance from cs. P-value key: 0.033 (* or ^), 0.002 (** or ^^), <0.001 (*** or ^^^), <0.0001 (**** or ^^^^). N = 32 for each genotype.

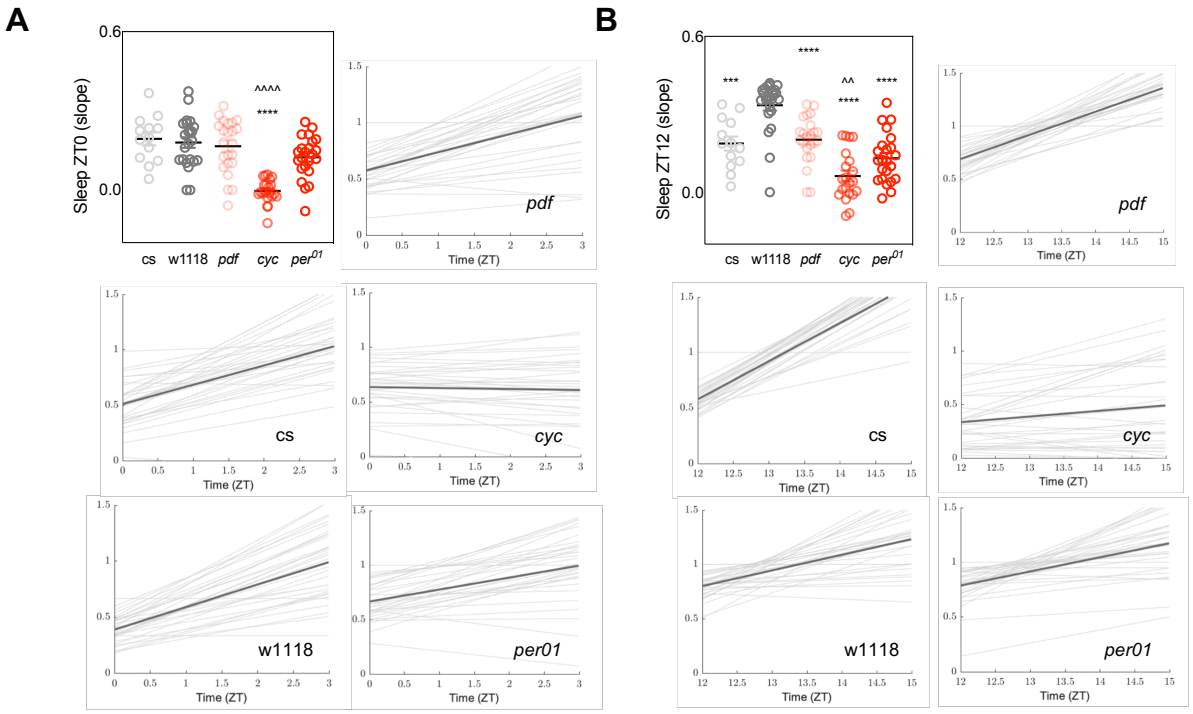

Figure 3.16. Morning and night sleep latency slope.
A, B. Flies were entrained for 2 days and left in 12:12 LD conditions for 4 subsequent days. LD. Data represent the genotype's average for the first 3 days of entrained 12:12 LD. PHASE converted 1-minute activity data to sleep using a binary function where sleep equals "1" for any 1-minute bin part of a 5-minute (or more) series of bins without IR beam crosses, and no sleep equals "0". Therefore, minutes are not true "minutes" as there is an effective 5-minute minimum. The binary nature of any given bin of sleep data makes sleep latency measures more discrete than activity anticipation (Figure 8). PHASE calculated each individual fly's average latency slope of a linear regression through *un*smoothed data in the 3-hour window after ZT0 (A) or ZT12 (B). Slopes were first averaged by day for individual flies, then by genotype for histograms. Slope plots represent each genotypes' unsmoothed sleep data for the 3-hour window before ZT0 or ZT12. Open circles represent all selected flies unsmoothed behavior data. Light grey lines are individual fly linear regressions. The dark grey line plots the population's average linear-regression. Error bars on histograms reflect SEM. P-values are reported if >0.05 by One-way ANOVA with Tukey correction for multiple comparisons between all groups. * indicates significant difference from w^{1118}. ^ indicates significance from cs. P-value key: 0.033 (* or ^), 0.002 (** or ^^), <0.001 (*** or ^^^), <0.0001 (**** or ^^^^). N= 32 for all genotypes.

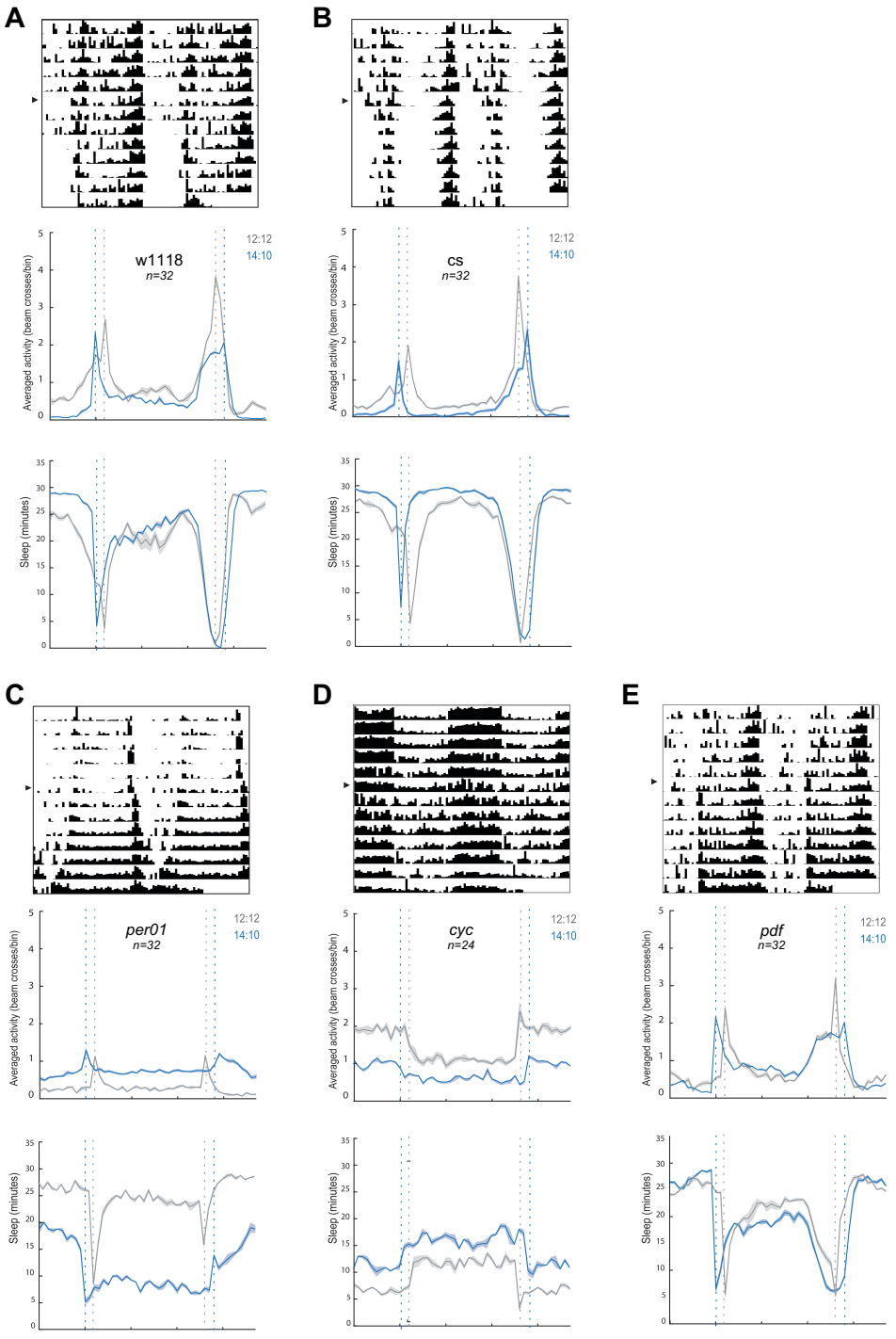

Figure 3.17. Activity and sleep of wildtype Canton-s and w^{1118}, and circadian mutants, per^{01}, cyc and pdf in equinox and long-days (14:10 LD).

A-E. Flies were entrained for 2 days and left in 12:12 LD conditions for 4 subsequent days before transitioning to 14:10 LD conditions for 7 days. Representative fly actograms (top) for the duration of the experiment for each genotype. Arrow represents first day of 14:10 long-day conditions. 30-minute binned averaged activity (middle) and sleep (bottom) line graphs represent the genotype's average of the first 3 days of entrained 12:12 LD (grey) or 14:10 LD (blue). Quantities were first averaged for individual flies across the 3 days of each LD condition, and then by genotype. These flies are the source data for Figures 17-23.

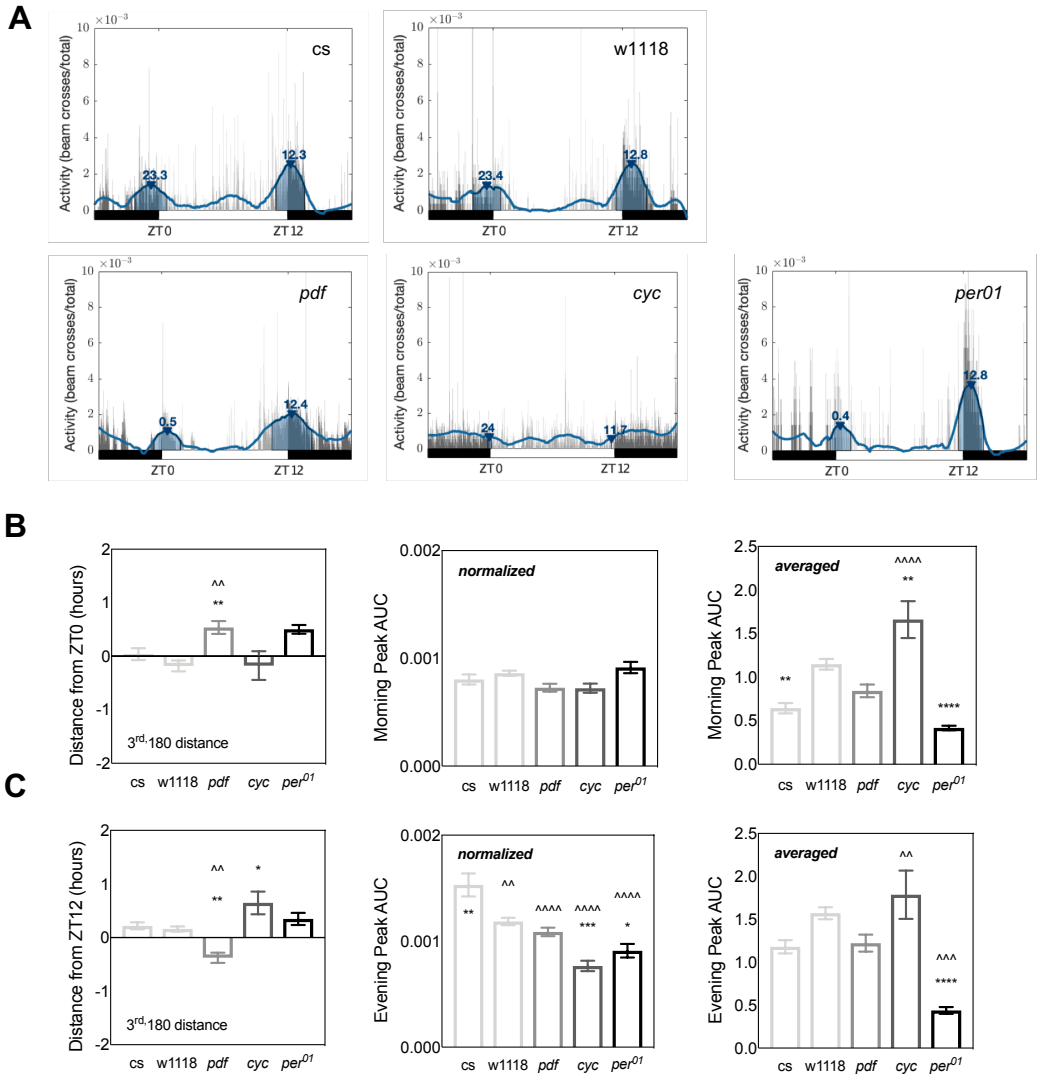

Figure 3.18. Equinox phase analysis using a Savitzky-Golay filter with 3rd –order polynomial, 241-minute frame, and 3-hour peak separation.
A-C. The first 3 days of entrained 12:12 LD activity data was averaged by day for individual flies, then by population, and fitted using Savitzky-Golay smoothing functions with a 3rd –order polynomial, 241-minute frame and a 180-minute or 3-hour minimum peak distance. PHASE applied *findpeaks* to smoothed data to determine the peak maximum, height (1-minute beam crosses) and width (minutes). 1-minute peak maximums were converted to ZT relative to the equinox paradigm specified in "Data Settings". A. Representative flies fitted with the Savitzky-Golay filter. Blue line over 1-minute normalized activity data represents Savitzky-Golay smoothed data. Blue shading represents peak area and blue carrots indicate peak maximums annotated with ZT. C. Average of each genotype's peak activity phase distance in hours from lights-on or lights off (left) and the associated peak's area under the smoothed curve (AUC) for normalized (middle) and averaged (right) activity in morning (B) and evening (C) peak calls. Error bars on histograms reflect SEM. P-values are reported if >0.05 by One-way ANOVA with Tukey correction for multiple comparisons between all groups. * indicates significant difference from w^{1118}. ^ indicates significance from cs. P-value key: 0.033 (* or ^), 0.002 (** or ^^), <0.001 (*** or ^^^), <0.0001 (**** or ^^^^).

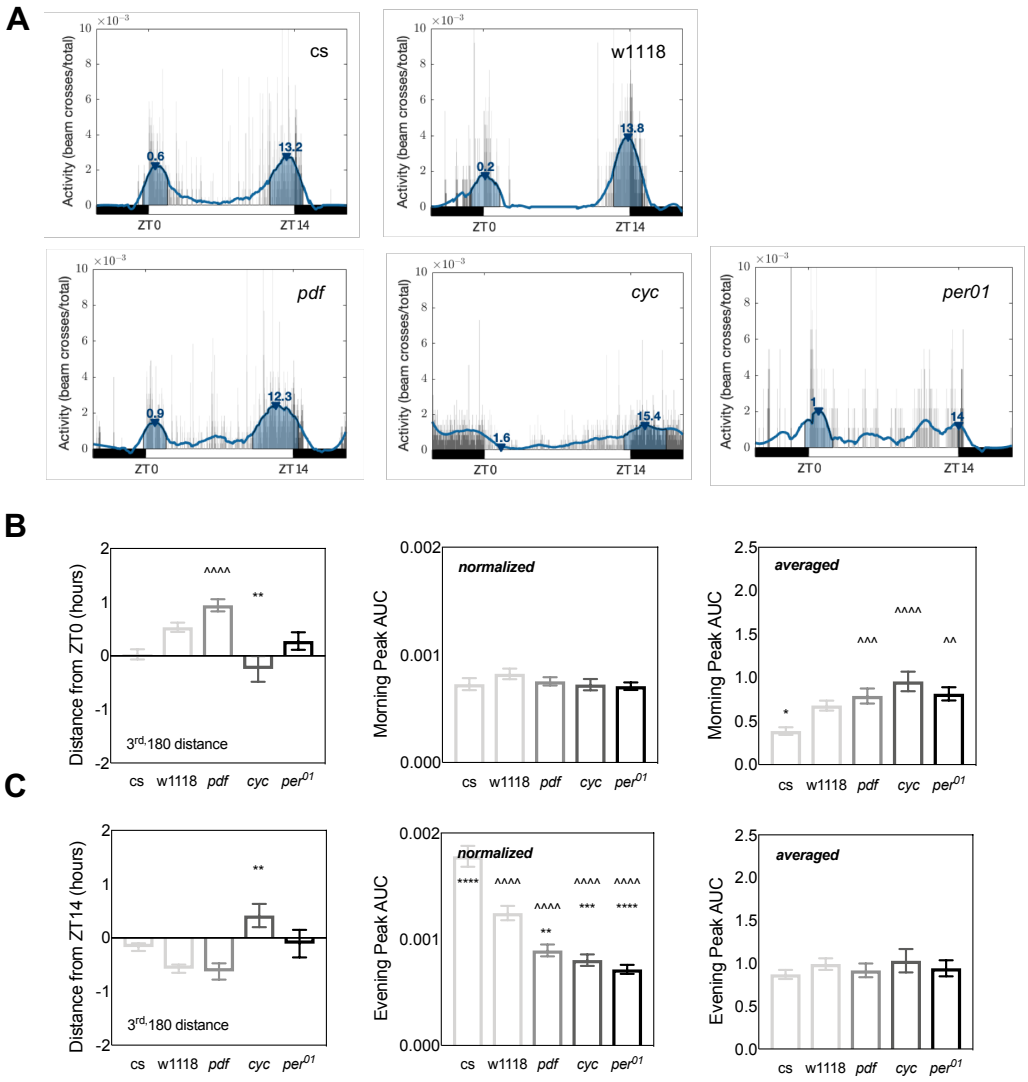

Figure 3.19. Long-day phase analysis using a Savitzky-Golay filter with 3rd –order polynomial, 241-minute frame, and 3-hour peak separation.

A-C. The first 3 days of entrained 14:10 LD activity data was averaged by day for individual flies, then by population, and fitted using Savitzky-Golay smoothing functions with a 3rd –order polynomial, 241-minute frame and a 180-minute or 3-hour minimum peak distance. PHASE applied *findpeaks* to smoothed data to determine the peak maximum, height (1-minute beam crosses) and width (minutes). 1-minute peak maximums were converted to ZT relative to the paradigm specified in "Data Settings". A. Representative flies fitted with the Savitzky-Golay filter. Blue line over 1-minute activity data represents Savitzky-Golay smoothed data. Blue shading represents peak area and blue carrots indicate peak maximums annotated with ZT. C. Average of each genotype's peak activity phase distance in hours from lights-on or lights off (left) and the associated peak's area under the smoothed curve (AUC) for normalized (middle) and averaged (right) activity in morning (B) and evening (C) peak calls. Error bars on histograms reflect SEM. P-values are reported if >0.05 by One-way ANOVA with Tukey correction for multiple comparisons between all groups. * indicates significant difference from w^{1118}. ^ indicates significance from cs. P-value key: 0.033 (* or ^), 0.002 (** or ^^), <0.001 (*** or ^^^), <0.0001 (**** or ^^^^).

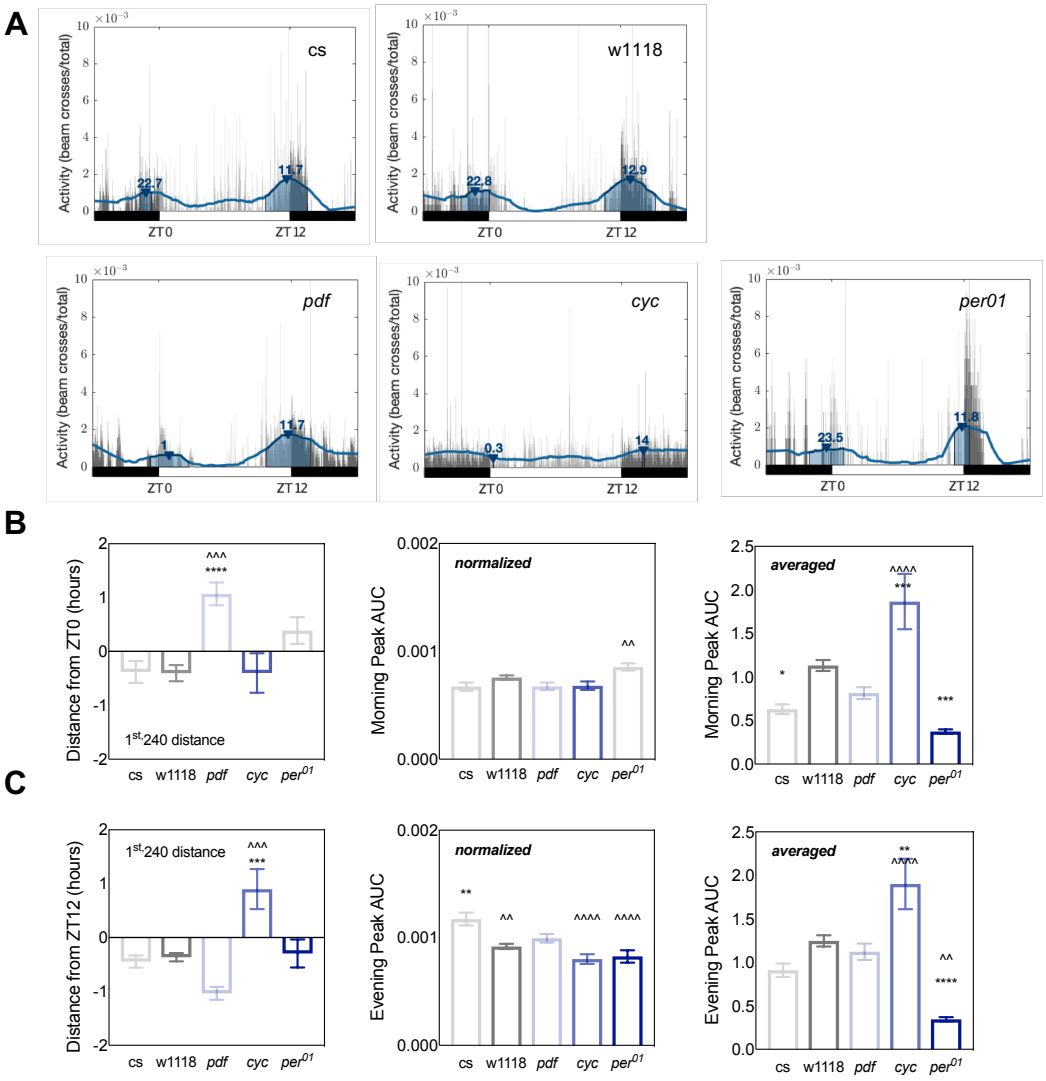

Figure 3.20. Equinox phase analysis using a Savitzky-Golay filter with 1st –order polynomial, 241-minute frame, and 4-hour peak separation.
A-C. The first 3 days of entrained 12:12 LD activity data was averaged by day for individual flies, then by population, and fitted using Savitzky-Golay smoothing functions with a 1st –order polynomial, 241-minute frame and a 240-minute or 4-hour minimum peak distance. PHASE applied *findpeaks* to smoothed data to determine the peak maximum, height (1-minute beam crosses) and width (minutes). 1-minute peak maximums were converted to ZT relative to the equinox paradigm specified in "Data Settings". A. Representative flies fitted with the Savitzky-Golay filter. Blue line over 1-minute activity data represents Savitzky-Golay smoothed data. Blue shading represents peak area and blue carrots indicate peak maximums annotated with ZT. C. Average of each genotype's peak activity phase distance in hours from lights-on or lights off (left) and the associated peak's area under the smoothed curve (AUC) for normalized (middle) and averaged (right) activity in morning (B) and evening (C) peak calls. Error bars on histograms reflect SEM. P-values are reported if >0.05 by One-way ANOVA with Tukey correction for multiple comparisons between all groups. * indicates significant difference from w^{1118}. ^ indicates significance from cs. P-value key: 0.033 (* or ^), 0.002 (** or ^^), <0.001 (*** or ^^^), <0.0001 (**** or ^^^^).

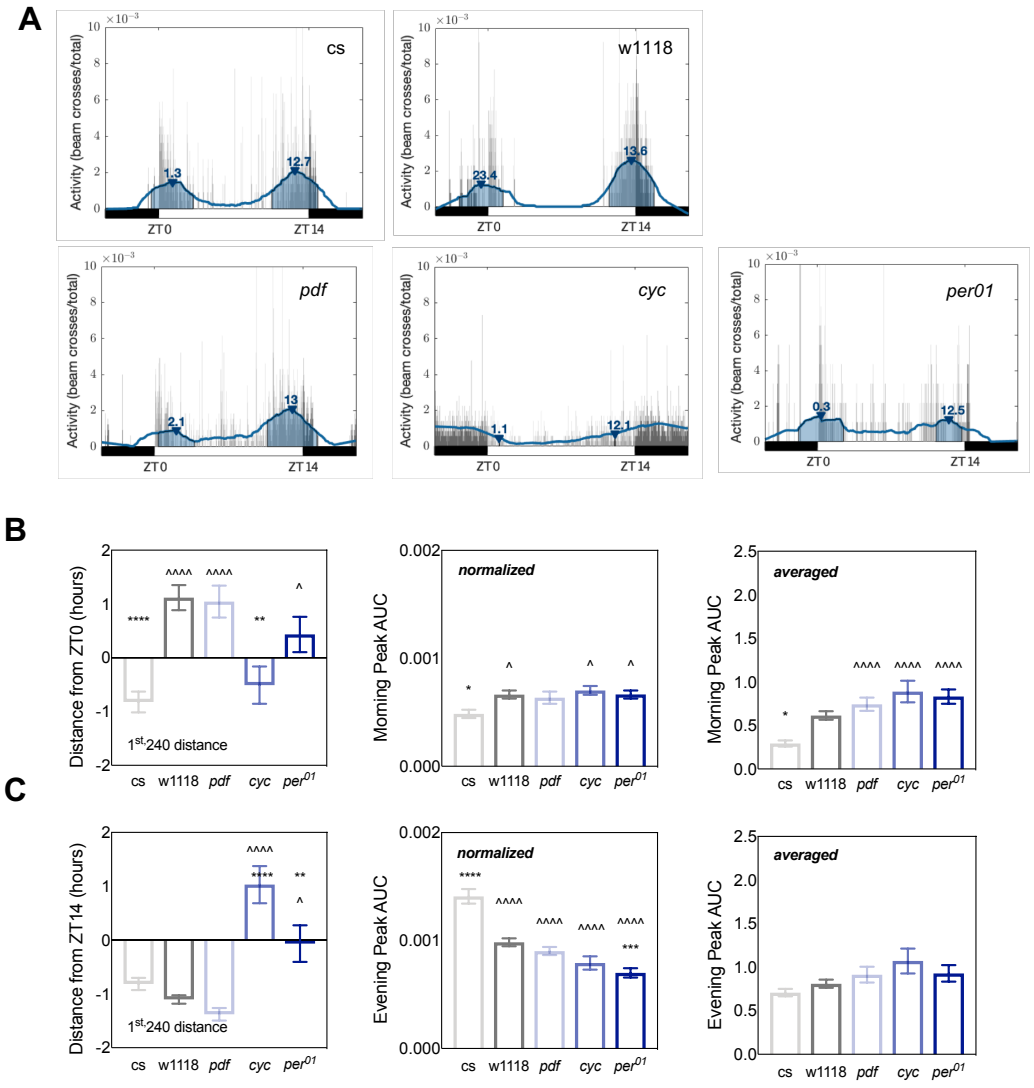

Figure 3.21. Long-day phase analysis using a Savitzky-Golay filter with 1st –order polynomial, 241-minute frame, and 4-hour peak separation.

A-C. The first 3 days of entrained 14:10 LD activity data was averaged by day for individual flies, then by population, and fitted using Savitzky-Golay smoothing functions with a 1st –order polynomial, 241-minute frame and a 240-minute or 4-hour minimum peak distance. PHASE applied *findpeaks* to smoothed data to determine the peak maximum, height (1-minute beam crosses) and width (minutes). 1-minute peak maximums were converted to ZT relative to the paradigm specified in "Data Settings". A. Representative flies fitted with the Savitzky-Golay filter. Blue line over 1-minute activity data represents Savitzky-Golay smoothed data. Blue shading represents peak area and blue carrots indicate peak maximums annotated with ZT. C. Average of each genotype's peak activity phase distance in hours from lights-on or lights off (left) and the associated peak's area under the smoothed curve (AUC) for normalized (middle) and averaged (right) activity in morning (B) and evening (C) peak calls. Error bars on histograms reflect SEM. P-values are reported if >0.05 by One-way ANOVA with Tukey correction for multiple comparisons between all groups. * indicates significant difference from w^{1118}. ^ indicates significance from cs. P-value key: 0.033 (* or ^), 0.002 (** or ^^), <0.001 (*** or ^^^), <0.0001 (**** or ^^^^).

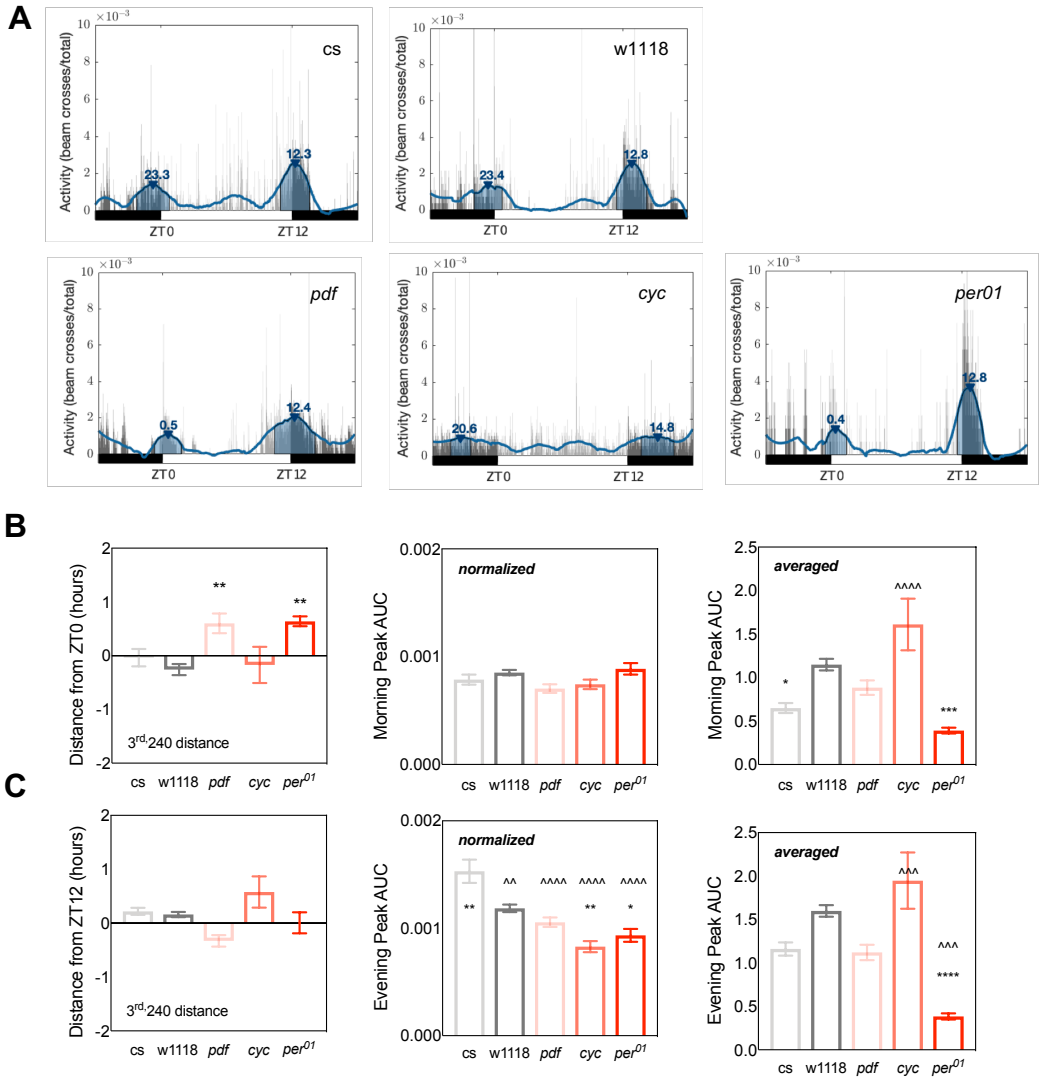

Figure 3.22. Equinox phase analysis using a Savitzky-Golay filter with 3rd –order polynomial, 241-minute frame, and 4-hour peak separation.

A-C. The first 3 days of entrained 12:12 LD activity data was averaged by day for individual flies, then by population, and fitted using Savitzky-Golay smoothing functions with a 3rd –order polynomial, 241-minute frame and a 240-minute or 4-hour minimum peak distance. PHASE applied *findpeaks* to smoothed data to determine the peak maximum, height (1-minute beam crosses) and width (minutes). 1-minute peak maximums were converted to ZT relative to the equinox paradigm specified in "Data Settings". A. Representative flies fitted with the Savitzky-Golay filter. Blue line over 1-minute activity data represents Savitzky-Golay smoothed data. Blue shading represents peak area and blue carrots indicate peak maximums annotated with ZT. C. Average of each genotype's peak activity phase distance in hours from lights-on or lights off (left) and the associated peak's area under the smoothed curve (AUC) for normalized (middle) and averaged (right) activity in morning (B) and evening (C) peak calls. Error bars on histograms reflect SEM. P-values are reported if >0.05 by One-way ANOVA with Tukey correction for multiple comparisons between all groups. * indicates significant difference from w^{1118}. ^ indicates significance from cs. P-value key: 0.033 (* or ^), 0.002 (** or ^^), <0.001 (*** or ^^^), <0.0001 (**** or ^^^^).

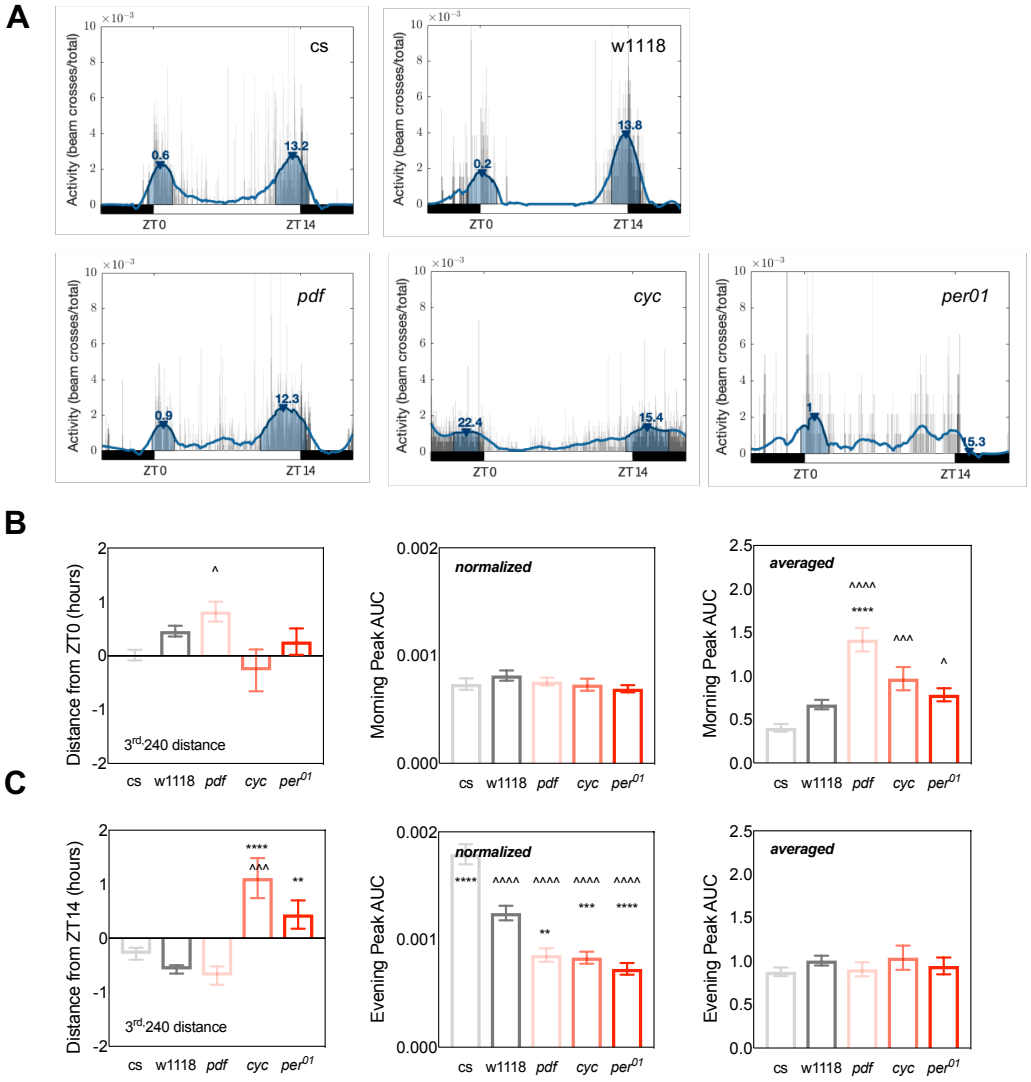

Figure 3.23. Long-day phase analysis using a Savitzky-Golay filter with 3rd –order polynomial, 241-minute frame, and 4-hour peak separation.

A-C. The first 3 days of entrained 14:10 LD activity data was averaged by day for individual flies, then by population, and fitted using Savitzky-Golay smoothing functions with a 3rd –order polynomial, 241-minute frame and a 240-minute or 4-hour minimum peak distance. PHASE applied *findpeaks* to smoothed data to determine the peak maximum, height (1-minute beam crosses) and width (minutes). 1-minute peak maximums were converted to ZT relative to the paradigm specified in "Data Settings". A. Representative flies fitted with the Savitzky-Golay filter. Blue line over 1-minute activity data represents Savitzky-Golay smoothed data. Blue shading represents peak area and blue carrots indicate peak maximums annotated with ZT. C. Average of each genotype's peak activity phase distance in hours from lights-on or lights off (left) and the associated peak's area under the smoothed curve (AUC) for normalized (middle) and averaged (right) activity in morning (B) and evening (C) peak calls. Error bars on histograms reflect SEM. P-values are reported if >0.05 by One-way ANOVA with Tukey correction for multiple comparisons between all groups. * indicates significant difference from w^{1118}. ^ indicates significance from cs. P-value key: 0.033 (* or ^), 0.002 (** or ^^), <0.001 (*** or ^^^), <0.0001 (**** or ^^^^).

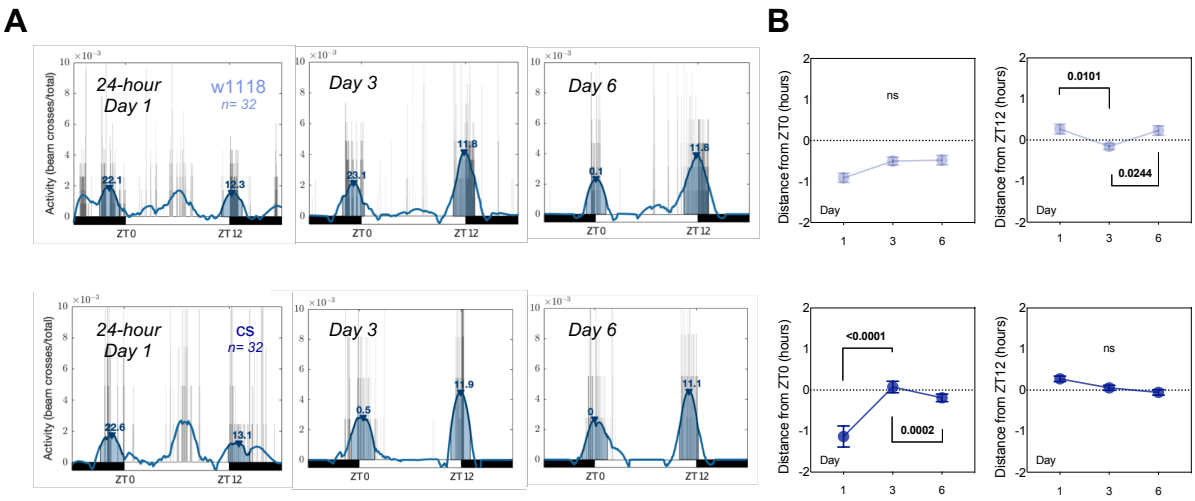

Figure 3.24. Phase analysis of 24-hour period using a Savitzky-Golay filter with 3rd –order polynomial, 241-minute frame, and 3-hour peak separation.

A-B. The first, third, and sixth days of entrained LD activity data in 24–hour periods was averaged by day for individual flies, then by population, and fitted using Savitzky-Golay smoothing functions with a 3rd –order polynomial, 241-minute frame and a 240-minute or 4-hour minimum peak distance. 1-minute peak maximums were converted to ZTs relative to period length, and then to distance in hours from light onset or offset. A. Representative flies from w^{1118} (light blue) or cs (dark blue) fitted with the Savitzky-Golay filter on day one and day six. Blue line over 1-minute activity data represents Savitzky-Golay smoothed data. Blue shading represents peak area and blue carrots indicate peak maximums annotated with ZT. B. Mean of w^{1118} (light blue) or cs (dark blue) population activity phase distance in hours from lights-on or lights off indicated on Y-axis. Number of flies in population average are indicated on representative plots in A. Error bars reflect SEM. P-values are reported with actual values if >0.05 by One-way ANOVA with Tukey correction for multiple comparisons between all days within genotype (w^{1118} or cs).

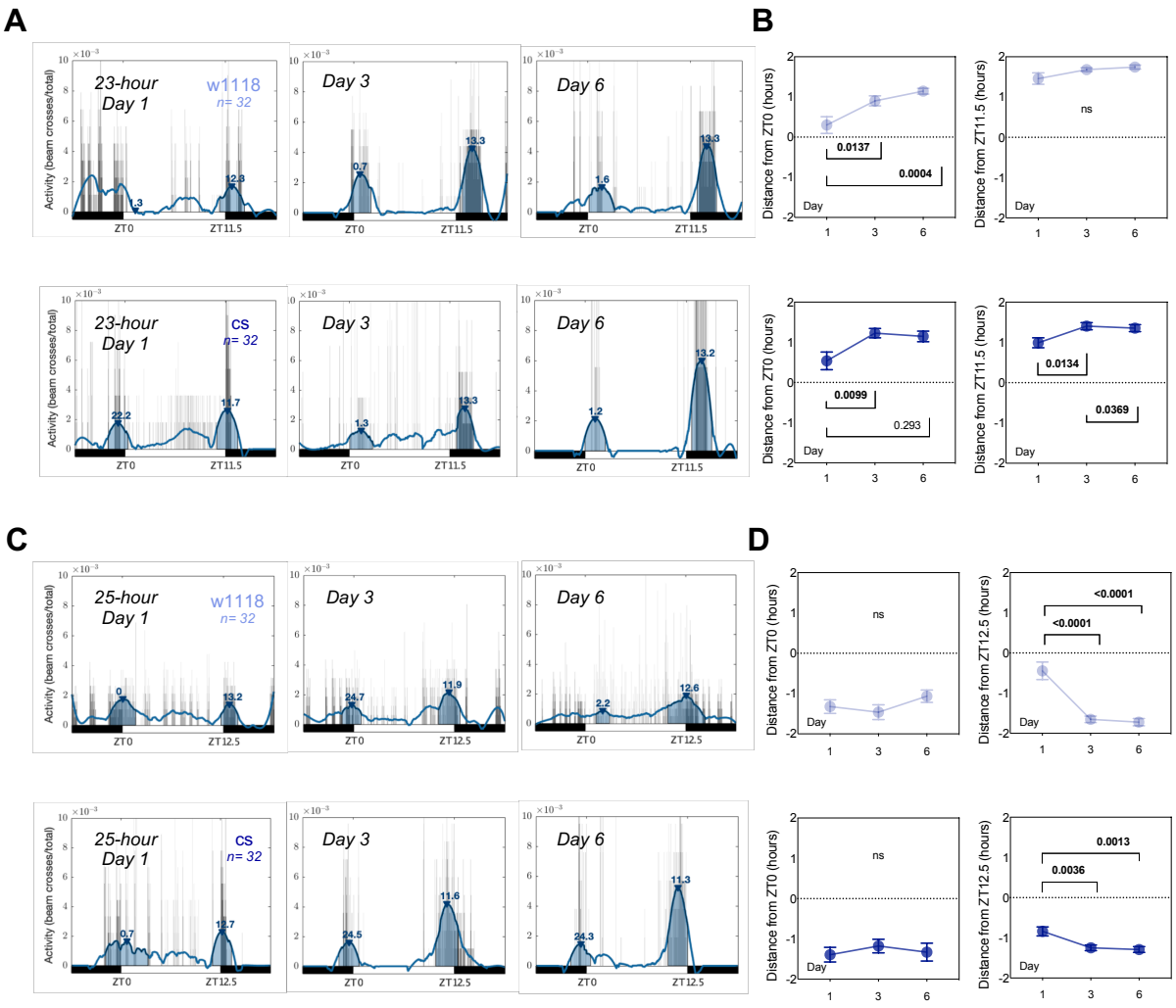

Figure 3.25. Phase analysis of 23 and 25-hour period using a Savitzky-Golay filter with 3rd –order polynomial, 241-minute frame, and 3-hour peak separation.

A-D. The first, third, and sixth days of entrained LD activity data in 23 (A-B) or 25 (C-D) –hour periods was averaged by day for individual flies, then by population, and fitted using Savitzky-Golay smoothing functions with a 3rd –order polynomial, 241-minute frame and a 240-minute or 4-hour minimum peak distance. 1-minute peak maximums were converted to ZTs relative to period length, and then to distance in hours from light onset or offset. A,C. Representative flies from w^{1118} (light blue) or cs (dark blue) fitted with the Savitzky-Golay filter on day one and day six. Blue line over 1-minute activity data represents Savitzky-Golay smoothed data. Blue shading represents peak area and blue carrots indicate peak maximums annotated with ZT. B,D. Mean of w^{1118} (light blue) or cs (dark blue) population activity phase distance in hours from lights-on or lights off indicated on Y-axis. Number of flies in population average are indicated on representative plots in A and C. Error bars reflect SEM. P-values are reported with actual values if >0.05 by One-way ANOVA with Tukey correction for multiple comparisons between all days within genotype (w^{1118} or cs).

References

Allada, R., and Chung, B.Y. (2010). Circadian organization of behavior and physiology in *Drosophila*. Annu. Rev. Physiol. 72, 605–624.

Allada, R., White, N.E., So, W.V., Hall, J.C., and Rosbash, M. (1998). A mutant *Drosophila* homolog of mammalian clock disrupts circadian rhythms and transcription of period and timeless. Cell.

Aton, S.J., Block, G.D., Tei, H., Yamazaki, S., and Herzog, E.D. (2004). Plasticity of circadian behavior and the suprachiasmatic nucleus following exposure to non-24 hour light cycles. J. Biol. Rhythms.

Bywalez, W., Menegazzi, P., Rieger, D., Schmid, B., Helfrich-Förster, C., and Yoshii, T. (2012). The dual-oscillator system of *Drosophila melanogaster* under natural-like temperature cycles. Chronobiol. Int.

Challet, E., Caldelas, I., Graff, C., and Pévet, P. (2003). Synchronization of the molecular clockwork by light- and food-related cues in mammals. Biol. Chem.

Cichewicz, K., and Hirsh, J. (2018). ShinyR-DAM: a program analyzing *Drosophila* activity, sleep and circadian rhythms. Commun. Biol.

Dissel, S., Hansen, C.N., Özkaya, Ö., Hemsley, M., Kyriacou, C.P., and Rosato, E. (2014). The logic of circadian organization in *Drosophila*. Curr. Biol.

Golombek, D.A., and Rosenstein, R.E. (2010). Physiology of Circadian Entrainment. Physiol. Rev.

Green, E.W., O'Callaghan, E.K., Hansen, C.N., Bastianello, S., Bhutani, S., Vanin, S., Armstrong, J.D., Costa, R., and Kyriacou, C.P. (2015). *Drosophila* circadian rhythms in seminatural environments: Summer afternoon component is not an artifact and requires TrpA1 channels. Proc. Natl. Acad. Sci.

Grima, B., Chélot, E., Xia, R., and Rouyer, F. (2004). Morning and evening peaks of activity rely on different clock neurons of the *Drosophila* brain. Nature.

Gronfier, C., Wright, K.P., Kronauer, R.E., and Czeisler, C.A. (2007). Entrainment of the human circadian pacemaker to longer-than-24-h days. Proc. Natl. Acad. Sci.

Guo, F., Cerullo, I., Chen, X., and Rosbash, M. (2014). PDF neuron firing phase-shifts key circadian activity neurons in *Drosophila*. Elife.

Harrison, E.M., Walbeek, T.J., Sun, J., Johnson, J., Poonawala, Q., and Gorman, M.R. (2016). Extraordinary behavioral entrainment following circadian rhythm bifurcation in mice. Sci. Rep.

Helfrich-Förster, C. (2000). Differential control of morning and evening components in the activity rhythm of *Drosophila melanogaster* - Sex-specific differences suggest a different quality of activity. J. Biol. Rhythms.

Helfrich-Förster, C., Yoshii, T., Wülbeck, C., Grieshaber, E., Rieger, D., Bachleitner, W., Cusumano, P., and Rouyer, F. (2007). The lateral and dorsal neurons of *Drosophila melanogaster*: New insights about their morphology and function. In Cold Spring Harbor Symposia on Quantitative Biology.

Hendricks, J.C., and Sehgal, A. (2004). Why a fly? Using *Drosophila* to understand the genetics of circadian rhythms and sleep. Sleep.

Hermann-Luibl, C., and Helfrich-Förster, C. (2015). Clock network in *Drosophila*. Curr. Opin. Insect Sci.

Hermann, C., Dircksen, H., Helfrich-Forster, C., and Yoshii, T. (2010). The neuropeptides

PDF, NPF and ITP operate synergistically in the endogenous clock of *Drosophila melanogaster*. J. Neurogenet.
Herzog, E.D. (2007). Neurons and networks in daily rhythms. Nat. Rev. Neurosci. 8, 790 802.
Houben, T., Coomans, C.P., and Meijer, J.H. (2014). Regulation of circadian and acute activity levels by the murine suprachiasmatic nuclei. PLoS One.
Huber, R., Hill, S.L., Holladay, C., Biesiadecki, M., Tononi, G., and Cirelli, C. (2004). Sleep homeostasis in *Drosophila melanogaster*. Sleep.
Johard, H.A.D., Yoishii, T., Dircksen, H., Cusumano, P., Rouyer, F., Helfrich-Förster, C., and Nässel, D.R. (2009). Peptidergic clock neurons in *Drosophila*: Ion transport peptide and short neuropeptide F in subsets of dorsal and ventral lateral neurons. J. Comp. Neurol.
Kempinger, L., Dittmann, R., Rieger, D., and Helfrich-Förster, C. (2009). The nocturnal activity of fruit flies exposed to artificial moonlight is partly caused by direct light effects on the activity level that bypass the endogenous clock. Chronobiol. Int.
Ko, C.H., and Takahashi, J.S. (2006). Molecular components of the mammalian circadian clock. Hum. Mol. Genet.
Konopka, R.J., and Benzer, S. (1971). Clock mutants of *Drosophila melanogaster*. Proc. Natl. Acad. Sci. U. S. A.
Levine, J.D., Funes, P., Dowse, H.B., and Hall, J.C. (2002). Signal analysis of behavioral and molecular cycles. BMC Neurosci.
Moore, R.Y. (1982). The suprachiasmatic nucleus and the organization of a circadian system. Trends Neurosci.
Nitabach, M.N. (2006). Electrical Hyperexcitation of Lateral Ventral Pacemaker Neurons Desynchronizes Downstream Circadian Oscillators in the Fly Circadian Circuit and Induces Multiple Behavioral Periods. J. Neurosci. 26, 479–489.
Nitabach, M.N., and Taghert, P.H. (2008). Organization of the *Drosophila* Circadian Control Circuit. Curr. Biol. 18.
Nitabach, M.N., Blau, J., and Holmes, T.C. (2002). Electrical silencing of *Drosophila* pacemaker neurons stops the free-running circadian clock. Cell.
Nitabach, M.N., Sheeba, V., Vera, D.A., Blau, J., and Holmes, T.C. (2005). Membrane electrical excitability is necessary for the free-running larval *Drosophila* circadian clock. J. Neurobiol.
Orfanidis, S.J. (1995). Introdction to Signal Processing. In Introdction to Signal Processing.
Pfeiffenberger, C., Lear, B.C., Keegan, K.P., and Allada, R. (2010a). Processing circadian data collected from the *Drosophila* activity monitoring (DAM) system. Cold Spring Harb. Protoc.
Pfeiffenberger, C., Lear, B.C., Keegan, K.P., and Allada, R. (2010b). Processing sleep data created with the *Drosophila* activity monitoring (DAM) system. Cold Spring Harb. Protoc.
Picot, M., Cusumano, P., Klarsfeld, A., Ueda, R., and Rouyer, F. (2007). Light activates output from evening neurons and inhibits output from morning neurons in the *Drosophila* circadian clock. PLoS Biol.
Pittendrigh, C.S., and Daan, S. (1976). A functional analysis of circadian pacemakers in nocturnal rodents. J. Comp. Physiol. A 106, 333–355.